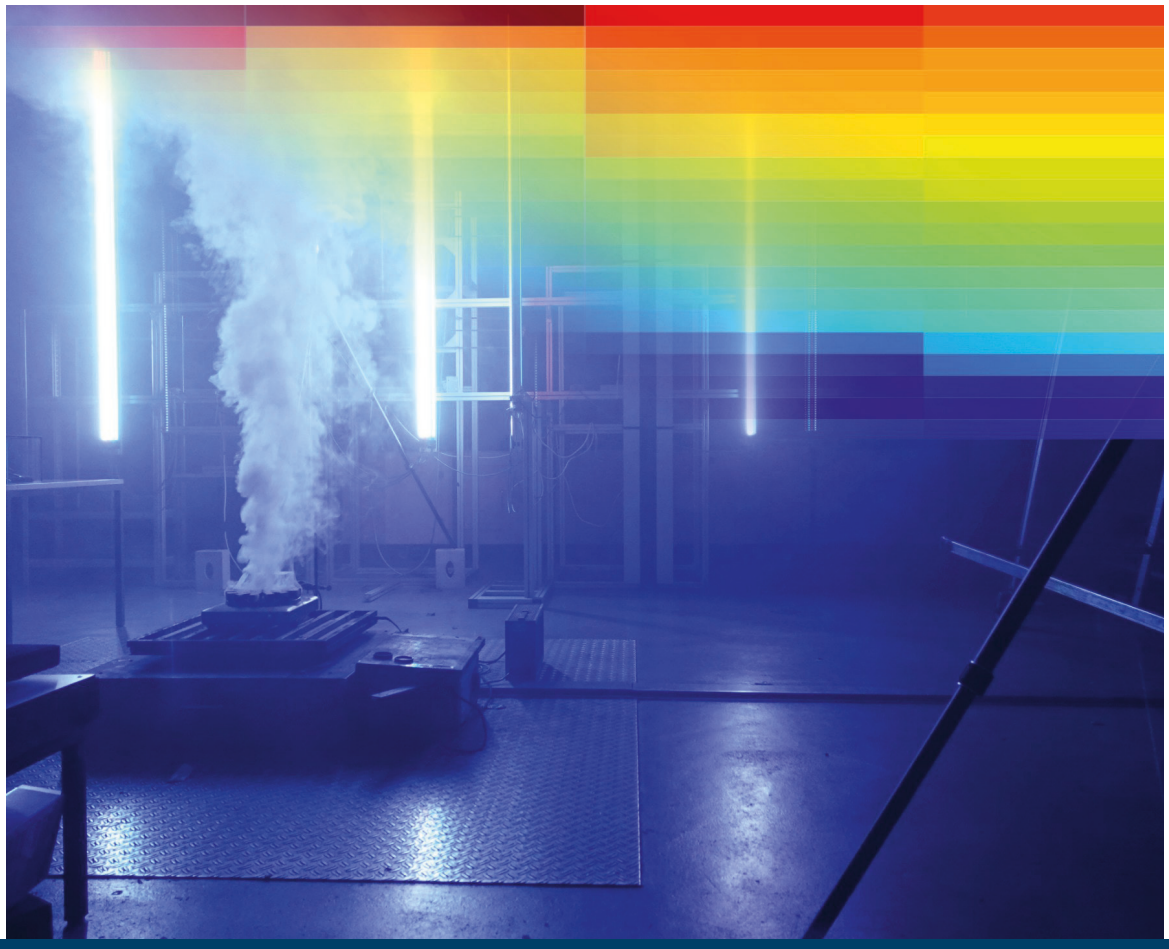

Improvement and Validation of Visibility Models in Fire Safety

Kristian Börger

IAS Series
Band / Volume 74
ISBN 978-3-95806-857-5

Mitglied der Helmholtz-Gemeinschaft

JÜLICH
Forschungszentrum

Schriften des Forschungszentrums Jülich
IAS Series Band / Volume 74

Forschungszentrum Jülich GmbH
Institute for Advanced Simulation (IAS)
Zivile Sicherheitsforschung (IAS-7)

Improvement and Validation of Visibility Models in Fire Safety

Kristian Börger

Schriften des Forschungszentrums Jülich
IAS Series

Band / Volume 74

ISSN 1868-8489

ISBN 978-3-95806-857-5

Bibliografische Information der Deutschen Nationalbibliothek.
Die Deutsche Nationalbibliothek verzeichnet diese Publikation in der
Deutschen Nationalbibliografie; detaillierte Bibliografische Daten
sind im Internet über http://dnb.d-nb.de abrufbar.

Herausgeber und Vertrieb:	Forschungszentrum Jülich GmbH Zentralbibliothek, Verlag 52425 Jülich Tel.: +49 2461 61-5368 Fax: +49 2461 61-6103 zb-publikation@fz-juelich.de www.fz-juelich.de/zb
Umschlaggestaltung:	Grafische Medien, Forschungszentrum Jülich GmbH
Druck:	Grafische Medien, Forschungszentrum Jülich GmbH
Copyright:	Forschungszentrum Jülich 2025

Schriften des Forschungszentrums Jülich
IAS Series, Band / Volume 74

D 468 (Diss. Wuppertal, Univ., 2024)

ISSN 1868-8489
ISBN 978-3-95806-857-5

The complete volume is freely available on the Internet on the Jülicher Open Access Server (JuSER)
at www.fz-juelich.de/zb/openaccess.

Abstract

In case of fire, smoke poses the major threat to the occupants of public or residential buildings. Notably, besides the smoke's toxicity, reduced visibility can prevent people from safe egress. Commonly applied fire models to assess visibility at the building's design stage often rely on input quantities that could not be consistently validated across multiple studies. Furthermore, the common interpretation of simulation results does not accurately mirror real-world conditions. This dissertation aims to develop robust methods for the experimental validation of visibility models and the enhanced post-processing of simulation results in the context of performance based design. The thesis comprises three publications exploring these topics.

The first publication introduces the improvement of an existing photometric method (LEDSA) to measure temporally and spatially resolved extinction coefficients in laboratory test fires. LEDSA involves capturing the smoke induced change in intensity of LEDs using consumer digital cameras. Validating against the established MIREX measurement system revealed, that utilizing RAW image data significantly improves measurement accuracy compared to the previously used JPG files. While using higher quality LEDs helped to increase reproducibility of the measurements, further uncertainties of the model and the experimental setup could be identified.

In the second publication, LEDSA is compared on multiple test fires to the Radiance Method, which was developed at the University of Waterloo. It involves measuring the contrast on adjacent light and dark areas in image or video footage. The Radiance Method measurements align well with LEDSA and the MIREX for smoke from n-heptane pool fires, with much lower computational effort than LEDSA. However, only LEDSA was in line with the MIREX measurements for wood smouldering fires, while the Radiance Method could only reproduce patterns of the reference measurement.

The third publication shifts focus from model validation to application, introducing visibility maps as a novel approach to assess visibility in performance based design. By post-processing existing data from fire simulations, the maps indicate areas where exit signs remain visible along the route of egress. Integrating the extinction coefficient along the line of sight allows applying Jin's empirical correlation to non-homogeneous smoke environments, providing for a more realistic assessment of visibility, than the classical way of treating it as a local quantity. Visibility maps can also account for additional factors like view angle and visual obstruction of exit signs.

Zusammenfassung

Im Brandfall stellt Rauch die größte Bedrohung für die Nutzer von öffentlichen Gebäuden oder Wohnhäusern dar. Abgesehen von der Toxizität des Rauchs kann dieser auch durch eine Einschränkung der Sichtweite eine sichere Flucht verhindern. Die üblicherweise verwendeten Brandmodelle zur Bewertung der Sichtweite in der Planungsphase eines Gebäudes beruhen häufig auf Eingangsgrößen, die über verschiedenen Studien hinweg nicht einheitlich validiert werden konnten. Darüber hinaus bildet die übliche Interpretation von Simulationsergebnisse die realen Verhältnisse oft nicht genau ab. Diese Dissertation zielt darauf ab, zuverlässige Methoden für die experimentelle Validierung von Sichtweitenmodellen und die verbesserte Aufbereitung von Simulationsergebnissen im Kontext leistungsorientierter Nachweise zu entwickeln. Die Arbeit umfasst drei Veröffentlichungen, die sich mit diesen Themen befassen.

Die erste Veröffentlichung stellt eine Verbesserung eines bestehenden photometrischen Verfahrens (LEDSA) zur Messung von zeitlich und räumlich aufgelösten Extinktionskoeffizienten bei Laborbränden vor. LEDSA erfasst die durch Rauch verursachte Änderung der Intensität von LEDs mit handelsüblichen Digitalkameras. Ein Vergleich mit dem etablierten MIREX-Messsystem zeigte, dass die Verwendung von RAW-Bilddaten die Messgenauigkeit im Vergleich zu den zuvor verwendeten JPG-Dateien erheblich verbessert. Obwohl der Einsatz hochwertigerer LEDs die Reproduzierbarkeit der Messergebnisse erhöhte, konnten weitere Unsicherheiten des Modells und des experimentellen Aufbaus identifiziert werden.

In der zweiten Veröffentlichung wird LEDSA in Brandversuchen mit mehreren Testbränden mit der Radiance Method verglichen, die an der University of Waterloo entwickelt wurde. Diese Methode beruht auf der Messung des Kontrasts zwischen angrenzenden hellen und dunklen Bereichen in Bild- oder Videoaufnahmen. Die Radiance Method zeigt gute Übereinstimmung mit den Messergebnissen von LEDSA und MIREX bei n-Heptan Poolbränden, benötigt jedoch deutlich weniger Rechenaufwand als LEDSA. Bei Holzschwelbränden stimmt lediglich LEDSA mit den MIREX Messungen überein, während die Radiance Method die Referenzmessung nur schematisch reproduzieren konnte.

Die dritte Veröffentlichung verlagert den Schwerpunkt von der Modellvalidierung auf die Anwendung und stellt Sichtweitenkarten als neuartiges Instrument zur Bewertung der Sichtweite im Rahmen leistungsorientierter Nachweise vor. Nach der Aufbereitung vorhandener Ergebnisdaten aus Brandsimulationen zeigen die Karten Bereiche an, in denen Notausgangsschilder entlang des Fluchtweges sichtbar bleiben. Durch die Integration des Extinktionskoeffizienten entlang der Sichtachse kann der

empirische Zusammenhang nach Jin auf inhomogene Rauchverteilung angewendet werden, was eine realistischere Bewertung der Sichtweite ermöglicht im Vergleich zu einer klassischen Behandlung als lokale Größe. Sichtweitenkarten können auch zusätzliche Faktoren wie den Betrachtungswinkel und die versperrte Sicht auf Notausgangsschildern berücksichtigen.

Acknowledgements

I would like to express my gratitude to all those who made it possible for me to write this dissertation and who supported me in the associated work over the last years. The journey was not without its challenges, but it was also filled with many rewarding and enjoyable moments. I am grateful to my colleagues at the Chair of Computational Civil Engineering at the University of Wuppertal and at IAS-7 at the Forschungszentrum Jülich for their ongoing support. To my great delight, some close, and lasting friendships have emerged from this collegial environment. Luckily, I had the opportunity of meeting many colleagues in person before the shift to remote work due to the COVID-19 pandemic.

My deepest thanks go to my partner, Inga, to whom I dedicate this dissertation. She has shown great understanding and endurance during intense periods of work, including late night work sessions, weekends spent working before important deadlines, many conferences and business trips and, last but not least, my three-month stay abroad in Canada. I particularly appreciate her dedication in taking care of our son, Jonte Michel, over the past months, which allowed me to focus on completing this thesis. Enduring all this and continuing to support me in my endeavour is by no means something to be taken for granted. Additionally, I thank her for her insightful feedback on typography and design issues during the preparation of numerous presentations.

A big thanks also goes to my supervisor, Prof. Lukas Arnold, who gave me the opportunity to enter a scientific career and encouraged me to pursue a doctorate in the field of visibility in fire conditions. Through his mentorship, I was able to gain and improve my skills in data analysis and scientific writing. His dedication to fostering a welcoming and familial working environment made a profound impact on my experience. I extend my sincere gratitude to my daily supervisor, Alexander Belt, for introducing me to the world of experimental research and consistently serving as a reliable point of contact for guidance and support. Both have always been by my side with valuable advice and were always good conversation partners in interesting and fulfilling discussions. Furthermore, my involvement in university teaching provided me with a fascinating and rewarding perspective.

I am also grateful to Prof. Elizabeth Weckman and Jennifer Ellingham from the University of Waterloo in Canada for their excellent partnership in our collaborative research project. Despite the challenges posed by COVID-related travel restrictions, we were able to conduct joint experiments that led to the publication of a co-authored scientific paper and a conference contribution. Subsequently, I experienced

excellent supervision and guidance during my research stay at the University of Waterloo.

My thanks also go to all the friends, colleagues, and individuals who have supported me both professionally and personally throughout this doctoral journey, even if their names are not mentioned here.

Lastly, I wish to thank my family for their support throughout my academic and professional life. They fully supported my decision to leave my position as a fire safety engineer to pursue this doctorate, and for that, I am sincerely thankful.

List of Publications

Publication I
Kristian Börger, Alexander Belt, Thorsten Schultze and Lukas Arnold. *Remote Sensing of the Light-Obscuring Smoke Properties in Real-Scale Fires Using a Photometric Measurement Method*. Fire Technol 60, 19–45, 2024.
https://doi.org/10.1007/s10694-023-01470-z.

Publication II
Kristian Börger, Jennifer Ellingham, Alexander Belt, Thorsten Schultze, Stefan Bieder, Elizabeth Weckman and Lukas Arnold. *Assessing Performance of LEDSA and Radiance Method for Measuring Extinction Coefficients in Real-Scale Fire Environments*. Fire Safety Journal, Volume 141, 2023. 103929, ISSN 0379-7112, https://doi.org/10.1016/j.firesaf.2023.103929.

Publication III
Kristian Börger, Alexander Belt and Lukas Arnold. *A Waypoint Based Approach to Visibility in Performance Based Fire Safety Design*. Fire Safety Journal, 2024. 104269, ISSN 0379-7112,
https://doi.org/10.1016/j.firesaf.2024.104269.

Table of Contents

CHAPTER 1

Introduction

1.1 Motivation

Smoke is the main cause of injuries and fatalities in fires in residential, public and industrial buildings. The various components of fire generated smoke pose a danger to humans in many ways. Particles from burned substances can penetrate the human body's respiratory system, while incomplete combustion in low oxygen environments can result in the formation of toxic gases. Some gases may also irritate the eyes of building occupants, making orientation considerably more difficult. Furthermore, smoke particles reduce visibility, making people incapable of finding an exit [1], particularly in unfamiliar environments. The effects of fire induced smoke on the visibility of guiding exit signs can be predicted and counteracted in the building design process by means of performance based design approaches incorporating the use of numerical fire models. However, the smoke characteristics utilized in most of these models are subject to considerable uncertainties, which can significantly compromise the predictive accuracy of corresponding fire simulations.

As visibility is often the first tenability criterion to be exceeded in performance based building designs, it is essential for the applied models to be sufficiently validated against real-world data. However, there are indications that visibility in smoke laden environments may be significantly underestimated by numerical fire models such as the Fire Dynamics Simulator (FDS) [2, 3]. Highly conservative predictions of the light obscuring effects may result in both uneconomical and unecological building designs, due to the implementation of excessive fire safety measures. Discrepancies between simulations and real-scale experiments are likely not to be attributed to the models themselves, but rather to the input quantities that describe the light extinction by smoke. Extensive research is still required to investigate all influences of both combustion and fluid dynamics effects on these discrepancies.

Current modelling practices to assess visibility in case of fire predominantly rely on investigations on human visual perception in fire conditions by Jin from the 1970s [4–7]. This empirical approach simplifies the complex dynamics of smoke and light interaction to a simple correlation of the light extinction coefficient and the visual range of exit signs at the obscuration threshold. Although the extinction

coefficient can be computed with temporal and spatial resolution using numerical fire models, the assessment of visibility is typically based on a local analysis. This approach does not adequately allow predicting visibility of exit signs in real-world conditions, as it fails to account for the nature of inhomogeneous smoke spread in actual compartment fires.

This dissertation aims to improve the understanding of how fire smoke interacts with light by developing a reliable measurement technique to gather temporally and spatially resolved smoke characteristics data from real-scale laboratory fire experiments. The collected data may serve to improve the accuracy of numerical fire models to predict visibility by revising input quantities. Furthermore, an advanced model is developed that allows a more realistic interpretation of the actual visibility in compartment fires based on simulation results than commonly applied approaches.

1.2 State of the Art in Science and Technology

1.2.1 Visibility in Performance Based Design

In order to enable safe egress in case of fire, building designs must prioritize occupants safety by minimizing potential hazards to their life and health. Accordingly, these fundamental requirements form the safety goals of most building codes. To meet these safety goals, specific objectives must be satisfied, detailing the respective requirements for the building or building components. Typically, compliance to these regulations involves implementing a variety of structural and technical measures that arise from prescriptive guidelines. Fire safety measures, for example, may include separating fire departments by creating physical barriers or incorporating systems for smoke control. However, as building designs become more complex, strict compliance to these requirements can become challenging from an economic and ecological perspective.

Performance based design in fire safety engineering offers a viable alternative to prescriptive design, encompassing a wide range of objectives outlined in most building regulations. The European Union's guidelines on fire safety [8] also encourage the use of engineering-based evidence to assess and design evacuation and rescue measures. In this context, performance is considered to be a quantitative expression of safety requirements for buildings, building products, services, and systems as well as fire protection equipment under fire conditions.

A comprehensive assessment of evacuation safety can be achieved using methods such as the ASET-RSET analysis [9], which compares the Available Safe Egress Time (ASET) with the Required Safe Egress Time (RSET). The ASET refers to the time until a predefined performance criterion is met or exceeded at a certain point in the area of interest. RSET, on the other hand, corresponds to the time it takes a person or agent, as modelled in pedestrian dynamics simulations, to reach an exit or place of safety. Fire smoke can affect ASET and RSET, as low visibility reduces the occupant's orientation and walking speed, while toxic products limit the tolerable time of exposure [10].

Until today, visibility in performance based design is usually modelled based on Jin's experimental investigations on human behaviour in fire. From the visual ob-

scuration threshold, he correlated the measured light extinction coefficient σ from smoke to the visual range V of exit signs as perceived from human observers by a single dimensionless factor C. The latter reflects the illumination type of the sign, typically being $2 \sim 4$ for light reflecting signs and $5 \sim 10$ for light emitting signs.

Visibility models based on this correlation have been widely adopted in fire safety engineering and are still implemented in numerical fire models like FDS, computing visibility as a function of the smoke density. In the context of performance based design, visibility is usually compared locally with performance criteria from the literature, showing considerable deviations from 4 m to 20 m, depending on the lighting conditions or how familiar people are with the architecture of the facilities [11]. However, this approach entails several uncertainties and limitations. First, the performance criteria are not related to the required visual range towards the actual exit signs. Second, Jin's correlation does not allow to map the inhomogeneous smoke distribution between a person and an observed target, that usually occurs in compartment fires. A local visual range gives no indication about the actual perception of the target.

1.2.2 Modelling Visibility in Smoke Laden Environments

The assessment of visibility in smoke laden environments by means of fire simulations requires users to be aware of the uncertainties and limitations associated with the applied models. Computational Fluid Dynamics (CFD) codes can compute the extinction coefficient σ as the product of local smoke density ρ_s and a mass specific extinction coefficient K_m. The extinction coefficient σ quantifies how much light is exponentially obscured along a certain distance in a damping medium like smoke. The phenomenon is described by the Beer-Lambert law [12], which is also utilized to determine σ in experimental studies based on measurements of light transmission.

Since a single value of K_m depicts the scattering and absorption characteristics of light by smoke particles as a simple damping of light, it does not allow for a dedicated analysis of both phenomena. While black smoke is more absorbent to light, white smoke predominantly causes a scattering effect, resulting in a blurred perception of the observed objects [13]. The mass specific extinction coefficient is a function of the size distribution and shape of the smoke particles, so it may be strongly related to boundary conditions of the combustion and differ between smoke from various fuels. However, in many fire models like FDS, a unique value of $K_\mathrm{m} = 8{,}700\,\mathrm{m^2\,kg^{-1}}$ is adopted as default. Mulholland and Croakin [14] introduced this as a mean value derived from an analysis of seven studies, involving smoke from flaming combustion of 29 different fuels and measuring light transmission at a wavelength of $\lambda = 633\,\mathrm{nm}$. They reported the value to be much lower for smoulder and pyrolysis generated smoke. The studies were conducted using bench-scale experimental setups that included optical and gravimetric measurements, such as those taken from the exhaust of a cone calorimeter.

Only few studies in the literature focus on examining these smoke characteristics in real-scale experimental setups, that allow unconstrained fluid dynamics. And yet, such research is crucial for understanding if scaling K_m is valid for applications in modelling compartment fires. Studies from Gottuk et al. [15] and Hamins

et al. [16] focussing on model validation revealed significant discrepancies in light extinction and smoke density relative to corresponding FDS simulations. Scaling effects of the mass specific extinction coefficient and soot yield, as well as soot loss by deposition, are discussed as key factors here. The experimentally determined extinction coefficient was overestimated by FDS by a factor of 4 to 5 when applying the default value of K_m. Comparable discrepancies were also observed in experiments conducted by the Chair of Computational Civil Engineering (CCE) at the University of Wuppertal and the Institute of Advanced Simulation (IAS-7) at the Forschungszentrum Jülich [17, 18]. Recent studies employing optical and aerosol measurement techniques in real-scale fire experiments support the assumption, that the mass specific extinction coefficient may highly depend on scaling effects [19]. Furthermore, K_m typically represents the light extinction of monochromatic light, as it varies exponentially with the wavelength λ, as demonstrated in an empirical study by Widmann [20]. Consequently, Jin's correlation fails to account for effects of ambient lightning, which may encompass a broad spectrum of wavelengths.

In real-scale fire tests, smoke spread usually does not exhibit a homogeneous density. Consequently, commonly applied apparatus for local measurements of the extinction coefficient are inadequate to fully capture the experimental dynamics, like changes in smoke stratification or ageing effects of aerosols. Inhomogeneous smoke distribution in compartment fires also complicates visibility assessment in performance based design, often restricting the application of Jin's correlation to a local analysis.

1.3 Research Objectives and Methodology

As outlined in the previous sections, numerical simulation models to predict visibility in case of fire pose an essential tool in performance based fire safety design. This dissertation aims to contribute to the validation of such models by developing a reliable methodology to investigate smoke characteristics in large-scale fires. Additionally, a model is developed to allow for a more realistic interpretation of simulation results. Accordingly, this thesis can be divided into an experimental part, covered in the first two publications, and an application-oriented part, covered in the third publication it is based on.

In a prior study [21], the photometric measurement method LEDSmokeAnalysis (LEDSA) was introduced for measuring spatially and temporally resolved extinction coefficients in laboratory test fires. LEDSA is an open source Python package that was developed at CCE and IAS-7 [22]. The method is based on measuring the smoke induced drop in light intensity of individual LEDs, using image data from consumer digital cameras. The tomographic approach of LEDSA is based on a discretisation of the measurement domain by horizontal layers, which are assumed to have a homogeneous smoke density. According to the principle of inverse modelling, a numerical model based on geometric optics and the Beer-Lambert law is used to compute extinction coefficients for the individual layers. A nonlinear system of equations is solved, by minimising a cost function that accounts for the differences between the measured intensities and model predictions, with additional terms to

ensure smoothness across adjacent layers and to stress the solution within bounding limits.

In a proof of concept study, the methodology has already been fundamentally verified, by comparing the computed extinction coefficients against local measurements of the established MIREX [23] apparatus. The MIREX measures the light transmittance of an infrared diode across a reflected path length of 2×1 m. It was shown, that LEDSA is able to capture the dynamics of the experiment but significantly underestimates the MIREX measurements. This observation contradicted expectations, as the LEDSA measurements are based on light in the visible range (red, green, blue) and the MIREX operates in the infrared range. According to the principles of classical electrodynamics and the empirical correlation according to Widmann, an exponential increase in the extinction coefficient with decreasing wavelength is to be expected.

The first publication outlines how LEDSA is optimised and validated against the MIREX on the basis of data from previously conducted experiments that have not yet been analysed. Based on the findings, uncertainties of the model and the experimental boundary conditions are recognised and, where possible, quantified. An enhanced experimental setup is employed in a follow-up series of experiments, as presented in the second publication. It features multiple cameras, higher quality LEDs and further measurement instrumentation to capture quantities like temperature or aerosol characteristics. Furthermore, other test fires (TF) than the previously investigated TF5 n-heptane pool fire according to the EN 54-7 standard [24] like a wood smouldering fire are investigated. The key aspect of this study, however, involves comparing LEDSA with the Radiance Method, developed at the Department of Mechanical and Mechatronics Engineering at the University of Waterloo in Canada. It originates from the field of air pollution measurement and was adapted to estimate the descent of a smoke layer in compartment fires. Following an analytical approach, the Radiance Method requires much less computational effort, than the numerical model of LEDSA. However, the latter is designed to perform a more detailed analysis of smoke characteristics under controlled laboratory boundary conditions. This publication investigates the suitability of both methods for measuring extinction coefficients produced by smoke from different fuels, and evaluates the balance between the required effort and measurement accuracy, using the MIREX as a reference.

The third publication focuses on the development of a new model for assessing visibility in the context of performance based fire safety design. The proposed visibility maps are intended to allow a straightforward and easy to understand evaluation of egress routes by identifying blind spots in the building floor plan where the perception of exit signs may not be sufficiently guaranteed. Generating the maps involves little additional effort and is based upon post-processed data from numerical fire simulations only. They offer an alternative to the conventional method of treating visibility as a localised measure and eliminate the need for defining arbitrary performance criteria.

CHAPTER 2

Results

2.1 Publication I: Remote Sensing of the Light-Obscuring Smoke Properties in Real-Scale Fires Using a Photometric Measurement Method

The first publication deals with the systematic analysis of weak points and uncertainties of the existing photometric measurement method LEDSA in order to improve its measurement accuracy.

The original approach utilized JPG image data to measure the change in LED intensities based on pixel values in the images. However, a side-by-side analysis of the unprocessed RAW image files showed that brightness measurement is inevitably distorted by the camera's internal post-processing like compression or gamma correction. The intensities read from the RAW data show a much higher attenuation through the smoke than those from the corresponding JPGs. This results in a significant underestimation of the computed extinction coefficients based on JPG images.

The experiments presented in this publication were conducted at the Heinz-Luck fire detection laboratory at the University of Duisburg-Essen. Both, the laboratory geometry and the conducted test fires resemble the EN 54-7 standard. The experiments feature a similar, but extended, setup to the original work. Tangent to a radius of 3 m around a central fire source, seven LED strips are installed vertically and diagonally aligned, each spanning from around 1 m above the floor to the ceiling at 3.37 m height. Two cameras, placed on the other side of the laboratory, are facing the LED strips, while the position of one camera was changed within two setups. Three MIREX devices were placed for reference measurements at the 3 m radius at heights 1.52 m, 2.3 m and 3.3 m above the floor.

Four experiments were conducted with 500 g n-heptane fuel in each setup, and two experiments with an n-heptane-toluene mixture in another setup. The extinction coefficients measured by the MIREX were compared to the LEDSA measurements

at the respective heights as a function of time. All measurements showed good reproducibility, with separate results from the red, green, and blue colour channels of the RAW images yielding the expected correlation with regard to the wavelength dependency according to Widmann.

As expected, the LEDSA measurements were also correspondingly higher than the MIREX measurements. Furthermore, analysing images from cameras positioned at different locations in the laboratory supported the initial hypothesis of homogeneous smoke layers, as the results showed consistent extinction coefficients.

Several uncertainties resulting from the experimental setup and the numerical model itself could be identified in a more detailed analysis of the measurement results. Varying weighting factors within the cost function of the numerical model of LEDSA indicated that weak solutions of the extinction coefficients may occur in the boundary layers of the domain. Here, information in the optimization procedure is sparse, because these layers are not crossed by many light beams between the camera and the LEDs.

An in-depth spectral analysis of the individual LEDs showed a broad bandwidth of the individual red, green, and blue colour components, so that the measurements cannot be precisely assigned to a certain wavelength. In addition, due to the broad response spectrum of the camera sensor, it is to be expected that the individual colour components of the LEDs are not captured exclusively in the corresponding colour channels of the camera. As the light of the individual LED colours is damped differently by the smoke, the measurement is additionally distorted. Furthermore, the measurement of light intensities is expected to be affected by the heating of the LEDs as a result of radiation and convection from the flame and hot smoke. Based on correlations in the literature [25], a considerable reduction in the emitted intensity can be assumed due to the maximum temperature measured in the course of the experiments. This effect is expected to be greatest for the red LED and smallest for the blue LED, but it was not quantified in detail in this study.

2.2 Publication II: Assessing Performance of LEDSA and Radiance Method for Measuring Extinction Coefficients in Real-Scale Fire Environments

Based on the findings of the previous laboratory fire experiments described in the first publication, an improved and more robust setup was developed for further investigations. In order to achieve better resistance to external temperature stress, higher quality LED strips with thermal insulation were used. To ensure uniform temperature dissipation, they were attached to vertically aligned aluminium columns using a thermally conductive adhesive.

In an elaborate series of experiments, this setup was used to test the performance of LEDSA against the Radiance Method to measure extinction coefficients in laboratory test fires with different fuels according to the EN 54-7.

Both methods involve measuring the intensity or transmission of light from image data. However, as they are based on different measuring equipment, the procedure differs accordingly. LEDSA detects the individual LEDs on an initial image using a maximum pixel search and defines ROIs (Regions Of Interest) with a defined size around them. The intensity of the individual LEDs is measured in each image during the experiment as the sum of all pixel values in the ROIs, normalised to the respective initial values. The Radiance Method measures transmission from the contrast between adjacent black and white ROIs on contrast boards. The contrast boards were placed on the opposite side of the laboratory to be directly illuminated by the LEDs of the LEDSA setup. The ROIs on the boards are defined manually by subdividing the black and white areas by a predefined number of sections. The Radiance Method utilises JPG images or video data, as it was built to work on footage from security cameras. Hence, an encoding procedure is applied to recover the linear radiance values, required for accurate measurements. To capture higher quality images, action cams were used in this study instead of security cameras. LEDSA bypasses this encoding step by using RAW image files, preserving the full dynamic range of the sensor.

LESDA is based on a numerical layer model, requiring significant computational effort and hence the use of an HPC (High Performance Computing) system. The Radiance Method, on the other hand, employs a straightforward analytical application of the Beer-Lambert law. It computes extinction coefficients under the simplified assumption that smoke density is constant along the measurement path. The required calculations can be carried out on a conventional desktop computer. However, since smoke density usually varies in height, the measured extinction coefficient, corresponds to the average extinction coefficient value integrated over the camera's line of sight. Since both methods are following a different approach, they are subject to different model-related uncertainties. The uncertainties were quantified using synthetically generated image data resulting from a constant, linear and quadratic height profile of the extinction coefficient. Virtual cameras were assumed to be at heights 1 m and 2 m above the floor. The LEDSA computed extinction coefficients closely follow the synthetic data for all three profiles. Notable deviations in the top and bottom layers can be attributed to the numerical model, as the camera captures only sparse information on light attenuation in the peripheral areas. The Radiance Method accurately measures the "real" extinction coefficients at the height of the camera but increasingly deviates towards lower and higher regions.

In the experiments, the MIREX extinction coefficient measurements were scaled according to Widmann's correlation, accounting for the peak wavelengths of the MIREX and the LEDs to allow for a comparability across the measurement methods. Despite the systematic discrepancies, the extinction coefficient measurements from both LEDSA and the Radiance Method for the TF5 n-heptane fire showed good agreement with the MIREX measurements at various heights, when analysing the red colour channel of the cameras. However, the Radiance Method was notably more sensitive to extraneous light than LEDSA. Since the contrast boards were illuminated by LEDs rather than being self-illuminating, the additional light from the flame had a much greater impact. This effect was largely mitigated by applying a correction procedure to adjust the measured light intensities accordingly.

For the TF2 wood smouldering pyrolysis fire tests, the LEDSA extinction coefficients again closely match the MIREX measurements, while the Radiance Method shows significant higher values. The direct exposure of the contrast boards by the LEDs likely caused significant back scattering from the white smoke particles, leading to reduced contrast and an overestimation of the extinction coefficient.

The TF5 experiments in general showed good reproducibility due to forced convection during the burning phase, while environmental factors became more significant after the fire was extinguished. In contrast, the TF2 tests had higher variability, as the negligible heat release results in low buoyancy of the smoke, making it more sensitive to environmental effects.

2.3 Publication III: A Waypoint Based Approach to Visibility in Performance Based Fire Safety Design

For use in the context of performance based design, a meaningful interpretation of the applied simulation models is just as important as an adequate validation. However, traditional visibility models based on Jin's correlation are usually accompanied by several limitations and uncertainties, as outlined in section 1.2.1. The third publication introduces visibility maps as an alternative and intuitive approach to assess visibility in compartment fires.

Visibility maps depict floor plans of a building, indicating, for a certain point in time, where exit signs remain visible or not along potential routes of egress in the presence of fire induced smoke. They are generated by post-processing the temporally and spatially resolved data of the computed extinction coefficients from numerical fire models like FDS. Representing Boolean type matrices, the maps are shaped in the same dimension as the mesh-grid of the respective fire simulation. Exit signs represent waypoints along potential routes of egress, being references for the computation of multiple quantities that are each computed as equally shaped matrices. Using ray-casting techniques, an averaged or integrated extinction coefficient is computed between all cells of the domain relative to a waypoint, allowing to apply Jin's correlation to an inhomogeneous smoke distribution. Visibility in all cells is reduced depending on the viewing angle relative to the exit sign or set to zero if it is concealed by architectural elements. For all cells, the computed or available visibility is matched against the required visibility, simply being the Euclidean distance between the cell and the waypoint. This results in a True or False declaration, depending on whether the exit sign is visible or not. Multiple waypoints along a route of egress require the generation of individual visibility maps for each waypoint and their superposition by logical operations. This also allows assigning different C factors to the individual exit signs, to account for different types of illumination. Furthermore, the assessment can be conducted across a period of time by aggregating multiple visibility maps for the corresponding time steps of the fire simulation. Likewise, the evaluation can be provided as ASET maps, locally indicating the time at which a performance criterion, here the required visibility, is violated for the first time.

To significantly reduce the computational effort for creating visibility maps, all computations are performed only at a two-dimensional level. Hence, the required data is read from horizontal slices of the simulation results, following the simplified assumption that all exit signs are placed at the same height above the floor as the observer's eye level.

A simple application example demonstrates the use of visibility maps based on the simulation of an emerging fire in a small office facility. The example reveals that the same simulation data can be interpreted fundamentally different when analysed as a local quantity or post-processed as visibility maps. In a sensitivity analysis, the influence of the mesh-grid resolution on the maps was examined. Only small discrepancies could be identified between simulations with a 5 cm, 10 cm and a 20 cm resolution. Although discretisation also affects the ray casting algorithm, its impact can primarily be attributed to the discretisation of the CFD simulation.

CHAPTER 3

Discussion

This dissertation aims at improving numerical models for the assessment of visibility in case of fire. The first two publications introduce methods for validating the input quantities of these models in the context of experimental investigations. In the third publication, a method is presented that enables a more realistic interpretation of such models by post-processing the result data.

Building upon an existing experimental dataset, the accuracy of the photometric measurement technique LEDSA was significantly improved over its original version. The empirical correlation by Widmann, linking the wavelength of light to the mass specific extinction coefficient, was utilised to account for the different wavelengths of the red, green, and blue colour components of the LED and the MIREX, operating in the infrared range. It should be noted that this is a simplification, not accounting for the dedicated physical effects of light interacting with smoke particles and certain experimental uncertainties that were not fully quantified within the scope of this thesis. First, employing only the peak wavelengths of the emitted light from MIREX and the LEDs neglects the broad spectrum of the light sources, which may lead to notable errors due to the exponential relationship between the mass specific extinction coefficient and the wavelength. Additionally, the response spectra of the cameras employed are not known, precluding any precise determination of which wavelength range is recorded most by the camera's sensors. Furthermore, the application of Widmann's fit function may also be subject to considerable uncertainties due to scaling effects of experimental measurements, as discussed in section 1.2.2.

The experimental setup itself introduces further uncertainties, particularly related to the LEDs, given a notable correlation between temperature and the emitted light intensity. An approach for quantifying the potential impact on the extinction coefficient measurements is provided in this work. The error can potentially be compensated for from measurements of the LED's working temperature and the increase in temperature resulting from radiative and convective thermal exposure by the smoke. For this purpose, separate investigations were conducted into the thermal behaviour of the employed LEDs [26]. Additionally, higher quality LEDs featuring a thermal insulation were used in an enhanced experimental setup. Various LED strips were spectrally analysed in preliminary experiments to investigate the

variation in peak wavelengths under operating temperature and external thermal stress. Another aspect to be addressed in future investigations is quantifying the effect of soot deposition, which was observed on all types of measurement equipment close to the ceiling. This deposition is expected to particularly impact measurement accuracy, especially in experiments with flaming combustion.

Given the good agreement with the MIREX measurements, LEDSA can still be regarded as an effective and low-cost technique for the experimental measurement of extinction coefficients and possibly for the validation of numerical fire models. However, certain limitations and constraints that are currently inherent with the method should be taken into account. LEDSA was designed to work under laboratory conditions, allowing the formation of a homogeneous smoke layer. Deviating boundary conditions such as multi-room geometries or aerodynamic flows from ventilation ducts may disrupt this homogeneity and distort the results. To address these limitations, further development of LEDSA into a three-dimensional tomographic model, utilising images captured from multiple cameras at different positions and angles, is conceivable. This in turn entails considerable additional computational effort, requiring a more efficient design of the numerical model. The proposed advancements would enable the use of LEDSA for the validation of compartment fires with complex geometries.

Further potential applications for LEDSA arise when compared with the Radiance Method. The Radiance Method offers comparable, although less precise, results with significantly lower computational effort for certain use cases. This suggests that a simplified and reduced version of LEDSA could be employed in fields such as fire detection.

Parallel to the improvements of the model and the experimental setup of LEDSA, a large data set of extinction coefficient measurements was collected during the conducted experiments, which can potentially contribute to the validation of numerical visibility models. Alongside the TF5 and TF2 fires already addressed in the publications, more test fires according to the EN 54-7 standard, like the TF3 (cotton smouldering fire) and TF4 (polyurethane fire) were also examined, with their analysis being the subject of future work. In particular, to further investigate scaling effects, additional experiments using the previously employed fuels with different heat release rates and room geometries are required.

Apart from experimental works, an application-oriented tool was developed to post-process data from numerical fire models for the assessment of visibility in the context of performance based design. Unlike traditional visibility models, the introduced visibility maps account for the actual inhomogeneous smoke spread, as well as the type, location, and orientation of exit signs. The maps enable not only a sectional view but also a comprehensive assessment of the entire route of egress, eliminating the need of defining arbitrarily chosen and highly subjective performance criteria for a minimum visibility threshold. They serve an intuitive interpretation of abstract simulation data, even by people without a professional qualification. This may encourage the use of numerical fire models in building design while strengthening credibility with approving authorities.

The model, however, still entails considerable potential for optimisation, both technically and conceptually. At present, the application is limited to flat floor plans,

as all geometric and physical computations are performed on a two-dimensional grid. To accommodate modern, complex building structures, involving open floor connections or staircases, the analysis must be extended to three dimensions.

Furthermore, direct coupling of visibility maps with models for pedestrian dynamics is possible. At spatial and temporal resolution, visibility can be read from the maps to adaptively control variable parameters of the pedestrian agents like walking speed or route decisions. A strong coupling between the fire model and the pedestrian dynamics model is even conceivable, so that the effects of people's actions, like opening doors on the course of the fire, can be taken into account. However, this would require appropriate interfaces between both models and could entail significant computational effort due to numerous iterations of the simulations.

It is crucial to note that the predictive validity of the visibility maps is constrained by the limitations of Jin's correlation, as discussed in section 1.2.2, not being able to mimic the actual human perception of exit signs. Moreover, physiological factors, like the effect of colour on the maximum cognitive distance and the perceptual processing, as investigated in [27, 28], are not considered.

A possible solution to provide a more sophisticated assessment of visibility involves the creation of synthetic images that mimic the actual perception of objects in a smoke laden environment. Models presented by Zhang [29] and Wahlqvist and Rubini [30], incorporate the actual smoke distribution from fire simulations to simulate the scattering and absorption of light on smoke particles, employing ray tracing technologies. Models like these can also account for additional factors that influence contrast perception, such as ambient lighting, reflections, or surface textures. However, current fire models cannot accurately map the exact processes of generation and transport of smoke particles, so simplified analytical approaches like the Henyey-Greenstein phase function [31] are typically used to map the processes of light scattering. The reliability of the above models is still limited by a lack of proper validation, currently constraining their applicability in performance based design. In order to derive threshold values for visibility, extensive validation against experimental studies with human participants is required, to compare perceptions of the synthetic images with real-world observations. In addition, these models are inherently affected by the uncertainties of the input quantities of the fire models, as discussed in section 1.2.2.

Visibility maps primarily provide a way of comparing predictive values against performance criteria. Consequently, further experimental investigations for the validation of fire models, as well as the proposed approaches for deriving visibility threshold values from synthetic image data, can contribute to improving both their accuracy and reliability.

Bibliography

[1] Accessed: 2024-09-03. URL: https://www.nfpa.org/about-nfpa/press-room/reporters-guide-to-fire/consequences-of-fire.

[2] Kevin McGrattan, Simo Hostikka, Jason Floyd, Randall McDermott, and Marcos Vanella. *Fire Dynamics Simulator User's Guide – Version 6.7.9*. Tech. rep. 2022.

[3] Kevin McGrattan, Simo Hostikka, Jason Floyd, Randall McDermott, and Marcos Vanella. *Fire Dynamics Simulator Technical Reference Guide Volume 3: Validation – Version 6.7.5*. Tech. rep. 2020. URL: https://github.com/firemodels/fds/releases/download/FDS6.7.5/FDS%5C_Validation%5C_Guide.pdf.

[4] Tadahisa Jin. "Visibility through Fire Smoke (I)". In: *Bulletin of Japan Association for Fire Science and Engineering* 19.2 (1970), pp. 1–8. DOI: 10.11196/kasai.19.2.1.

[5] Tadahisa Jin. "Visibility through Fire Smoke (II)". In: *Bulletin of Japan Association for Fire Science and Engineering* 21.1,1 (1971), pp. 17–23. ISSN: 18835600. DOI: 10.11196/kasai.21.17.

[6] Tadahisa Jin. "Visibility through Fire Smoke (III)". In: *Bulletin of Japan Association for Fire Science and Engineering* 22.1,2 (1972), pp. 11–15. DOI: 10.11196/kasai.22.11.

[7] Tadahisa Jin. "Visibility through Fire Smoke (IV)". In: *Bulletin of Japan Association for Fire Science and Engineering* 23.1,2 (1973), pp. 1–8. DOI: 10.11196/kasai.23.1_2_1.

[8] European Union. "Interpretative Document Essential Requirements No 2 'Safety in Case of Fire'". In: *Official Journal of the European Communities* (1994).

[9] Leonard Y. Cooper. "A concept for estimating available safe egress time in fires". In: *Fire Safety Journal* 5.2 (1983), pp. 135–144. ISSN: 0379-7112. DOI: 10.1016/0379-7112(83)90006-1.

[10] David A Purser and Jame L McAllister. "Assessment of Hazards to Occupants from Smoke, Toxic Gases, and Heat". In: *SFPE Handbook of Fire Protection Engineering*. Ed. by Morgan J. Hurley. New York: Springer, 2016. ISBN: 9781493925643. DOI: 10.1007/978-1-4939-2565-0.

[11] Tadahisa Jin. "Visibility and Human Behavior in Fire Smoke". In: *SFPE Handbook of Fire Protection Engineering*. Ed. by Philip J DiNenno. Third Edition. New York: National Fire Protection Association, 2002. ISBN: 087765-451-4.

[12] M. Pierre Bouguer and William Edgar Knowles Middleton. *Optical Treatise on the Gradation of Light. Translated, with Introduction and Notes, by WE Knowles Middleton*. University of Toronto Press, 1961.

[13] E.M Patterson, R.M Duckworth, C.M Wyman, E.A Powell, and J.W Gooch. "Measurements of the optical properties of the smoke emissions from plastics, hydrocarbons, and other urban fuels for nuclear winter studies". In: *Atmospheric Environment. Part A. General Topics* 25.11 (1991), pp. 2539–2552. ISSN: 0960-1686. DOI: 10.1016/0960-1686(91)90171-3.

[14] George W. Mulholland and Carroll Croarkin. "Specific extinction coefficient of flame generated smoke". In: *Fire and Materials* 24.5 (2000), pp. 227–230. ISSN: 1099-1018. DOI: 10.1002/1099-1018(200009/10)24:5<227::aid-fam742>3.0.co;2-9.

[15] Daniel Gottuk, Christopher Mealy, and Jason Floyd. "Smoke Transport and FDS Validation". In: *Fire Safety Science* 9 (2008), pp. 129–140. ISSN: 1817-4299. DOI: 10.3801/iafss.fss.9-129.

[16] Anthony Hamins, Alexander Maranghides, Rik Johnsson, Michelle Donnelly, Jiann Yang, George Mulholland, and Robert L Anleitner. *Report of experimental results for the international fire model benchmarking and validation exercise #3*. Tech. rep. 2005.

[17] Lukas Arnold, Alexander Belt, Thorsten Schulze, and Abdul Wahab Mughal. "Experimental and Numerical Investigation of Visibility in Compartment Fires". In: *AUBE 21*. 2021.

[18] Kristian Börger, Alexander Belt, Alica Kandler, Thorsten Schultze, and Lukas Arnold. "Investigation of smoke characteristics by photometric measurements". In: *Fire and Evacuation Modeling Technical Conference (FEMTC) 2022*. 2022, p. 14.

[19] Christoph Gnendiger, Thorsten Schultze, Kristian Börger, Alexander Belt, and Lukas Arnold. "Extinction coefficients from aerosol measurements". In: *Fire Safety Journal* 146 (2024), p. 104110. ISSN: 03797112. DOI: 10.1016/j.firesaf.2024.104110.

[20] John F. Widmann. "Evaluation of the planck mean absorption coefficients for radiation transport through smoke". In: *Combustion Science and Technology* 175.12 (2003), pp. 2299–2308. ISSN: 0010-2202. DOI: 10.1080/714923279.

[21] Lukas Arnold, Alexander Belt, Thorsten Schultze, and Lea Sichma. "Spatiotemporal measurement of light extinction coefficients in compartment fires". In: *Fire and Materials* (2020). ISSN: 0308-0501. DOI: 10.1002/fam.2841.

[22] Kristian Börger and Lukas Arnold. *LEDSA - Github repository*. 2024. URL: https://github.com/FireDynamics/LEDSmokeAnalysis.git.

[23] Cerberus. *Ionization measuring chamber MIC Extinction measuring equipment MIREX*. Technical description. 1992.

[24] The European Committee for Standardization. *EN 54— Fire detection and fire alarm systems, part 7: smoke detectors point detectors using scattered light, transmitted light or ionization*. 2000.

[25] E. Fred Schubert. *Light-Emitting Diodes*. Vol. Second edition. New York: Cambridge University Press, 2006. DOI: 10.1017/BO9780511790546.

[26] Niklas Brutscheid. *Photometrische Analyse der Intensität einer LED infolge thermischer Beanspruchung*. BA thesis. Wuppertal, 2023.

[27] Jiguang Shi, Ning Ding, and Fan Jiang. "The influence of color and direction on the perceptual processing of standard evacuation signs and the effect of attention bias". In: *Fire Safety Journal* 132 (2022), p. 103638. ISSN: 03797112. DOI: 10.1016/j.firesaf.2022.103638.

[28] Ryun-Seok Oh, Young-Chan Kim, Young-Hoon Bae, and Jun-Ho Choi. "Evaluation of the Maximum Cognitive Distance Per Emergency Exit Sign Colour in a Smoke-Filled Environment Simulated Using a Translucent Eye Patch". In: *Fire Technology* (2023). ISSN: 0015-2684, 1572-8099. DOI: 10.1007/s10694-023-01474-9.

[29] Qihui Zhang. "Image based analysis of visibility in smoke laden environments". PhD thesis. Hull: University of Hull, 2010.

[30] Jonathan Wahlqvist and Philip Rubini. "Real-time visualization of smoke for fire safety engineering applications". In: *Fire Safety Journal* 140 (2023), p. 103878. ISSN: 03797112. DOI: 10.1016/j.firesaf.2023.103878.

[31] L. C. Henyey and J. L. Greenstein. "Diffuse radiation in the Galaxy". In: *The Astrophysical Journal* 93 (1941), p. 70. ISSN: 0004-637X, 1538-4357. DOI: 10.1086/144246.

PUBLICATION I

Remote Sensing of the Light-Obscuring Smoke Properties in Real-Scale Fires Using a Photometric Measurement Method

Note: This article was published as Kristian Börger, Alexander Belt, Thorsten Schultze and Lukas Arnold. *Remote Sensing of the Light-Obscuring Smoke Properties in Real-Scale Fires Using a Photometric Measurement Method*. Fire Technol 60, 19–45, 2024. https://doi.org/10.1007/s10694-023-01470-z.

Author Contributions

Conceptualization: Kristian Börger, Alexander Belt and Lukas Arnold
Methodology: Kristian Börger, Alexander Belt and Lukas Arnold
Software: Kristian Börger and Lukas Arnold
Validation: Kristian Börger, Alexander Belt, Thorsten Schultze and Lukas Arnold
Formal analysis: Kristian Börger
Investigation: Kristian Börger
Resources: Lukas Arnold, Alexander Belt and Thorsten Schultze
Data curation: Kristian Börger
Writing–original draft: Kristian Börger
Writing–review and editing: Kristian Börger, Alexander Belt, Thorsten Schultze and Lukas Arnold
Visualization: Kristian Börger
Supervision: Lukas Arnold
Project administration: Lukas Arnold
Funding acquisition: Lukas Arnold

Remote Sensing of the Light-Obscuring Smoke Properties in Real-Scale Fires Using a Photometric Measurement Method

Kristian Börger[1 2], Alexander Belt[2], Thorsten Schultze[3] and Lukas Arnold[1 2]

[1] Computational Civil Engineering, University of Wuppertal, Germany
[2] Institute for Advanced Simulation, Forschungszentrum Jülich, Germany
[3] Communication Systems (NTS), University of Duisburg-Essen, Duisburg, Germany

Abstract

A new photometric measurement method for the determination of temporally and spatially resolved light extinction coefficients in laboratory fire tests was recently presented. The approach relies on capturing the change in intensity of individual light sources (LEDs) due to fire smoke using a commercially available digital camera. Comparing the results for red light LEDs to measurements of the well-established MIREX system indicates the model is capable of capturing the investigated phenomena. However, a significant underestimation of this reference measurement taken in the infrared range is inconsistent with the expected increase of the extinction coefficients with lower wavelengths. In the context of new experimental investigations, this deficiency was remedied by evaluating multiple colour channels of RAW image data instead of the previously used JPG files. Furthermore, extending the experimental setup by several LED strips as well as a second camera allows to verify the hypothesis of a homogeneous smoke layering. The study covers eight experiments including n-heptane fuel in style of the well documented EN 54 TF5 test fire as well as two additional experiments with an n-heptane-toluene mixture. Considering spatial resolution as well as the high reproducibility of the results, the method appears to be a convenient tool for the validation of numerical visibility models. Nevertheless, a sensitivity analysis identified uncertainties that need to be addressed in upcoming investigations to further improve the accuracy.

Keywords: Compartment fire, visibility, soot, extinction coefficients, optical measurement, photometry

1 Introduction

On the occurrence of a fire, smoke usually poses the greatest danger to the building's occupants, as it can make it difficult or even impossible to escape to a safe area. It affects both, the Available Safe Egress Time (ASET) and the Required Safe Egress Time (RSET). The occupants' movement speed and the capability of wayfinding are

impaired by the smoke's irritating products and its optical opacity. Likewise, the conditions for self-rescue become untenable when the exposure to heat or toxic smoke products exceed a critical level [1]. When modelling escape scenarios in performance based safety designs within the ASET-RSET [2] concept, corresponding threshold values are matched against the predicted exposures. The FED (Fractional Effective Dose) model proposed by Hartzell and Emmons [3] is commonly used to assess the hazardous effects of fire induced smoke. A time-dependent incremental exposure dose is related to the total exposure dose required to cause a toxicological effect. The time at which the continuously integrated fractional effective dose for a person exceeds a certain limit indicates the time available until the person is incapable of escaping. An approach for applying both of these concepts in numerical fire simulations is outlined in [4] and [5].

In contrast, modelling visibility is much more complex. It has to be considered as a spatial phenomenon rather than a local quantity. Numerical models like the Fire Dynamics Simulator (FDS) [6] rely on the concept of Jin [7], defining visibility as the distance at which a visual target can still be recognized in a smoke laden environment as the contrast to the background is sufficiently large. This approach, see Eq. 1, is highly simplified, as it merely maps visibility V as a ratio of the local extinction coefficient σ to an empirical factor C for the contrast threshold.

$$V = \frac{C}{\sigma} \tag{1}$$

Furthermore, considerable uncertainties within the modelling of visibility can arise from the experimentally obtained input parameters, that are usually encapsulated by the extinction coefficient. Gottuk et al. reported deviations by a factor of 4 - 5 of the optical density between large-scale experiments and simulations with FDS. They primarily attributed this to scaling effects of the soot yield, as well as soot loss due to deposition effects [8]. Similar discrepancies between experiments and corresponding simulations with FDS have been reproduced in [9].

Computational fluid dynamics (CFD) models such as FDS allow for the prediction of smoke propagation in turbulent systems on a spatial scale, which is a major advantage over zone models and hand formulas. However, spatially and temporally resolved measurements from experimental studies are in general needed to validate such complex models. In order to obtain spatially and temporally resolved extinction coefficients from the optical observation of a single LED strip within laboratory experiments, a photometric method was recently presented [10]. It relies on capturing the smoke induced attenuation of light by a digital camera. Local values of the extinction coefficient can be deduced by an inverse modelling approach based on the Beer-Lambert law and simple geometrical optics. Besides the validation of numerical fire models, the method can contribute to the development of photometric smoke detection systems. The presented study primarily addresses the assessment of its general applicability as a photometric measurement method in laboratory test fires. In this context, the adaptability to different experimental setups, different types of fuels as well as the influence from the experimental boundary conditions are investigated. The goal of the study is to develop a reliable measurement method for the comprehensive investigation of fire smoke characteristics. A similar approach

for analysing smoke density using video data from conventional security cameras is presented in [11].

The above-mentioned photometric method provides some substantial advantages, since it is easily applicable with small technical effort. Moreover, smoke propagation is not disturbed by air ducts or filters as part of a measuring apparatus. Comparison of the computed extinction coefficients within an n-heptane test fire in style of the EN 54 TF5 with measurements of the well-established MIREX system shows that the method is reasonably capable of capturing the light obscuring phenomenon of the smoke. However, the observation of the results being significantly lower than the MIREX measurement does not agree with expected behaviour of the extinction coefficient increasing with decreasing wavelengths. Examining those issues is an essential part of this work.

The next section will first discuss the characteristics and properties of fire smoke, and the associated effects on light obscuration. Hereafter, the setup and procedure of the conducted experiments will be presented. An outline on the data acquisition and the methodology is provided, although it is primarily limited to the enhancements of the original approach. The subsequent section addresses the application of the method to experimental data, as well as its validation by reference measurements. Here, the focus is on investigating the temporal and spatial resolution of the computed extinction coefficients for light at different wavelengths. Finally, the uncertainties of the model and the experiments are assessed by means of a sensitivity analysis. The article closes with a conclusion and an outlook on future work.

2 Light Obscuring Effects of Fire Smoke

Investigating the effects of fire induced smoke on visibility requires an understanding of its characteristics along with the associated light obscuring properties. Mulholland provides a convenient definition of smoke as the condensed phase component of the combustion products that widely varies in appearance and structure [12]. Light-coloured aerosols, essentially containing droplets, produced by smouldering fires and pyrolysis have a strong scattering effect on light. Dark and solid carbonaceous soot particles produced by flaming combustion from fuels such as n-heptane, on the other hand, are highly absorbent [13]. Both effects are induced by the particle size distribution of the aerosol, mainly related to the geometric mean volume to surface diameter of the particles [14]. For post-flame smoke particles, the absorbing effect can be expressed in terms of an almost fuel type independent, mass specific extinction coefficient, subsequently denoted K_m. This simplification assumes that soot essentially comprises spherical carbonaceous particles significantly smaller than the wavelength of light so that scattering effects are negligible [15]. The light obscuring effect of smoke therefore is proportional to the smoke density ρ_s. Both quantities can be summarized into the extinction coefficient σ. It can be obtained by applying Beer-Lambert's law, see Eq. 2, to optical measurements of the light transmission T along a known path length l. However, this only accounts for the damping effect on the initial light intensity I_0 to the intensity I in the presence of smoke due to absorption and scattering, since both effects can not easily be separated.

$$T = \frac{I}{I_0} = \exp\left(-K_\mathrm{m} \cdot \rho_\mathrm{s} \cdot l\right) = \exp\left(-\sigma \cdot l\right) \tag{2}$$

Mulholland and Croarkin estimated K_m to be $8{,}700\,\mathrm{m^2\,kg^{-1}}$ with an extended uncertainty of $1{,}100\,\mathrm{m^2\,kg^{-1}}$ as a mean value from the analysis of seven studies involving 29 fuels in flaming fires [15]. It is frequently referenced as a default quantity in various numerical fire models, such as FDS [16]. Optical measurements each were performed at a wavelength of $\lambda = 633\,\mathrm{nm}$ in post-flame generated smoke from stoichiometric or over-ventilated combustion. For smoulder and pyrolysis generated smoke, the value is reported to be much lower and more variable. A similar study was conducted by Widmann based on a literature review of data from stoichiometric and over-ventilated combustion [17]. He deduced a correlation of K_m with wavelength λ, based on the least square fit of measurements mainly in the visible spectrum and in the near infrared range, described by Eq. 3.

$$K_\mathrm{m} = 4.8081 \cdot \lambda^{-1.0088} \tag{3}$$

The value of K_m can change over time, caused by ageing processes of the aerosol. Due to agglomeration, the particle concentration decreases while the size distribution shifts towards a larger mean particle diameter [18]. The difference in scattering and absorption characteristics of particles at different wavelengths can be used to estimate the mean particle size diameter. A potential approach relying on a combination of optical measurements and theoretical calculations based on Mie scattering theory is presented in [19] and [20]. These procedures follow a correlation of the logarithms of the measured light transmission at different wavelengths with the calculated extinction efficiency as a function of the particle diameter. Węgrzyński et al. have examined several multi-wavelength densitometers following a similar approach in a literature study [21]. They summarized that most of the apparatus are connected to bench-scale experimental setups like cone calorimeters, while only few devices exist that are meant to be used in compartment-scale fires. Still, such investigations are even more important in terms of modelling visibility, since scaling effects regarding the extinction coefficient can not be precluded.

3 Experimental Setup and Procedure

The presented experiments were conducted in the Heinz-Luck fire detection laboratory at the university of Duisburg-Essen, Germany. The study is based on the concept introduced in [10] and therefore features a similar design and procedure. A fundamental assumption of the model is the extinction coefficient being homogeneous within horizontal layers. To investigate this hypothesis, seven of the same type as the previously used LED strips were installed vertically (three strips) and diagonally (four strips) in the laboratory, see Fig. 1. The assembly roughly spans a plane, tangent to a circle with a 3 m radius around the fire source. It extends from a height of 1 m above the floor to the ceiling at 3.37 m. Each of the strips measures an equal length of approximately 2.35 m and contains 141 RGB LEDs. The experimental setup features two DSLR cameras facing the LEDs from different locations and

heights. Within two setups, the position of the second camera is varied. In setup 1, camera 1 and camera 2 are positioned on opposite sides of the room to the left and right in front of the LEDs. In setup 2, the position of camera 1 remains constant, while camera 2 is placed directly next to it, but at a slightly elevated position. Since it covers a similar distance to both cameras in setup 1, the centre LED strip serves as a reference for investigating symmetry effects. Three MIREX devices are located behind it at heights of 1.52 m, 2.3 m and 3.3 m above the floor. The MIREX apparatus measures the smoke density on a 2×1 m reflected path length according to the light transmission in the infrared regime, with a maximum intensity at a wavelength of $\lambda_{\mathrm{IR}} = 880\,\mathrm{nm}$ [22].

Data acquisition by the cameras as well as the MIREX covers a period of about 20 minutes and is performed at a 1 Hz sampling rate. In order to investigate the reproducibility of the experiments, all measurement sequences are evaluated starting with the time of the fuel ignition. The laboratory ventilation system is activated 6 minutes after that time.

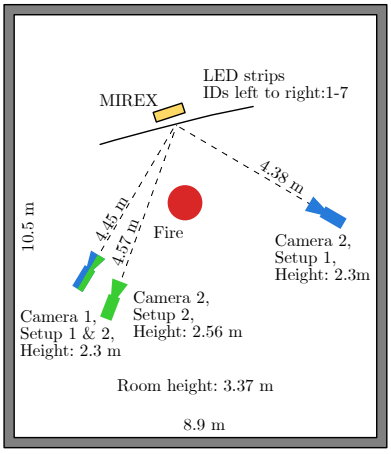

(a) Floor plan of the experimental setup. Three MIREX devices are located behind the centre LED strip. The position of the second camera varies within two setups.

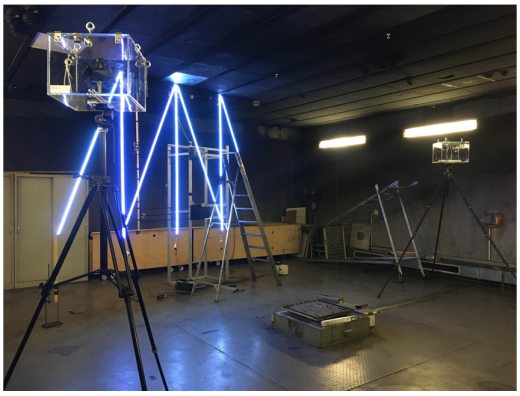

(b) Experimental setup before ignition of the fuel. Two cameras facing the LEDs are located left and right of the pool fire (setup 1).

Figure 1: Experimental setup in style of EN 54

3.1 Heat Release Rate

The test fires of the EN 54 standard [23] form the basis for the classification of smoke detectors and therefore should be easily reproducible. A total of eight n-heptane fires in style of the TF5 test fire were investigated within the scope of the experiments. In each case, 500 g of n-heptane fuel were burned in a 335 mm × 335 mm fuel pan,

resulting in an average burning duration of approximately 225 s. Compared to the EN 54 standard, the amount of fuel was reduced from 650 g to account for the reduced ceiling height. The mass loss rate was determined from continuous weighing so that the Heat Release Rate (HRR) could be derived from 44.6 MJ kg^{-1} for the effective heat of combustion [24]. Another series of two experiments was performed, adding 15 g of toluene to the fuel, yielding similar heat release rates.

Fig. 2 shows the mass loss and the corresponding HRR as mean values from eight experiments with n-heptane fuel. All data were smoothed by a 5 s moving average. The narrow standard deviation confirms the good reproducibility in terms of the burning progression.

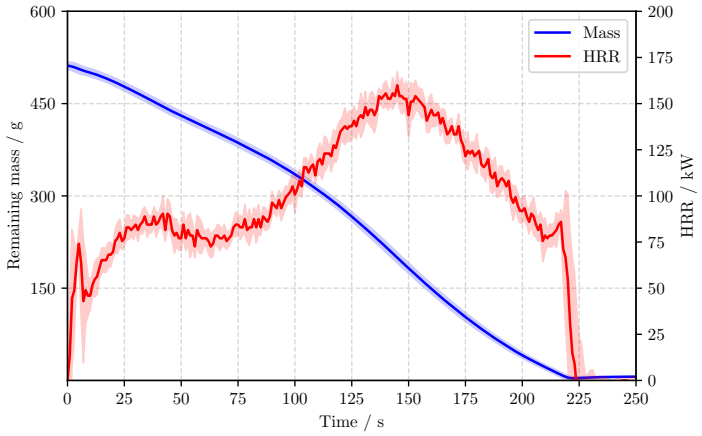

Figure 2: Mass loss and HRR for the 500 g n-heptane pool fires in style of the TF5 according to EN 54. Solid lines indicate mean values, while shaded areas depict the standard deviation. The maximum HRR of approx. 159 kW is reached at about 145 s.

4 Methodology

4.1 Raw Data Acquisition

The photometric measurement method described in [10] is based on the time-resolved acquisition of LED intensities from images series. The original approach followed the procedure outlined subsequently.

Using a reference image taken before the start of the experiment, all visible LEDs are detected that exceed a certain threshold in luminosity. Iteratively, the pixel with the highest value including a peripheral area is excluded from the further search. The width of these regions of interest, further denoted ROI, is chosen to be uniform and sufficiently large. It must be ensured that the relevant pixels do not shift outside these areas due to refraction of the incident light. An image model of each LED is fitted to the experimentally obtained pixel values by means of an

Table 1: Manual settings of the used cameras

Camera	Model	ISO	Shutter speed	Aperture	Focal length
1	Canon 80D	100	1/500 s	f/16	18 mm
2	Canon 70D	100	1/250 s	f/22	18 mm

algebraic model. The approach allows determining the position and magnitude of the amplitude from the shape of the modelled LED. Acquiring these quantities potentially allows for the consideration of extensive phenomena, such as refraction. However, since this process has to be repeated for all images and LEDs, it requires an enormous computational effort.

As the focus of the current study is on the acquisition of significant amounts of data, a simplified approach to determine the LED intensities is used for that purpose. At each time step, the LED intensity is calculated separately for all three colour channels (CH) as the sum of all pixel values within the respective ROI.

The camera exposure is primarily determined by shutter speed, aperture, and the sensor sensitivity (ISO). For photometric measurement, it therefore is essential to operate the camera in manual mode (see Table 1) and to deactivate any internal image optimization.

Nevertheless, luminosity measurements based on JPG images are inevitably biased by camera-internal pre-processing. For example, a correction function (e.g. gamma correction) is usually applied to scale linear sensor data according to the logarithmic light sensitivity of human perception. However, high-quality CCD or CMOS cameras do allow direct access to the unprocessed sensor data via RAW image files.

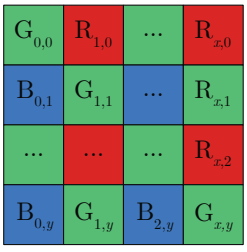

Figure 3: Bayer filter array is the most common CFA used in modern digital cameras. Red (R), green (G), and blue (B) filters are placed on the sensor by a 4×4 repeating pattern.

The camera sensor is covered with a spectrally sensitive colour filter array (CFA) arranged according to a particular mosaic pattern, of which each element only samples a single colour. The resulting intermediate greyscale image can be converted to a true-colour image by various interpolation techniques referred to as "demosaicing", in which each pixel typically maps independent levels for red (R), green (G), and blue (B) [25]. The most common CFA is the Bayer filter array, which is also used in

the employed cameras. A regularly repeating 4×4 pixel section of this pattern is shown in Fig. 3. Like most CFAs, it contains twice as many green-sensitive filters, which is supposed to match human perception in terms of higher resolution for green light.

4.2 Determining the LED Intensities

Since the unprocessed RAW images are encoded in a native camera file format, the embedded data is accessed by a Python wrapper for the LibRaw library [26]. The obtained sensor readings can be represented as a matrix $S(x, y)$ of elements with positions x, y, that has the same resolution as the visible part of the sensor. In order to convert this matrix into a greyscale image with pixels $P(x, y)$, the individual elements must be mapped to a fixed tonal range [27] by Eq. 4.

$$P(x, y) = (S(x, y) - B) \cdot \frac{2^{b-1}}{W - B} \tag{4}$$

B and W indicate the black level and the saturation point of the sensor. The black level is measured using masked pixels, i.e. pixels which are not illuminated by construction, and thus serves as a calibration point for the sensor noise, e.g. due to temperature influences. After linearizing the sensor readings within those bounds, they are scaled back to integer values according to the target tonal range b. JPG images usually feature a tonal range of 8 bit, allowing each colour channel to be shaded in 256 increments. The sensor data, on the other hand, are typically recorded at a 14-bit resolution. However, the higher dynamic range of RAW images is also relevant for accurate brightness measurement. It prevents details in regions with particularly high or low exposure from being irreversibly clipped by the camera's post-processing.

According to their position in the CFA, the three colour channels (RGB) can be separated as independent pixel arrays:

$$\begin{aligned}
P_{\mathrm{R}}(x, y) &= \begin{cases} P(x, y) & \text{if } x \text{ is odd and } y \text{ is even} \\ 0 & \text{otherwise} \end{cases} \\
P_{\mathrm{G}}(x, y) &= \begin{cases} P(x, y) & \text{(if } x \text{ is odd and } y \text{ is odd) or (if } x \text{ is even and } y \text{ is even)} \\ 0 & \text{otherwise} \end{cases} \\
P_{\mathrm{B}}(x, y) &= \begin{cases} P(x, y) & \text{if } x \text{ is even and } y \text{ is odd} \\ 0 & \text{otherwise} \end{cases}
\end{aligned} \tag{5}$$

Fig. 4 shows an example of the pixel values within the ROI of a single LED, separated for the three colour channels of the camera.

For the individual colour channels, the experimental intensity I_{e} simply results as the sum of the pixel values within the respective ROIs, see Eq. 6, normalized to their initial values.

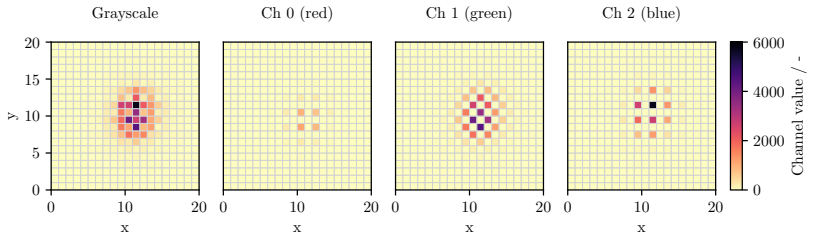

Figure 4: ROI of a greyscale image and RGB components according to the Bayer filter pattern.

$$I_\mathrm{e} = \sum_{\text{all pixels } x,y} P(x,y) \tag{6}$$

The initial intensity I_0 of each LED indicates the mean value from ten images taken before the fuel is ignited. It is assumed to be constant throughout the experiment and therefore serves as a reference according to Eq. 2. The influence of the variability of I_0 due to intrinsic as well as extrinsic influences by e.g. temperature on the computation of extinction coefficients is discussed in section 5.2.

Splitting the greyscale image into the individual colour channels implies that, unlike the JPG image, much fewer pixels are involved in determining the LED intensities. This can slightly increase noise. Especially within the blue and red colour channel, individual peaks of luminosity may not be detected due to a refraction induced shift of the incident light.

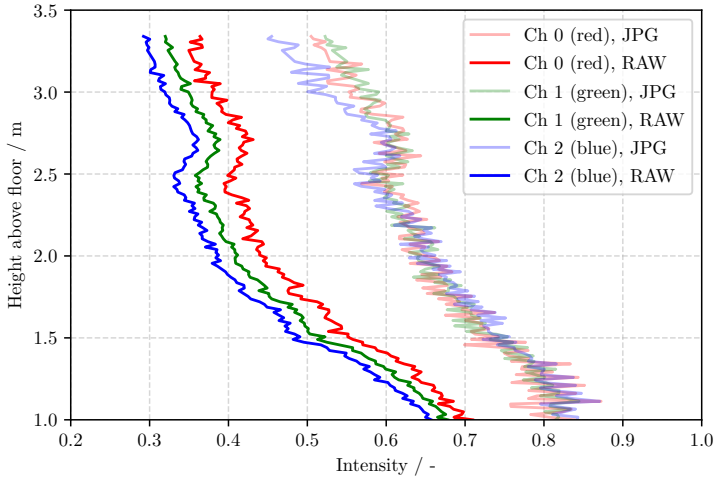

Figure 5: Normalized intensities of all 141 LEDs from the centre strip, acquired from RAW and JPG image data at t = 300 s. The relative deviation in the drop of intensities increases towards the lower regions.

An instantaneous comparison of the measured intensities from a single RAW image and the corresponding JPG is given in Fig. 5. It depicts the intensities for all LEDs of the centre strip about 300 s after the ignition, scaled to their initial value. The intensities from the RAW data show considerably higher attenuation than those from the corresponding JPGs, with the relative deviation in the drop of intensities increasing towards lower regions. This results in a significant underestimation of the computed extinction coefficients based on JPG images. It also entails that the wavelength influence on light obscuration can be detected exclusively in high smoke density regions. The main reason for these errors is likely to be the nonlinear scaling of the pixel values by the gamma correction.

Unlike the original approach, the experiments presented in this study are entirely analysed on the basis of RAW image files.

4.3 Computation of Extinction Coefficients

The conducted experiments are analysed by an enhanced version of the method introduced in [10]. The software LEDSA (LED Smoke Analysis) used for data analysis is written in Python [28]. An inverse modelling approach based on geometrical optics and the Beer-Lambert law is applied to obtain temporally and spatial resolved extinction coefficients σ. Therefore, a model for the intensities of individual LEDs is formulated as a line of sight integral corresponding to a spatial discretization as horizontal layers. The underlying assumption of the model is that σ is homogeneous within horizontal layers. A non-linear system of equations comprising the model intensities $I_{\mathrm{m},j}$ and the experimental intensities $I_{\mathrm{e},j}$ for all LEDs then is to be solved to find the best matching set of the extinction coefficients for each time step. $I_{\mathrm{e},j}$ corresponds to the accumulated pixel values according to Eq. 6 as a mean value of two consecutive images. The computation is performed separately for the three colour channels of the camera, as well as the seven LED strips.

By means of a cost function Ω_σ, additional boundary conditions besides the L2-norm between $I_{\mathrm{e},j}$ and $I_{m,j}$ can be considered.

$$\Omega_\sigma = \sum_{j=1}^{N_{\mathrm{LEDs}}} (I_{\mathrm{m},j} - I_{\mathrm{e},j})^2 + \phi_{\mathrm{s}} \sum_{i=2}^{N_{\mathrm{layers}}-1} (\sigma_{i-1} - 2\sigma_i + \sigma_{i+1}) + \phi_{\mathrm{a}} \sum_{i=1}^{N_{\mathrm{layers}}} \sigma_i \qquad (7)$$

The factor ϕ_{s} weights the requirement of a smoothness of the solution as a numerical approximation of the second derivative. Furthermore, an upper or lower limit can be defined via ϕ_a, so that either large or small values for the extinction coefficient are preferred when there is little impact of the L2-norm. This is crucial in the boundary layers, which are only crossed by few light beams. Here the information used in the optimization procedure is sparse, which leads to a weak solution, i.e. a not unique solution. By using the weighting factors, ϕ_{a} the solution is stressed towards bounding limits of possible values. In layers which are crossed by many light beams the solution is rigid, thus a stressing by the ϕ_{a} leads to same solutions Fig. 6 depicts the impact of featuring high or low values and no preference for the extinction coefficient using data from the centre LED strip. As the whole study, the analysis is based on a model with 20 equally sized layers extending from 0.99 m above the floor to the ceiling at 3.37 m height.

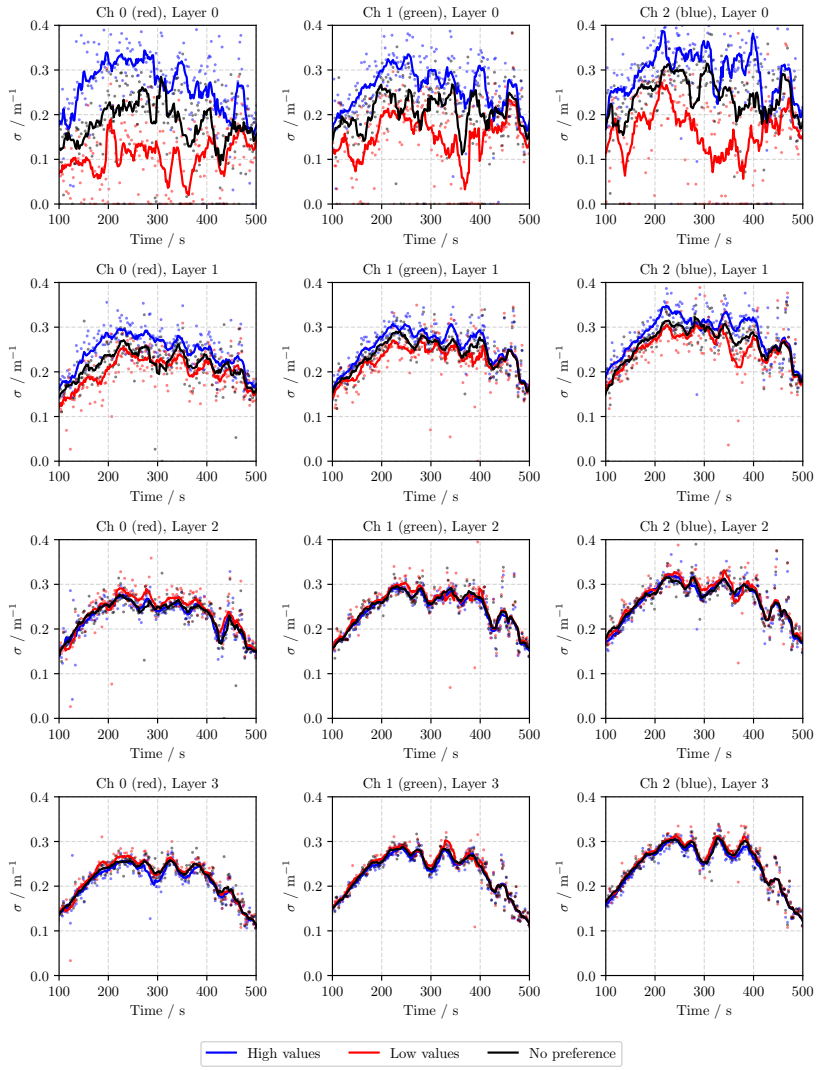

Figure 6: Influence of the weighting factor ϕ_a on the temporal evolution of the extinction coefficient for the three colour channels on the layers 0 to 3 (from top down). The investigation was carried out for $\phi_a = -1 \times 10^{-6}$ (low values), $\phi_a = 1 \times 10^{-6}$ (high values) and $\phi_a = 0$ (no preference). Scattered dots show the computed extinction coefficients based on the average intensities of two consecutive images each. Lines represent the smoothed data by a 10 s moving average over 5 time steps each.

The extinction coefficients obtained at different wavelengths may finally serve for the remote estimation of the mean particle size. Techniques as described in [14, 19] rely on the log ratios of extinction coefficients and therefore are highly sensitive to uncertainties, e.g., from numerical artefacts. The major impact of ϕ_a as well as the

significant differences among the individual colour channels in the top layers indicate that the obtained data may not be used unrestricted for this purpose.

5 Results

5.1 Extinction Coefficients

Eight experiments were performed with n-heptane fuel and two more with an n-heptane toluene mixture. The location of the second camera was varied among the experiments according to Fig. 1. Therefore, the following experiments, given an identical setup, were aggregated within the evaluation:

1. Four experiments with n-heptane fuel in setup 1
2. Four experiments with n-heptane fuel in setup 2
3. Two experiments with n-heptane toluene mixture in setup 2

Fig. 7 shows the extinction coefficients for the centre LED strip based on the photometric measurements from both cameras in setup 1. The results for layers 0, 8 and 15 correspond to the respective heights above the floor at which the reference measurements were acquired by the MIREX devices (3.30 m, 2.30 m, 1.52 m).

The LEDSA results as well as the MIREX reference measurements confirm a good reproducibility of the experiments, which has already been shown for the mass loss. Results from both cameras are in the same order of magnitude. As expected, the extinction coefficients from LEDSA are much higher than those from the MIREX, which can be attributed to the difference in wavelengths. A strong wavelength dependence is also evident in the colour channels of the cameras. The phenomenon of increasing light obscuration with decreasing wavelength, as described by Widmann, can be observed for all data sets. According to Eq. 3, a rough estimate of the expected ratio of extinction coefficients can be established based on the peak wavelengths of the LEDs. Referring to the red LED at $\lambda_R = 630\,\mathrm{nm}$, the expected ratios are 1.24 for the green ($\lambda_G = 510\,\mathrm{nm}$), 1.37 for the blue LEDs ($\lambda_B = 462\,\mathrm{nm}$) and 0.71 for the MIREX ($\lambda_{IR} = 880\,\mathrm{nm}$) which is a good approximation especially for the eighth layer. It must be noted, however, that the light sources used are not perfectly monochromatic and the LEDs in particular have a relatively broad spectrum, which may bias this correlation. In layer 0, there is a significantly smaller discrepancy between LEDSA and the MIREX, although a distinct wavelength dependency remains evident. Potential reasons for this may be attributed to e.g. different particle sizes of the smoke or an inhomogeneous smoke layering that effects the LEDSA layer model. However, the exact causes for this are not yet understood and will be the subject of future research.

Fig. 8 shows the extinction coefficients for another series of four experiments on the setup 2. The experimental boundary conditions as well as the analysis match the one from the first setup, except that both cameras were placed side by side with a difference in height of 25 cm.

Both cameras show similar results to the first setup, but still match closer, especially in the range between 200 and 400 s. This suggests that the discrepancies are

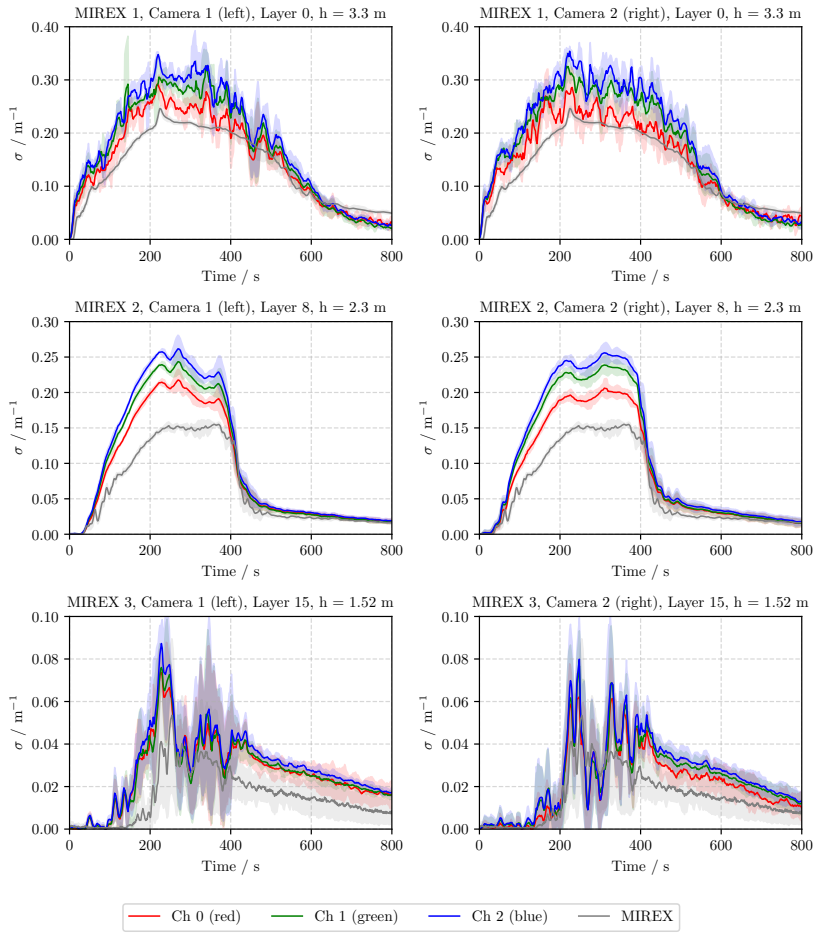

Figure 7: MIREX and LEDSA (Camera 1 and Camera 2) extinction coefficients in setup 1. The plot shows mean values (solid lines) and standard deviation (shaded areas) from four experiments with the n-heptane fuel.

related to the viewing angle as well as local variations in smoke density rather than intrinsic camera characteristics.

In setup 2, an additional series of two experiments was performed with toluene added to the n-heptane fuel (see Fig. 9). The computed extinction coefficients as well as the MIREX measurements are significantly higher than for the pure n-heptane fire. Although the recorded dynamics of both methods match well again, it can be seen that the wavelength related ratio is not consistent with Eq. 3. The computed extinction coefficients for the red channel are of the same order of magnitude as the corresponding MIREX 1 and MIREX 2 measurements after about 300 s. A possible contribution to this may be related to a much larger mean particle diameters reported for smoke of toluene fires [29]. Jin concluded from his experiments that the

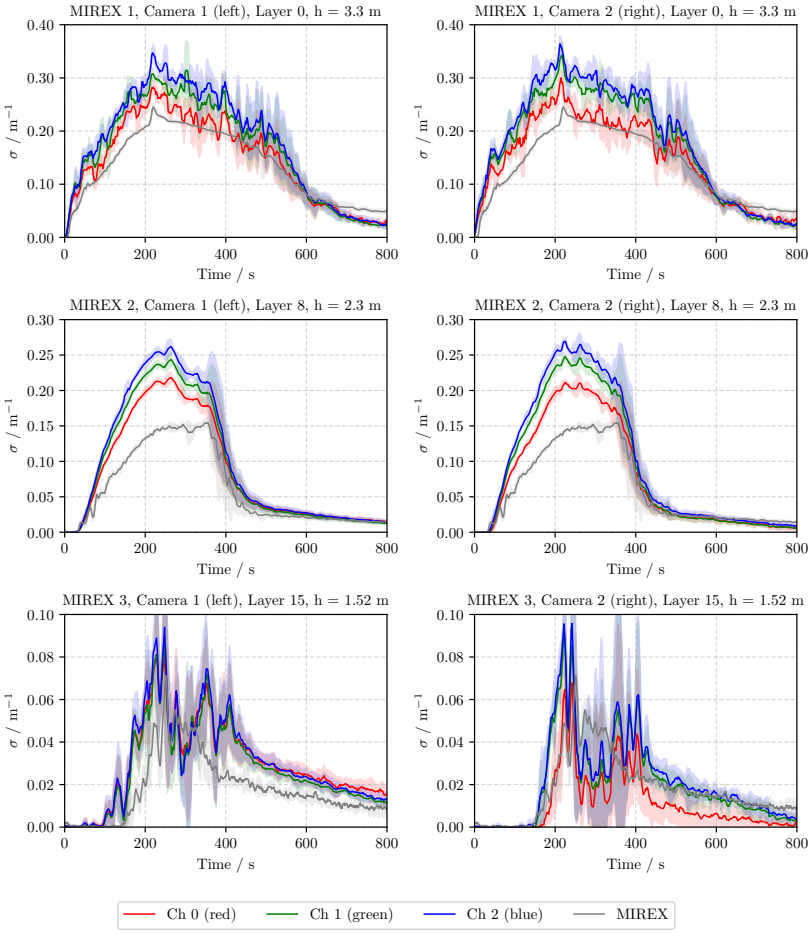

Figure 8: MIREX and LEDSA (Camera 1 and Camera 2) extinction coefficients in setup 2. The plot shows mean values (solid lines) and standard deviation (shaded areas) from four experiments with the n-heptane fuel.

dependence on wavelength vanishes or reverses for particles larger than 1 µm [30]. However, this effect was not further investigated in this study.

Fig. 10 depicts the layer wise extinction coefficients for both of the outer and the centre LED strip at 300 s as a 10 s average. For reference, the extinction coefficients were computed considering all the 987 LEDs in the setup, referred to as 'merged strips" in the plot. The minimization procedure requires the weighting of the smoothness condition to be reduced via $\phi_s = 1 \times 10^{-7}$ in order to compute reasonable results.

The extinction coefficients of all LED strips follow a similar profile over the height. Especially, the results from the centre strip are in a good agreement with those from the merged strips. It should be noted that the extinction coefficients each increase

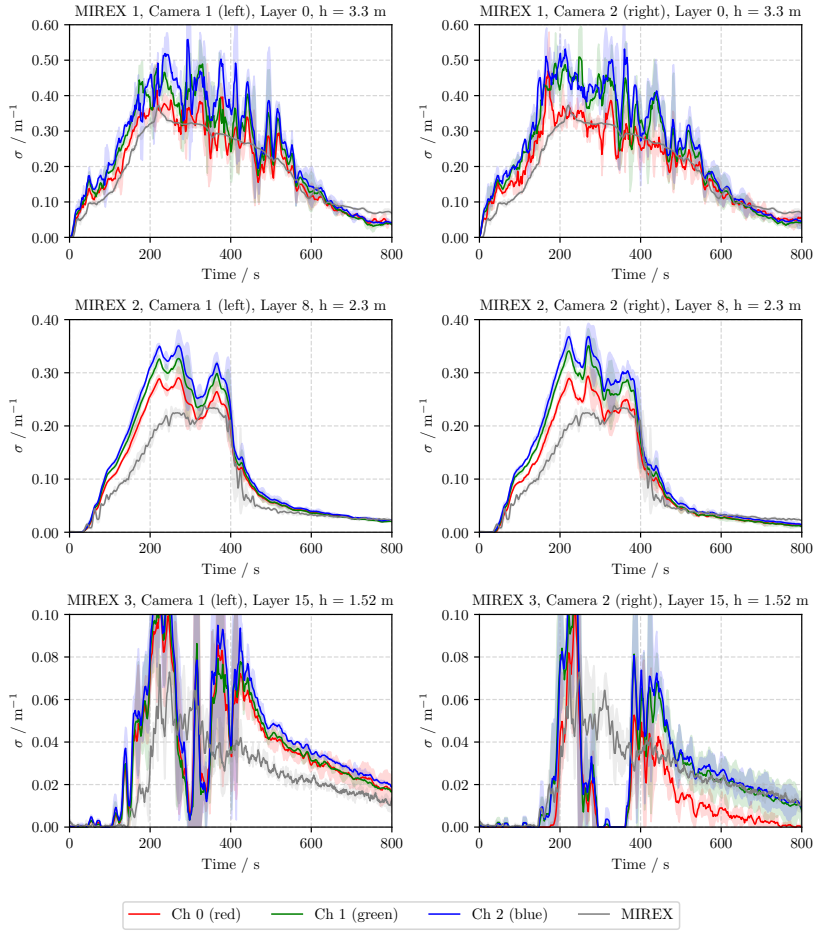

Figure 9: MIREX and LEDSA (Camera 1 and Camera 2) extinction coefficients in setup 2. The plot shows mean values (solid lines) and standard deviation (shaded areas) from 2 experiments with a mixed fuel from n-heptane and toluene.

with shorter distance between the reference point and the camera. The effect is significantly larger for the red than for the green and blue camera channel.

The phenomenon also occurs in reverse for the second camera, as can be seen from the aggregated results of all strips in Fig. 11. This cannot be attributed exclusively to an inhomogeneity of the smoke layering, since the influence on all colour channels would be equivalent. A change in particle size distribution could have a different effect on light opacity at various wavelengths, but this cannot be accounted for the dependence on the distance between the camera and the light source.

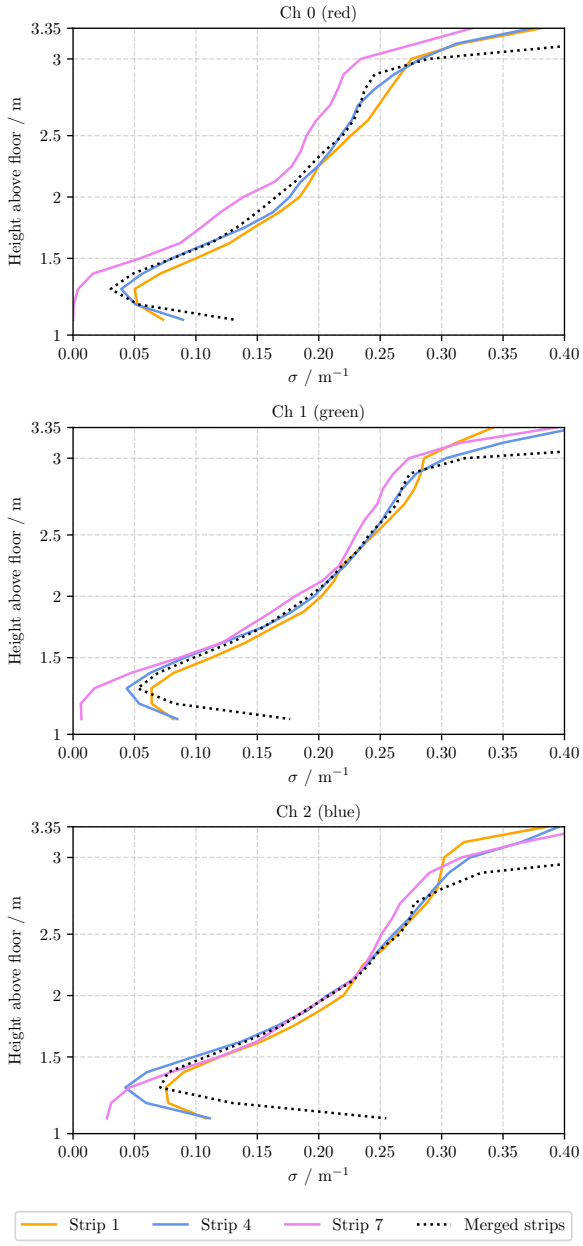

Figure 10: Computed extinction coefficients at t = 300 s of a single experiment for camera 1 as a function of height. The results of all three colour channels are shown for the two outer (1, 7) and the middle (4) LED strip, as well as a merged computation from all strips.

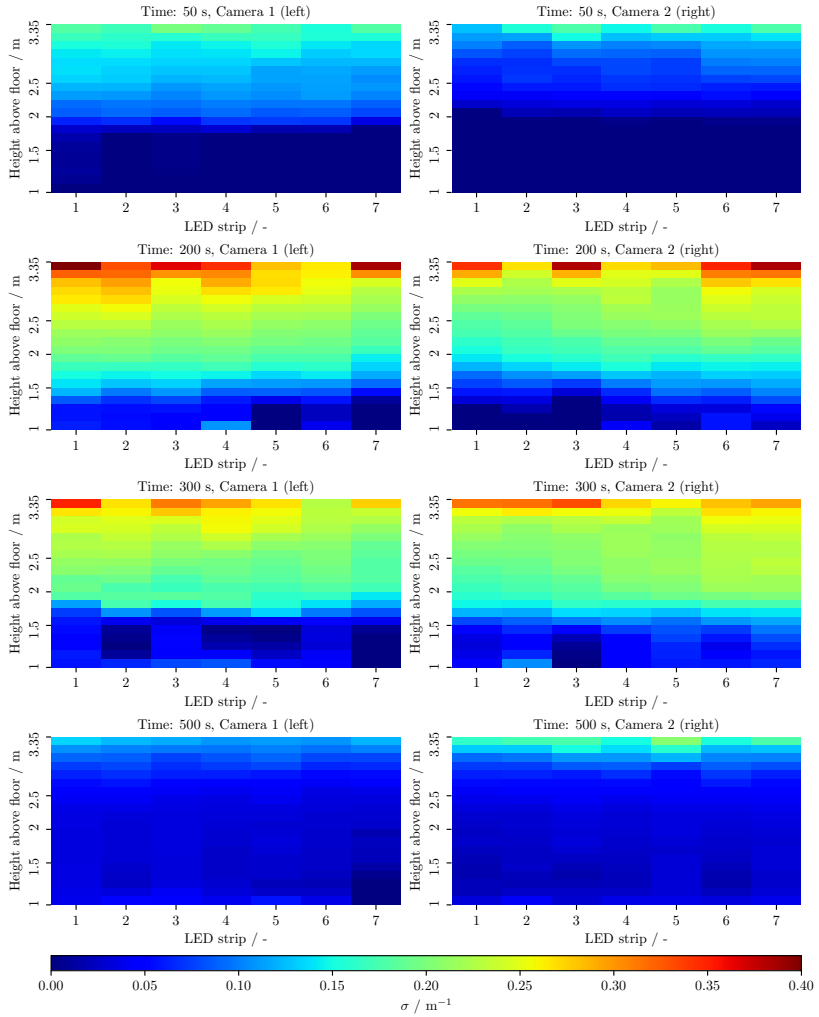

Figure 11: 2D spatial resolution of the computed extinction coefficients for the red camera channel (Channel 0) at different times for both cameras. The computed values from both cameras show a roughly point-symmetric behaviour around the centre LED strip. This phenomenon can be attributed to temperature-related influences on the LEDs as well as to a slightly homogeneous smoke layering.

The observations suggest that the photometric measurement could be biased by a change in the initial luminosity of the individual light sources. A potential temperature-related effect on the emitted intensity is discussed in the following section.

Plots of the spatially resolved extinction coefficients corresponding to Fig. 11 are provided in Appendix A for the other colour channels.

5.2 A Study on Experimental Parameters

The Beer-Lambert law imposes some limitations that involve certain simplifications and inaccuracies for the present model. No distinction is made between effects from absorption and scattering by smoke particles, since it only describes the attenuation of a single light beam. This approach can be considered sufficiently accurate for point light sources as long as the absorbing influence is dominant over the scattering effect. For most smoke products, this assumption is valid, as the particle diameter is usually well below the wavelength of the light [15].

Another simplification of the applied method results from how the interaction between the light source and the detector is processed. For simplicity, the employed RGB LEDs are considered as three independent light sources each, which are detected solely in the respective colour channels of the camera. Since a real light source is not perfectly monochromatic and σ is a function of the wavelength, the total transmission T would be obtained by integration over its spectral bandwidth [31]:

$$T = \frac{I}{I_0} = \frac{\int_{\lambda_1}^{\lambda_2} I_0(\lambda) \cdot e^{-\sigma \cdot l} d\lambda}{\int_{\lambda_1}^{\lambda_2} I_0(\lambda) d\lambda} \tag{8}$$

Furthermore, it is assumed that the sensor's colour filters have a perfectly flat spectral response. The related error is difficult to quantify as it results from various influences:

1. Due to the broad response spectra of the colour filters, contributions from all three colour components of the LEDs are detected in all colour channels of the camera.

2. Temperature-related influences may cause the emitted spectrum to vary in intensity as well as in bandwidth and peak wavelength.

3. The light attenuation caused by smoke depends on the wavelength.

The response spectrum as well as the sensitivity of the camera can be assumed to be invariable, since they are shielded from thermal exposure.

To better understand the above influences, the LEDs used in the experiment were spectrally analysed. Fig. 12 shows an example of the mean emitted spectrum of eleven RGB LEDs from three repetitive measurements with a BTS256-LED spectroradiometer device from Gigahertz-Optik [32]. All measurements were performed at ambient temperature after a ten-minute warm-up period with all three colour components turned on.

The standard deviation of the peak wavelength is relatively small, although significantly larger for the red (1.36 nm) and blue (1.37 nm) than for the green (0.37 nm) LEDs. The coefficient of variation (CV) denotes the relative standard deviation and thus serves as a reference value that is independent of the absolute intensity. It is likewise higher for red (CV = 11.6%) and blue (CV=15.9%) than for green

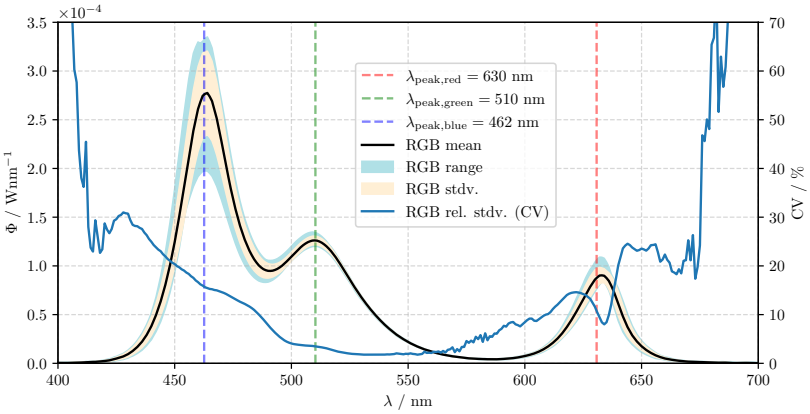

Figure 12: Mean emitted spectra of eleven RGB LEDs at ambient temperature from three repetitive measurements after a ten minutes warm-up period. Furthermore, the measurement range and the standard deviation are shown. The blue line indicates the relative standard deviation (coefficient of variation (CV) of the measured LED intensity.

(CV = 3.5%) LEDs. The RGB light sources of the individual LEDs were each analysed simultaneously, so that uncertainties in the measurements can be excluded from being a potential cause for the magnitude of deviations. Since the LED intensities are scaled to towards their initial values in the experiments, those deviations do not pose a fundamental issue for the photometric measurement. However, an uncertainty arises from the captured light in a colour channel of the camera being composed of varying contributions from the LED colour components.

Thermal exposure of the LEDs due to convective heat transfer and radiation from the plume could pose a significant error on the measured intensities. An empirical correlation between ambient temperature T and the relative emission intensity I for red AlGaInP/GaAs, green GaInN/GaN and blue GaInN/GaN LEDs from data of the Toyoda Gosei Corporation is reported in [33]:

$$I = I_{300\mathrm{K}} \cdot \exp\left(-\frac{T - 300\,\mathrm{K}}{T_1}\right) \tag{9}$$

$I_{300\mathrm{K}}$ is the initial intensity at room temperature, here 300 K, and T_1 is the characteristic temperature. The latter is an empirical quantity characterizing the temperature dependence of the LED. Reported characteristic temperatures of $T_1 = 199\,\mathrm{K}$ for red ($\lambda_\mathrm{R} = 625\,\mathrm{nm}$), $T_1 = 341\,\mathrm{K}$ for green ($\lambda_\mathrm{G} = 525\,\mathrm{nm}$) and $T_1 = 1{,}600\,\mathrm{K}$ for blue ($\lambda_\mathrm{B} = 460\,\mathrm{nm}$) LEDs imply a much higher temperature dependence for red than for green and blue LEDs. The exact specifications of the LEDs used in the presented experiments are not known. However, it can be assumed that these are the same types as in the reported study, since they are the most commonly used today.

Temperature measurements taken close to the ceiling during the experiments allow a rough estimate of the influence on the emitted intensity based on these correlations.

Maximum temperatures between 60°C and 75°C would estimate attenuation against room temperature according to Eq. 9 as follows:

- red: 85% - 79%
- green: 91% - 87%
- blue: 98% - 97%

The actual error with respect to the measurement of light transmission is likely to be smaller due to the inherent heating of the LEDs themselves, which sets in even before the external temperature exposure.

Based on this thermally induced reduction of the initial intensity I_0, a geometric influence on the measurement of the extinction coefficient occurs. Beer-Lambert's law assumes I_0 of the emitted light to remain constant over the entire course of the experiment. A shift of this reference thus also has an effect on the extinction coefficients computed by LEDSA. The initial intensity I_0 of an LED may be reduced to a fraction α due to thermal exposure. Following Eq. 2 the measured intensity I_α can be expressed as a function of α and l

$$I_\alpha = \exp(-\sigma_\mathrm{r} \cdot l) \cdot I_0 \cdot \alpha \tag{10}$$

Here σ_r denotes the "real" extinction coefficient that would result from a measurement with an undisturbed reference quantity I_0. Substituting Eq. 10 into Eq. 2 and solving for σ provides the distorted extinction coefficient computed by the model, subsequently referred to as σ_m, see Eq. 11. In case $\alpha < 1$, σ_m increases against the real value σ_r with decreasing path length l through the smoke layer.

$$\sigma_\mathrm{m} = \sigma_\mathrm{r} - \frac{\ln \alpha}{l} \tag{11}$$

Eq. 11 potentially allows determining the attenuation α of the initial intensity using the extinction coefficient calculated with LEDSA at different path lengths. However, this would require σ_r to be perfectly uniform along both measurement paths.

6 Conclusion

Experiments in style of EN 54 were conducted in order to investigate the light obscuring effects of fire smoke using a photometric method. This involves capturing the light attenuation of individual RGB LEDs on seven strips by two cameras from different perspectives. Comparing the results with local measurements of the well-established MIREX system reveals that the method is capable of computing spatially and temporally resolved extinction coefficients. The LEDSA extinction coefficient values show higher fluctuations than the MIREX, which may be related to a longer measurement distance as well as the numerical optimisation procedure. However, there is no information about an internal smoothing of the raw data by the MIREX. Due to the different wavelengths of the light sources, the LEDSA extinction

coefficient values are generally higher than the MIREX values at the respective measurement locations. For the MIREX at heights 1.52 m and 2.3 m, the discrepancies approximately correspond to the expected ratio according to Widmann's empirical law. For the MIREX at 3.3 m, the results of LEDSA and the MIREX are closer than expected, given the different wavelengths. A reasonable reproducibility can be verified by data from ten experiments with n-heptane fuel and a mixture of n-heptane and toluene. Furthermore, the experimental setup allows verifying the hypothesis of homogeneous smoke properties within horizontal layers.

Significant improvements of the previously introduced photometric approach could be achieved in particular by evaluating RAW image data instead of common JPG files. The luminosity can thus be determined separately for three colour channels of a common digital camera without being corrupted by camera-internal post-processing. However, a sensitivity analysis involving experimental data indicates that the measurement may still be biased due to a considerable temperature dependence of the LEDs.

The experimental uncertainties, especially with respect to the intrinsic properties of the LEDs, are still too large at the present stage to derive further conclusions about smoke properties such as particle size. Nevertheless, the method can be considered as a promising approach for the validation of numerical fire simulation models due to the temporal and spatial resolution. Simulations with FDS have already shown that the method is able to roughly capture the local dynamics of the smoke density. However, the results still show significant deviation, indicating the choice of unsuitable input quantities, e.g., the mass specific extinction coefficient or the soot yield for the simulation model.

The software LEDSA which is used for data analysis was written in Python and is made freely available by the authors [28]. Additionally, all data associated with the presented experiments are publicly accessible in a Zenodo repository [34]. This involves both image files and input files comprising the geometric parameters of the setup and the boundary conditions of the model.

7 Outlook

As stated above, the applied method can be generally validated within the scope of the conducted experiments. Nevertheless, both the experimental setup and the data analysis reveal a considerable potential for improvement. To enhance the accuracy of the photometric measurement, it is essential to minimize the temperature related influences on the light sources. Higher quality LED strips with thermal insulation may therefore be used in upcoming experiments. It has been found that the latter usually also show smaller deviations in the spectrum of the individual colour sources.

The experimental setup is to be extended by further measuring devices for local detection of temperatures, light transmission and particle size distribution in order to validate the spatial resolution of the model.

Along with the data analysis from several LED strips, the employed layer model is capable to confirm the assumption of an adequate homogeneous smoke stratification. Nevertheless, it can be expected that by extending the model to a true three-dimensional scale, based on data from multiple cameras and viewpoints, local

variations in smoke density can be detected. The development of such a model will include the use of synthetic measurement data from CFD simulations.

The results from the experiments with an n-heptane toluene mixture indicate that the fuel-specific properties affecting the particle size distribution have a measurable influence, being accounted for by this approach. Further experiments will be conducted to investigate such effects, taking into account additional test fires in accordance with EN 54, including smouldering fires and pyrolysis.

Acknowledgements

The authors gratefully acknowledge the financial support of the German Federal Ministry of Education and Research. The extensive LEDSA computations were performed largely on the high-performance computer system funded as part of the CoBra project with the grant number 13N15497.

Funding

Open Access funding enabled and organized by Projekt DEAL.

Appendix

Appendix A – Spatiotemporal Extinction Coefficients

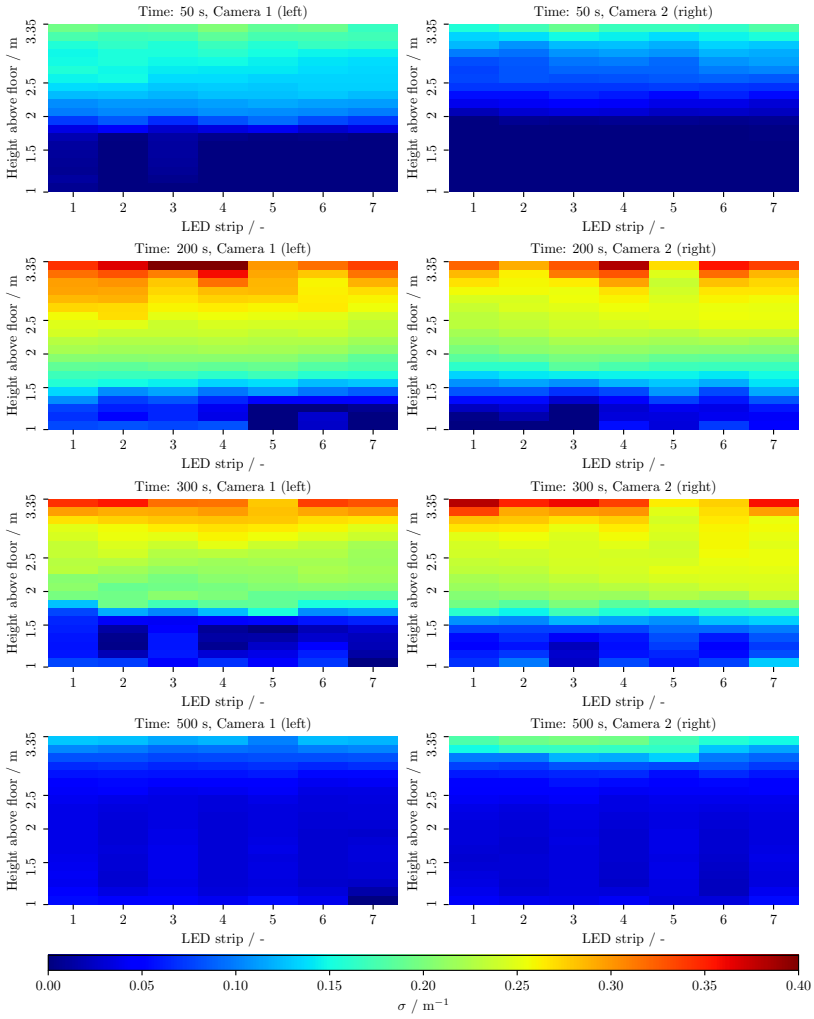

Figure 13: 2D spatial resolution of calculated extinction coefficients for the green camera channel (Channel 1) at different times for both cameras.

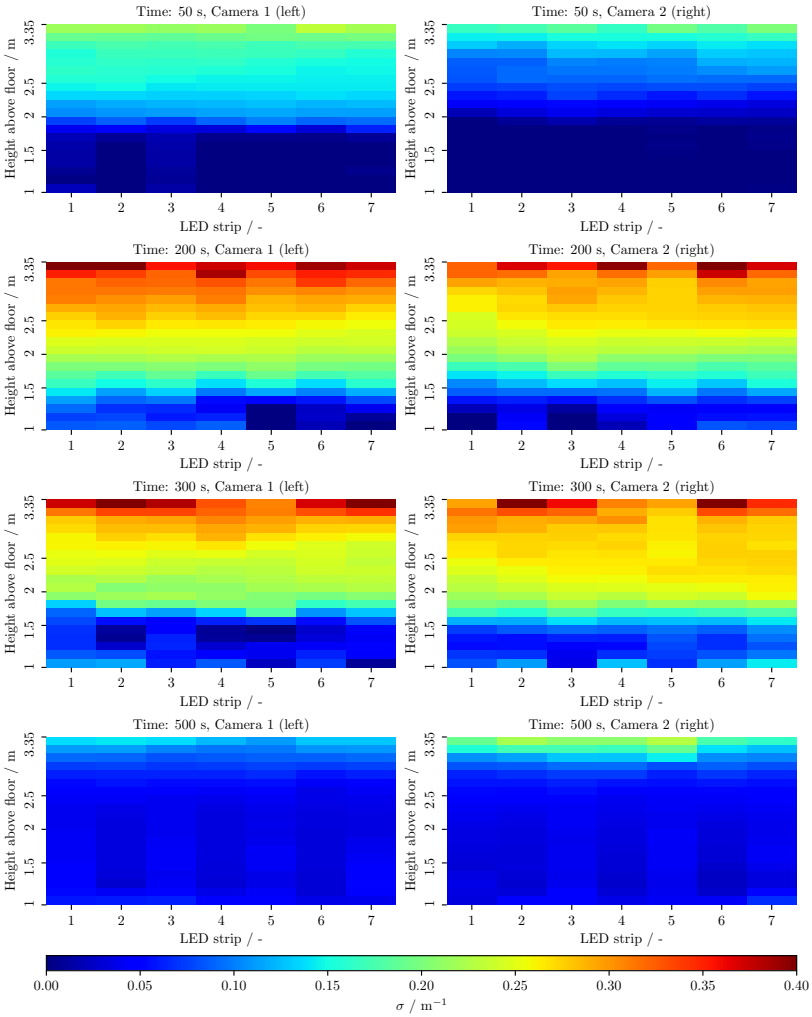

Figure 14: 2D spatial resolution of calculated extinction coefficients for the blue camera channel (Channel 2) at different times for both cameras.

References

[1] David A Purser and Jame L McAllister. "Assessment of Hazards to Occupants from Smoke, Toxic Gases, and Heat". In: *SFPE Handbook of Fire Protection Engineering*. Ed. by Morgan J. Hurley. New York: Springer, 2016. ISBN: 9781493925643. DOI: 10.1007/978-1-4939-2565-0.

[2] Leonard Y. Cooper. "A concept for estimating available safe egress time in fires". In: *Fire Safety Journal* 5.2 (1983), pp. 135–144. ISSN: 0379-7112. DOI: 10.1016/0379-7112(83)90006-1.

[3] Gordon E. Hartzell and Howard W. Emmons. "The Fractional Effective Dose Model for Assessment of Toxic Hazards in Fires". In: *Journal of Fire Sciences* 6.5 (1988), pp. 356–362. ISSN: 0734-9041. DOI: 10.1177/073490418800600504.

[4] Benjamin Schröder. "Multivariate Methods for Life Safety Analysis in Case of Fire". PhD thesis. University of Wuppertal, 2016.

[5] Benjamin Schröder, Lukas Arnold, and Armin Seyfried. "A map representation of the ASET-RSET concept". In: *Fire Safety Journal* 115 (2020), p. 103154. ISSN: 0379-7112. DOI: 10.1016/j.firesaf.2020.103154.

[6] Kevin McGrattan, Simo Hostikka, Jason Floyd, Randall McDermott, and Marcos Vanella. *Fire Dynamics Simulator User's Guide – Version 6.7.9*. Tech. rep. 2022.

[7] Tadahisa Jin. "Visibility through Fire Smoke (I)". In: *Bulletin of Japan Association for Fire Science and Engineering* 19.2 (1970), pp. 1–8. ISSN: 0546-0794. DOI: 10.11196/kasai.19.2.1.

[8] Daniel Gottuk, Christopher Mealy, and Jason Floyd. "Smoke Transport and FDS Validation". In: *Fire Safety Science* 9 (2008), pp. 129–140. ISSN: 1817-4299. DOI: 10.3801/iafss.fss.9-129.

[9] Lukas Arnold, Alexander Belt, Thorsten Schulze, and Abdul Wahab Mughal. "Experimental and Numerical Investigation of Visibility in Compartment Fires". In: *AUBE 21*. 2021.

[10] Lukas Arnold, Alexander Belt, Thorsten Schultze, and Lea Sichma. "Spatiotemporal measurement of light extinction coefficients in compartment fires". In: *Fire and Materials* (2020). ISSN: 0308-0501. DOI: 10.1002/fam.2841.

[11] Jennifer Ellingham and Elizabeth Weckman. "Video analysis of smoke density in full-scale fires". In: *Combustion Institute – Canadian Section Spring Technical Meeting 2019*. Kelowna: The University of British Columbia, 2019.

[12] George W Mulholland. "Smoke Production and Properties". In: *SFPE Handbook of Fire Protection Engineering*. Ed. by Philip J DiNenno. Third Edition. New York: National Fire Protection Association, 2002. ISBN: 087765-451-4.

[13] E.M Patterson, R.M Duckworth, C.M Wyman, E.A Powell, and J.W Gooch. "Measurements of the optical properties of the smoke emissions from plastics, hydrocarbons, and other urban fuels for nuclear winter studies". In: *Atmospheric Environment. Part A. General Topics* 25.11 (1991), pp. 2539–2552. ISSN: 0960-1686. DOI: 10.1016/0960-1686(91)90171-3.

[14] Richard A Dobbins and G Stephen Jizmagian. "Particle Size Measurements Based on Use of Mean Scattering Cross Sections*". In: *Journal of the Optical Society of America* 56.10 (1966), p. 1351. ISSN: 0030-3941. DOI: 10.1364/josa.56.001351.

[15] George W. Mulholland and Carroll Croarkin. "Specific extinction coefficient of flame generated smoke". In: *Fire and Materials* 24.5 (2000), pp. 227–230. ISSN: 1099-1018. DOI: 10.1002/1099-1018(200009/10)24:5<227::aid-fam742>3.0.co;2-9.

[16] Kevin McGrattan, Simo Hostikka, Jason Floyd, Randall McDermott, and Marcos Vanella. *Fire Dynamics Simulator Technical Reference Guide Volume 2: Verification – Version 6.7.9*. Tech. rep. 2022.

[17] John F. Widmann. "Evaluation of the planck mean absorption coefficients for radiation transport through smoke". In: *Combustion Science and Technology* 175.12 (2003), pp. 2299–2308. ISSN: 0010-2202. DOI: 10.1080/714923279.

[18] A. Keller, M. Loepfe, P. Nebiker, R. Pleisch, and H. Burtscher. "On-line determination of the optical properties of particles produced by test fires". In: *Fire Safety Journal* 41.4 (2006), pp. 266–273. ISSN: 0379-7112. DOI: 10.1016/j.firesaf.2005.10.001.

[19] Konrad Wilkens Flecknoe-Brown and Patrick van Hees. "Obtaining Additional Smoke Characteristics Using Multi-Wavelength Light Transmission Measurements". In: *14th International Conference and Exhibition on Fire and Materials 2015*. San Francisco, 2015.

[20] Kenneth L Cashdollar, Calvin K Lee, and Joseph M Singer. "Three-wavelength light transmission technique to measure smoke particle size and concentration". In: *Applied Optics* 18.11 (1979), p. 1763. ISSN: 0003-6935. DOI: 10.1364/ao.18.001763.

[21] Wojciech Węgrzyński, Piotr Antosiewicz, and Jadwiga Fangrat. "Multi-Wavelength Densitometer for Experimental Research on the Optical Characteristics of Smoke Layers". In: *Fire Technology* (2021), pp. 1–24. ISSN: 0015-2684. DOI: 10.1007/s10694-021-01139-5.

[22] Cerberus. *Ionization measuring chamber MIC Extinction measuring equipment MIREX*. Technical description. 1992.

[23] The European Committee for Standardization. *EN 54— Fire detection and fire alarm systems, part 7: smoke detectors point detectors using scattered light, transmitted light or ionization*. 2000.

[24] Mohammed M Khan, Archibald Tewarson, and Marcos Chaos. "Characteristics of Materials and Generation of Fire Products". In: *SFPE Handbook of Fire Protection Engineering*. Ed. by Morgan J. Hurley. New York: Springer, 2016. ISBN: 9781493925643. DOI: 10.1007/978-1-4939-2565-0.

[25] O. Losson, L. Macaire, and Y. Yang. "Comparison of Color Demosaicing Methods". In: *Advances in Imaging and Electron Physics* 162 (2010), pp. 173–265. ISSN: 1076-5670. DOI: 10.1016/s1076-5670(10)62005-8.

[26] Alex Tutubalin. *LibRaw*. 2021. URL: https://www.libraw.org.

[27] P. Rotjberg. *Processing RAW images in Python*. Tech. rep. 2017.

[28] Kristian Börger, Alexander Belt, and Lukas Arnold. "LEDSA: A Python package for determining spatially and temporally resolved extinction coefficients of fire smoke". In: *Submitted to JOSS, The Journal of open source software* (2023).

[29] Sean P. Kearney and Flint Pierce. "Evidence of soot superaggregates in a turbulent pool fire". In: *Combustion and Flame* 159.10 (2012), pp. 3191–3198. ISSN: 0010-2180. DOI: 10.1016/j.combustflame.2012.04.011.

[30] Tadahisa Jin. "Visibility through Fire Smoke (IV)". In: *Bulletin of Japan Association for Fire Science and Engineering* (1974).

[31] George W. Mulholland. "How well are we measuring smoke?" In: *Fire and Materials* 6.2 (1982), pp. 65–67. ISSN: 1099-1018. DOI: 10.1002/fam.810060205.

[32] *Gigahertz Optik BTS256-LED Tester*. Technical description. 2020.

[33] E. Fred Schubert. *Light-Emitting Diodes*. Vol. Second edition. New York: Cambridge University Press, 2006. DOI: 10.1017/BO9780511790546.

[34] Kristian Börger, Alexander Belt, Thorsten Schultze, and Lukas Arnold. *Remote sensing of the light-obscuring smoke properties in real-scale fires using a photometric measurement method-Data Set*. 2023. DOI: 10.5281/zenodo.7016689.

PUBLICATION II

Assessing Performance of LEDSA and Radiance Method for Measuring Extinction Coefficients in Real-Scale Fire Environments

Note: This article was published as Kristian Börger, Jennifer Ellingham, Alexander Belt, Thorsten Schultze, Stefan Bieder, Elizabeth Weckman and Lukas Arnold. *Assessing Performance of LEDSA and Radiance Method for Measuring Extinction Coefficients in Real-Scale Fire Environments.* Fire Safety Journal, Volume 141, 2023. 103929, ISSN 0379-7112, https://doi.org/10.1016/j.firesaf.2023.103929.

Author Contributions

CONCEPTUALIZATION: Kristian Börger, Jennifer Ellingham, Alexander Belt, Elizabeth Weckman and Lukas Arnold
METHODOLOGY: Kristian Börger, Jennifer Ellingham, Alexander Belt, Elizabeth Weckman and Lukas Arnold
SOFTWARE: Kristian Börger, Jennifer Ellingham and Lukas Arnold
VALIDATION: Kristian Börger, Jennifer Ellingham, Alexander Belt, Thorsten Schultze, Stefan Bieder, Elizabeth Weckman and Lukas Arnold
FORMAL ANALYSIS: Kristian Börger and Jennifer Ellingham
INVESTIGATION: Kristian Börger and Jennifer Ellingham
RESOURCES: Lukas Arnold, Alexander Belt, Thorsten Schultze, Stefan Bieder
DATA CURATION: Kristian Börger and Jennifer Ellingham
WRITING–ORIGINAL DRAFT: Kristian Börger
WRITING–REVIEW AND EDITING: Kristian Börger, Jennifer Ellingham, Alexander Belt, Thorsten Schultze, Elizabeth Weckman and Lukas Arnold
VISUALIZATION: Kristian Börger
SUPERVISION: Lukas Arnold and Elizabeth Weckman
PROJECT ADMINISTRATION: Lukas Arnold and Elizabeth Weckman
FUNDING ACQUISITION: Lukas Arnold and Elizabeth Weckman

Assessing Performance of LEDSA and Radiance Method for Measuring Extinction Coefficients in Real-Scale Fire Environments

Kristian Börger[1 3], Jennifer Ellingham[2], Alexander Belt[3], Thorsten Schultze[4], Stefan Bieder[4], Elizabeth Weckman[2] and Lukas Arnold [1 3]

[1] Computational Civil Engineering, University of Wuppertal, Germany
[4] Department of Mechanical and Mechatronics Engineering, University of Waterloo, Waterloo, Canada
[3] Institute for Advanced Simulation, Forschungszentrum Jülich, Germany
[4] Communication Systems (NTS), University of Duisburg-Essen, Duisburg, Germany

Abstract

Two photometric measurement methods (Radiance Method and LEDSA) were compared against the established MIREX measurement apparatus under controlled laboratory conditions to assess their capability of measuring extinction coefficients in real-scale fires on a temporal and spatial scale. LEDSA is a tomographic technique based on direct measurements of light intensity from individual LEDs using commercially available DSLR cameras. By discretizing the domain into horizontal layers with homogeneous smoke density, values of the extinction coefficient can be computed using an inverse model based on Beer Lambert's law. The Radiance Method involves measuring the contrast of light and dark areas in images and/or video footage. It was originally developed to investigate the descent of the smoke layer in high-temperature fire events. In this work, the extinction coefficient was deduced from measurements on a contrast board by a straightforward analytical approach. Both methods were shown to yield similar extinction coefficient results in line with the MIREX for an EN 54-7 TF5 n-heptane fire. The Radiance Method is able to generate accurate patterns but not values for a TF2 wood smouldering fire, while LEDSA is generally able to reflect the MIREX measurement values, yet requires higher computational effort.

Keywords: Compartment fire experiments; smoke characteristics; visibility; extinction coefficient; Radiance Method; LEDSA

1 Introduction

Understanding propagation and characteristics of smoke in real-scale fires is crucial for fire safe building design. In particular, hazards arise from toxic components of fire smoke and from an impairment in visibility [1]. The latter can be estimated, for

example, from numerical fire models such as the Fire Dynamics Simulator (FDS) [2] following the theory of Jin [3]. In this context, smoke density and the light extinction coefficient serve as key metrics commonly employed for quantification and model validation. Measurement techniques to assess these quantities usually rely on Beer Lambert's law [4] (see Eq. 1), which expresses the transmission T through a homogeneous absorbing and/or scattering medium as a function of the extinction coefficient σ and the measurement path length L. This usually involves measuring the incident intensity I_0 of a light source and the transmitted intensity I in the presence of smoke from a photoelectric sensor.

$$T = \frac{I}{I_0} = \exp(-\sigma \cdot L) = \exp(-K_\mathrm{m}(\lambda) \cdot \rho_\mathrm{s} \cdot L) \tag{1}$$

The correlation of the smoke density ρ_s [$\mathrm{kg\,m^{-3}}$] and the extinction coefficient σ [$\mathrm{m^{-1}}$] can be established by a mass specific extinction coefficient $K_\mathrm{m}(\lambda)$ [$\mathrm{m^2\,kg^{-1}}$]. $K_\mathrm{m}(\lambda)$ is reported to be almost fuel independent for smoke from well-ventilated, stoichiometric, flaming combustion [5]. However, the absorption and scattering behaviour of light by smoke particles depends on the wavelength. Widmann determined an empirical law (Eq. 2) from a comprehensive literature review [6].

$$K_\mathrm{m} = 4.8081 \cdot \lambda^{-1.0088} \tag{2}$$

Established devices for local smoke density measurements, such as the *Measuring InfraRed EXtinction* (MIREX) apparatus [7], rely on the Beer Lamber's law. However, it would be prohibitively expensive to use these sensors for spatially resolved smoke density measurements, e.g. for the validation of CFD (computational fluid dynamics) models. This prompted the development of the two new image-based photometric measurement methods, LEDSA (LED Smoke Analysis) [8] and the Radiance Method [9], which are able to determine spacially resolved extinction coefficients.

The Radiance Method is a technique for measuring smoke density in real-scale fires by analysing video and/or image data. The method involves identifying contrasting light (white) and dark (black) areas in the footage to evaluate smoke progression in the compartment. The Radiance Method has been tested in full-scale furniture fire experiments based on the recordings from security cameras [9]. The approach showed promise when comparing the numerical rank of smoke density results generated by human observers and from smoke density chamber [10] results for different fuels. While the Radiance Method relies on capturing the contrast on externally illuminated surfaces, LEDSA is based on the direct measurement of transmission from individual light sources such as Light-Emitting Diodes (LEDs). The smoke-induced drop in light intensity can be read from sequential images recorded by consumer digital cameras. Local values of the extinction coefficient can then be deduced by an inverse modelling approach based on geometric optics and Beer Lambert's law. LEDSA was validated by local measurements of the extinction coefficient using multiple MIREX apparatus in laboratory experiments [11] similar to EN 54-7 [12] test fires. Although both methods rely on measuring intensity from image data, they originally target a different field of application. The Radiance Method is intended as a robust method for analysing smoke propagation in high-temperature fire events,

while LEDSA aims at the detailed analysis of smoke characteristics in controlled laboratory conditions.

Investigation into both methods under the same boundary conditions will assess the extent to which they are suitable for gauging the evolution of smoke from a fire. For this purpose, experiments were conducted involving the TF5 n-heptane flaming fire and the TF2 wood smouldering pyrolysis similar to the EN 54-7 test fires. This will provide the basis for comparing the spatially resolved measurements of the extinction coefficient obtained using LEDSA and the Radiance Method with the local measurements of the MIREX.

2 Experimental Setup

The Heinz-Luck fire detection laboratory at the University of Duisburg-Essen, where the experiments were conducted, resembles the standardized cubic test chamber according to EN 54-7. The compartment dimensions correspond to the floor plans shown in Fig. 1, while the height-adjustable ceiling was set at 3.37 m. The laboratory is equipped with a variety of sensors including three MIREX apparatus for local measurements of smoke density at 1.6 m, 2.3 m and 3.3 m above the floor. The MIREX measures transmission within a fixed two-meter path length from a pulsed infrared diode, to a reflector, and back to a detector. The documentation indicates a peak wavelength in the $\lambda_{IR} = 880\,\text{nm}$ range [7].

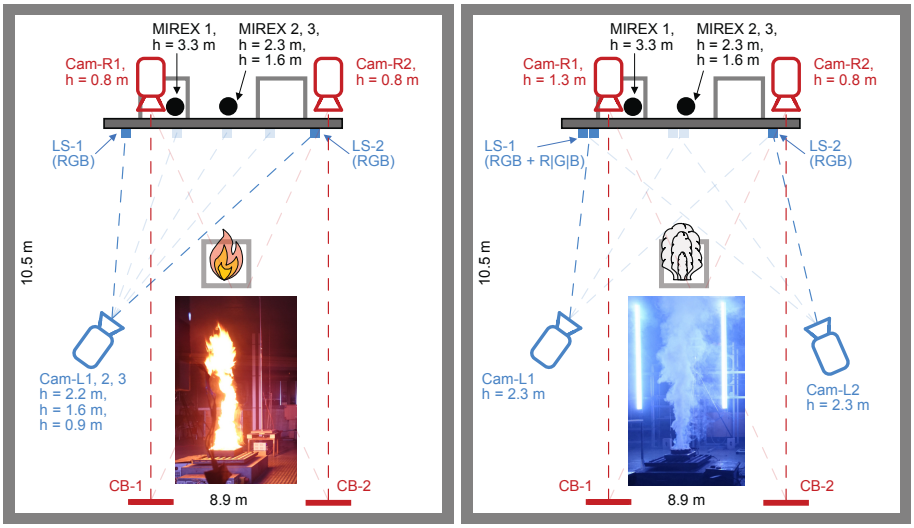

(a) Setup 1 (TF5) **(b)** Setup 2 (TF2)

Figure 1: Floor plans of the laboratory showing the (a) TF5 and (b) TF2 experimental setups. Camera locations were altered, while the relevant LED strips (LS) and contrast boards (CB) stayed in place.

In the experiments, two test fires similar to the EN 54-7 standard were examined. An n-heptane pool fire, similar to the EN 54-7 TF5 test fire, was burned in a

0.33 m × 0.33 m fuel tray. Unlike the standard, only 500 g fuel was used here to account for the reduced ceiling height. The laboratory ventilation was activated 420 s after the n-heptane fire extinguished, until the smoke was completely exhausted. Fire TF2 corresponds to a pyrolysis-driven smouldering fire from 13 beech wood sticks, heated on a hot plate to 600 °C within 11 minutes. Each stick was 75 mm × 25 mm × 20 mm with a relative moisture below 5%. Moisture was determined using a wood moisture meter for building materials with a sampling range between 5% and 50%. Since the full consumption of the fuel requires a considerable amount of time, the ventilation was activated ∼ 1,200 s after the start of the heating phase. Within a total of 17 TF5 and 9 TF2 experiments, the arrangement of the LEDSA and Radiance Method components was varied in the context of different setups, with 3 - 4 identical tests being carried out on each day. This study focuses on experimental setups 1 and 2, as shown in Fig. 1, encompassing one repeat set from each fuel arrangement. The results of three tests from one day were compared for both setups in order to ensure the most identical boundary conditions possible, such as the ambient and wall temperature. The experimental repeatability is evaluated on the basis of local measurements with the established MIREX system. Each of the three repeat experiments for both setups (six experiments total) was analysed as detailed below. A comparison of the three methods is shown here with plots from a single representative experiment in each case, in order to display the emerging phenomena at the most precise level possible. Deviations of the measurements with LEDSA and the Radiance Method between the individual experiments are slightly larger than those of the respective MIREX measurements, but are in the same order of magnitude. The experimental procedure for each setup is outlined in Fig. 2.

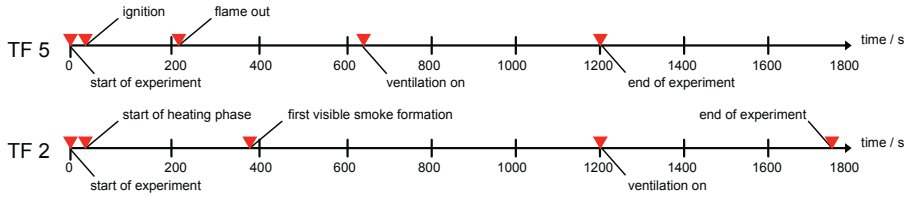

Figure 2: Timeline of the experimental procedure.

Multiple 2.4 m long RGB LED strips (LS), each featuring 144 uniformly distributed individual LEDs, served as the light sources for LEDSA. They were attached to vertically aligned aluminium columns by a thermally conductive adhesive to allow for uniform temperature dissipation. The columns were mounted on a supporting substructure with the bottom edge 0.95 m above the floor. Each of the RGB LEDs featured individual colour components with peak wavelengths measured as $\lambda_R = 632$ nm (red), $\lambda_G = 512$ nm (green), and $\lambda_B = 430$ nm (blue) using a dedicated LED spectrometer [13]. Each LED strip was operated in either single colour ($R \mid G \mid B$, setup 2) or multicolour (RGB, setup 1 & 2) mode. However, only the RGB strips were analysed by LEDSA for this study, since the Radiance Method only allows a clear separation via the colour channels of the camera and not by the light source. Measurements using the Radiance Method were made on two contrast boards (CB), each illuminated by the aforementioned LEDs, on the opposite side

of the room. Both boards spanned the entire height of the room, with a width of 0.3 m. Each of the black and white stripes for contrast measurement were 0.1 m wide. Additionally, horizontal markers at 1 m increments from the ground served as a height reference.

Two Canon 80D cameras (*Cam-L1* and *Cam-L2* in Fig. 1) and one Canon 70D camera (*Cam-L3* in Fig. 1) were used to capture images of the LED strips. A low ISO number of 100 was selected to minimise signal noise from the camera sensor. An F/16 aperture setting was found to keep all observed LEDs in focus. The shutter speed of the camera was set to a fixed value between 1/500 s and 1/2000 s to allow maximum use of the dynamic range of the pixels while avoiding saturation. For measurements by the Radiance Method, two Sony RX 100 II cameras were employed (*Cam-R1* and *Cam-R2* in Fig. 1). The cameras had a fixed focal length of 7.9 mm and a fixed aperture of f/4. Since the targeted contrast boards were not self-illuminating, the images were weakly exposed. Accordingly, the cameras needed to be operated at a high ISO value of 800 and a slow shutter speed of 1/25 s. All cameras used in the experiments were operated in manual mode to allow unbiased photometric measurements. Images were each captured at a sampling rate of 1 Hz, starting a few seconds before the ignition.

In setup 1, a general dependence of the camera height on the measured intensities and the computed extinction coefficients was investigated from the LEDSA cameras. Furthermore, two measurements each of LEDSA (*Cam-L1* on *LS-1*, *Cam-L1* on *LS-2*) and the Radiance Method (*Cam-R1* on *CB-1* and *Cam-R2* on *CB-2*) are compared with the MIREX measurements. Setup 2 focuses on examining the general applicability of both methods for the TF2 test. For this purpose, the measurements of *Cam-L1* on *LS-1*, *Cam-L2* on *LS-2*, *Cam-R1* on *CB-1* and *Cam-R2* on *CB-2* are compared to the MIREX measurements.

3 Methodology

3.1 Measuring Intensity From Image Data

Photometric measurement methods such as LEDSA and the Radiance Method used in the present study are based on reading light intensity from image data. Per Eq. 1, transmittance T of the smoke, as an absorbing and/or scattering medium, is the ratio of measured intensity of a light source when obscured by smoke (I) and in clear condition (I_0). Hence, it corresponds to the measured luminosity of the LEDs, and the contrast measured on the contrast boards, relative to an initial value. The baseline intensities are determined from one image (Radiance Method) or the average of ten images (LEDSA) taken just before the experiment, i.e. the fire, started. Hereafter, the normalized intensities will be referred to as the experimental intensity I_e.

LEDSA utilizes high-resolution image data from DSLR cameras that feature high dynamic and tonal ranges. By using RAW image files, the in-camera post-processing can be bypassed, allowing the individual red, green, and blue ($R \mid G \mid B$) pixel values to be retrieved linearly from the camera's sensor readings. Conversely, the Radiance Method is intended to work with relatively low-resolution image or video data, e.g.

from security cameras. Such videos and JPG images are usually encoded by the camera to match human perception of luminosity, requiring a decoding scheme to be determined [9]. Accordingly, for calibration, images were taken of a standardized colour checker (see Fig. 3a) from each camera and setup.

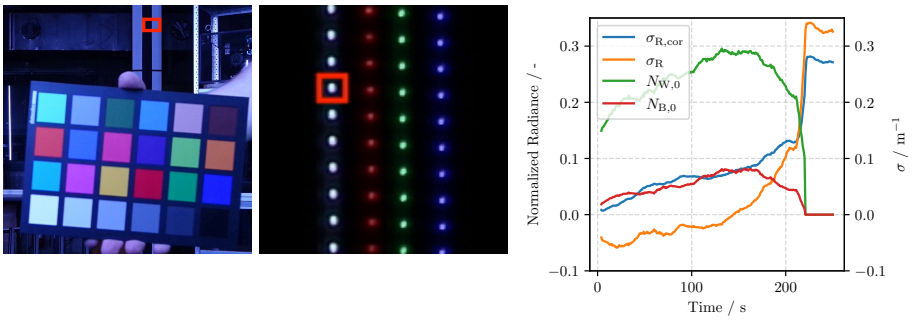

(a) **(b)** **(c)**

Figure 3: (a) Image of the colour checker in front of a contrast board with marked ROI (red rectangle), (b) image of the LEDs as used for reading the intensities by LEDSA with marked ROI (red square), (c) example of the applied flame correction in the burning phase

The Radiance Method uses the ImageJ software [14] to determine the mode $R \mid G \mid B$ pixel values from all 24 colour checker fields in each image. The cameras' encoding schemes were determined by matching measured values against the listed manufacturer $R \mid G \mid B$ radiance values of the colour checker. Finally, the decoding scheme is obtained by inverting the encoding scheme. Consequently, in this work, the actual radiance normalized by the available pixel range (255/3=85), N, can be calculated from the pixel values, P, according to Eq. 3. The pixel values P are read from separate $R \mid G \mid B$ images that were extracted from the original JPG images. It takes ImageJ approximately 20 minutes per colour channel to separate $R \mid G \mid B$ images for analysis for 1200 high-resolution JPG images. ImageJ takes an additional 20 minutes to extract the pixel values once the images are prepared. Both tasks are carried out on a conventional desktop computer.

$$N_{R|G|B} = P/85 \tag{3}$$

Deducing the experimental intensities I_e from the image data works differently for the measurement methods. For LEDSA, I and I_0 are computed as the accumulated pixel values in the same Region Of Interest (ROI) surrounding the individual LEDs (see Fig. 3b). For 1200 RAW images on a desktop computer, the pixel data for all three colour channels is extracted in about 20 minutes from the underlying images. This needs to be done only once per camera and experiment. The ROIs are automatically detected on a reference image and centred around the maximum pixel of each LED with a fixed and predefined size (usually 20×20 pixels). The method captures small movements of the LEDs' position on the image, due to temperature dependent refraction in the compartment.

I_e according to the Radiance Method is given by Eq. 4. Here, $N_{W,0}$ and $N_{B,0}$ denote the initial radiance and $N_{W,S}$ and $N_{B,S}$ denote the radiance in the presence of smoke on adjacent ROIs on the white (W) and black (B) areas, respectively. This assumes transmission losses for both surfaces are equal for every point in time. All radiance values are calculated as mean pixel values of manually selected $\sim 0.03\,\mathrm{m} \times 0.03\,\mathrm{m}$ areas corresponding to 13×13 pixel ROIs (e.g. red rectangle in Fig. 3a). 100 ROIs were analysed between 0.18 m and 3.35 m height on each contrast board.

$$I_e = \frac{N_{W,S} - N_{B,S}}{N_{W,0} - N_{B,0}} \tag{4}$$

In the burning period of the TF5 ($0 - 220\,\mathrm{s}$), the flame provides additional illumination of the contrast boards. Thus, for correctness, $N_{W,0}$ and $N_{B,0}$ of the actual ROIs are substituted with the $N_{W,S}$ and $N_{B,S}$ values from the lowest ROI instead, assuming there is no smoke in the camera's line of sight. This correction reduces the error due to the additional illumination, such that the extinction coefficient is within the bounds of acceptable outcomes (i.e., positive values). Though it reduces error in all cases, this correction is most effective lower in the compartment due to proximity to the lowest measurement.

3.2 Computing Extinction Coefficients

The Radiance Method was designed to estimate smoke density directly from the measured transmission as $1 - T$ which differs from the common definition used in fire safety engineering [9]. Consequently, to generate results directly comparable to those from LEDSA and MIREX, the Radiance Method was adapted to calculate extinction coefficients in the present study. Eq. 5 is a straightforward application of the Beer Lambert's law with $I_e(z_{CB})$ being the normalized intensity and $L_R(z_{CB})$ being the path length from the camera towards the observed ROI at height z_{CB} on the contrast board. This approach provides an analytical calculation of the extinction coefficient from the measured transmission under the simplified assumption that the smoke density is constant along the measurement path. The effect of flame correction as described in section 3.1 on the extinction coefficient is illustrated in Fig. 3c. With flame correction applied, the corrected extinction coefficient $\sigma_{R,cor}$ significantly increases over the uncorrected value σ_R.

$$\sigma_R(z_{CB}) = -\frac{\ln\left(I_e(z_{CB})\right)}{L_R(z_{CB})} \tag{5}$$

LEDSA, on the other hand, relies on a tomographic model designed to evaluate extinction coefficients by means of a spatial discretization. The fundamental assumption of the model is that the smoke density, and hence the extinction coefficients $\sigma_{L,i}$, are constant within horizontal layers i with a predefined thickness. At a certain time, the best matching set of extinction coefficients can be computed by fitting a model for the LED intensity I_m (Eq. 6) to the actual measured intensities I_e. Here, Eq. 6 is basically the numerical integration of Eq. 1 in the camera's line of sight according to the selected layer discretization.

$$I_{\mathrm{m},j} = \exp\left(-\sum_{i=1}^{N_{\mathrm{Layers}}} \sigma_{\mathrm{L},i} \cdot \Delta L_{\mathrm{L},i,j}\right) \tag{6}$$

As outlined in Fig. 4, $L_{\mathrm{L},i,j}$ corresponds to the travelled distance within the layer i between the camera and the LED j. The target nonlinear system of equations spanned by $I_{\mathrm{m},j}$ and $I_{\mathrm{e},j}$ is solved for every image by minimizing a cost function that includes additional criteria for the optimization. This optimization requires significant computational effort, increasing almost linearly with the number of layers. The applied inverse model is described in detail in the original work [15]. Data processing on the individual time-steps can be parallelised across several threads, allowing an almost lossless speed up to be achieved. At present, a simulation based on 1200 images for one colour channel and one LED strip takes about 20 minutes when parallelised to 60 CPU threads of a modern HPC system. The computation of the extinction coefficients with the Radiance Method is negligible due to the analytical model, which is carried out using spreadsheet software on a desktop computer.

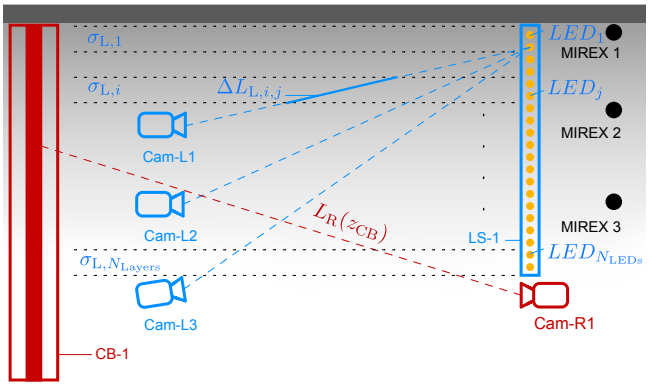

Figure 4: Cross-sectional view through the laboratory showing the arrangement of the cameras as well as a contrast board (*CB-1*) and an LED strip (*LS-1*) in setup 1. $L_{\mathrm{L},i,j}$ is the path length in layer i in the camera's line of sight to LED j. $L_{\mathrm{R}}(z_{\mathrm{CB}})$ is the full sensing path for the Radiance Method from the camera to a specific ROI at height z_{CB} on the contrast board.

3.3 Model Uncertainties

Both the LEDSA and Radiance Method approaches are subject to model-related uncertainties in computing extinction coefficients from measured intensities. In order to quantify these uncertainties and isolate them from instrumental and environmental influences, both methods are verified with synthetic data. Here, $\sigma_{\mathrm{S}}(z)$ depicts the prescribed synthetic extinction coefficient of the smoke as a function of height z, assumed to be constant on a horizontal level. Supposing the camera is in line with the light source and the contrast board, the examination is simplified to a two-dimensional scale.

Smoke density, and thus the extinction coefficient, usually varies in height. σ_R, as measured by the Radiance Method, therefore corresponds to the average extinction coefficient value integrated over the camera's line of sight and can be calculated analytically. For the numerical simulation with LEDSA, artificial image data is generated with 100 equidistant LEDs corresponding to the intensities that a camera at height z_C would see according to the given smoke distribution $\sigma_\mathrm{S}(z)$. The domain is discretized into 20 equally sized layers in the range between $z = 0\,\mathrm{m}$ and $z = 3\,\mathrm{m}$. Increasing the number of layers results in a higher spatial resolution, but does not yield better results, as it reduces the amount of information for each layer for the optimization. A sensitivity analysis in this regard was conducted in the original work [15].

Fig. 5 shows the resulting extinction coefficients by LEDSA (σ_L) and the Radiance Method (σ_R) that would result from a constant, linear, and quadratic profile of σ_S with the cameras being at $z_\mathrm{C} = 1\,\mathrm{m}$ and $z_\mathrm{C} = 2\,\mathrm{m}$. Positions of the cameras and light sources used in this example are chosen for simplicity and to highlight comparisons, and thus differ from the actual experiments.

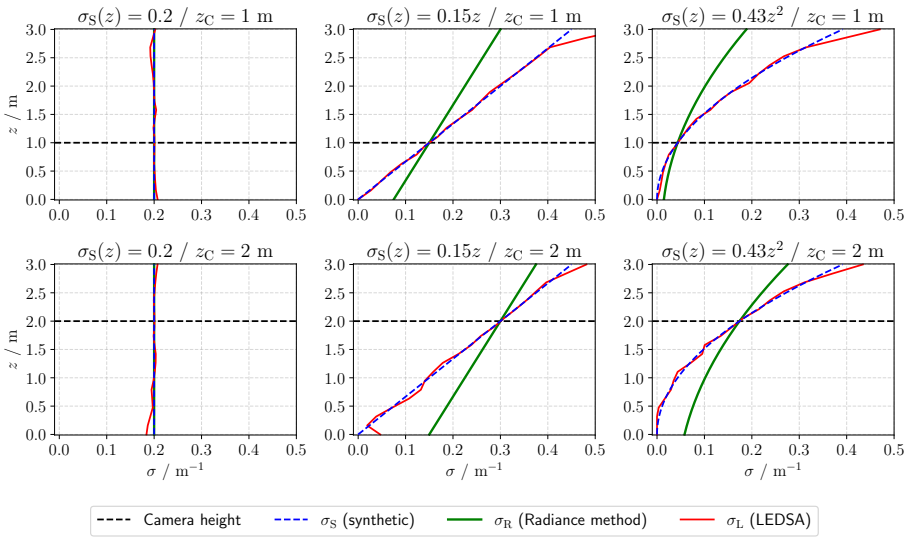

Figure 5: Example based on synthetic data, showing the model-conditioned systematic and numerical deviations between the real extinction coefficient σ_S and as measured by LEDSA (σ_L) and the Radiance Method (σ_R).

The LEDSA extinction coefficient σ_L closely follows the synthetic extinction coefficient σ_S for all three profiles, with the only notable deviations (up to $\sim 0.1\,\mathrm{m}^{-1}$) in the top two or bottom two layers. σ_R accurately estimates the constant profile of σ_S while for the linear and quadratic profiles, it matches at the camera height but increasingly deviates with $\Delta z = |z_\mathrm{C} - z|$. Accordingly, correct measurement of the extinction coefficient by the Radiance Method as presently formulated should only be possible at the height of the camera or when the smoke density is perfectly uniform across the sensing range. With smoke density increasing upward, the measured

value gets overestimated below the camera and underestimated above the camera. It should be noted, that this may be due to the fact, that Eq. 5 is providing the extinction values with regard to the target position on the contrast board (z_{CB}). Although LEDSA aims at computing the real extinction coefficients, it is subject to numerical uncertainties. As noted, deviations from σ_{S} arise especially in the peripheral areas. A steeper viewing angle from the camera results in shorter sensing ranges, so the edge layers are less weighted by the cost function. The presented model can only give a broad outline of the model-related uncertainties and therefore misses some crucial parameters related to the instrumental and environmental effects.

3.4 Instrumental and Environmental Uncertainties

The uncertainties in the experimental determination of the extinction coefficient can be attributed to both the instrumentation and the experimental boundary conditions. Besides intrinsic noise, both the detector and the light sources can be systematically affected by extrinsic influences. As ambient temperature increases, the emitted intensity of LEDs generally decreases exponentially, depending on the type of semiconductor and thus the colour of the LED [16]. The uncertainty from the internal thermal induced drift was reduced by turning on the LEDs at least 20 minutes before the experiments until a constant operating temperature of about 40 °C was reached on the LED surfaces. It was measured by exposed thermocouples that were attached to the LEDs below the thermally insulated silicone coating. The influence of external thermal stress on the measurement accuracy is discussed in [11]. Changes in LED lighting inherently influence Radiance Method results. However, no advantageous correction for the LED light impact could be found, so no correction for this effect was applied. All cameras were housed in PMMA and glass boxes and should therefore remain insensitive to the convective effects of hot smoke. The MIREX incorporates a reference receiver to compensate for thermal drift and ageing of the light source. Temperature influence is likely to be relevant only for TF5 tests, since no significant increase in temperature was measured in the laboratory for the TF2 tests. For the application in high-temperature tests, it might be advisable to place the cameras and LEDs in cooled boxes or even outside the compartment. In this context, the effects of the respective protective layers, such as glass panes, on the light spectrum may have to be taken into account.

Deposition of smoke particles on the instrumentation increasingly distorts the measured light intensity during the course of the experiment. This particularly applies to the MIREX lenses and detectors, LEDs, cameras, and contrast boards close to the ceiling where smoke density is the highest. Comparing the initial extinction coefficient and the asymptotic values post ventilation, this soot deposit impact increases at higher measurement points for all three methods (see Figs. 7, 8). As expected, the effect is negligible for white smoke, such as in the case of TF2, since the particles have an absorbance much lower than the scattering effect [17]. The MIREX, as well as both of the introduced novel measurement methods, can currently only measure light extinction as a whole. However, LEDSA also may potentially provide the means to derive refraction and scattering phenomena from the detected

shape and position of the individual LEDs in the future. The original paper also presents an approach to these issues [15].

Since the flame is not shielded from the experimental setup, it poses an additional light source that can distort the measured transmission in the TF5 tests. This effect increases if the reference source for the light measurement has a comparatively low intensity, as for the contrast boards. It can be quantified by measuring the light intensity gradient in an area not affected by smoke obscuration while the fire goes out. Corresponding to the emitted light spectrum of a diffuse n-heptane flame, the effect should be greatest on the red colour channel of the cameras. The intensity drop on an LED near the ground was observed to be less than 2% for *Cam-L3*. As shown in Fig. 3c, the effect is much higher for Radiance Method results, but was significantly reduced with the flame light correction applied. Furthermore, environmental influences affecting the smoke stratification can have a significant impact on the measurement accuracy. LEDSA assumes the smoke density to be homogeneous on a horizontal level. This assumption is likely to be a good approximation for the MIREX, as it covers a comparatively low measuring distance. In [11], it was shown that the computed extinction coefficients by LEDSA show notable deviations as the camera is shifted horizontally. However, the effect was not observed until the flame was extinguished. Most likely, the descent of the smoke layer in the post flame phase is affected by different wall temperatures of the laboratory.

3.5 Influence of Camera Height

Measuring the intensities of the corresponding light sources provides the raw data for calculating the extinction coefficient using LEDSA and the Radiance Method. Since the smoke is usually not homogeneously distributed over the observed domain, the intensity measurement (I_e) is significantly affected by the position of the camera in the smoke laden environment. The cameras *Cam-L1* - *Cam-L3* in setup 1 were placed at the same location, but at different heights, so the above-mentioned influences can be demonstrated from comparing the respective normalized intensities.

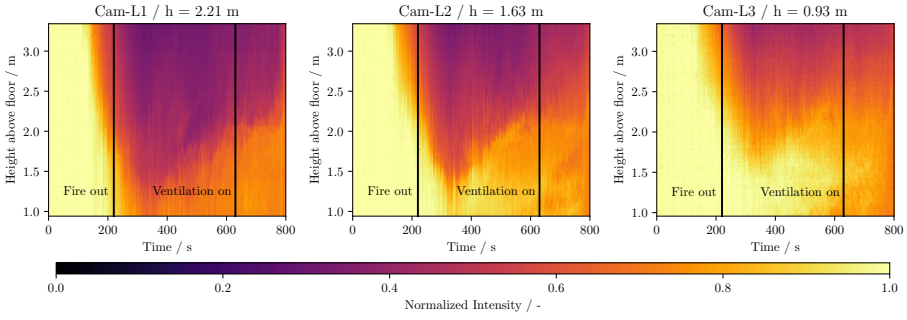

Figure 6: Intensity as a function of height and time, measured on a single RGB LED strip. Cameras are located in the same position in the laboratory at heights of 2.21 m, 1.63 m and 0.93 m above the floor. Data is shown for the red colour channel of the cameras.

Fig. 6 depicts the normalized LEDSA intensities for a TF5 test from all 144 LEDs of the same strip (*LS-1*) as a function of time and height. In the burning period, the descending smoke layer can be observed for each camera, which is characterized by distinctly lower intensities. With maximum depth around the time of flame out, it slightly retreats as mixing occurs with ambient air, and then rapidly draws back when the ventilation is turned on.

Comparing between cameras, the measured intensities decrease across all LEDs when captured from an elevated perspective. Despite a considerably higher optical path, the maximum drop on the top LED, for example, is 77% for *Cam-L1* and 65% for *Cam-L3*. This difference indicates the smoke density increases with height above floor level. Data from *Cam-L3* further reveals that the camera remains outside the smoke until about 200 s after ignition. This allows for a rough estimate on the smoke layer to drop to about 1.5 m. LEDSA is capable to deal with different camera positions and yield similar extinction coefficients, see section 3.3. Yet, it is expected that the intensities measured by the Radiance Method will also be influenced by camera height, though quantifying the impact on the resulting extinction coefficients is future work.

4 Results and Discussion

4.1 Evaluation of Repeatability Using Established Measurement Methods

The overall repeatability of the experiments can best evaluated based on the MIREX readings, as these are expected to provide the lowest measurement uncertainty (see Fig. 7).

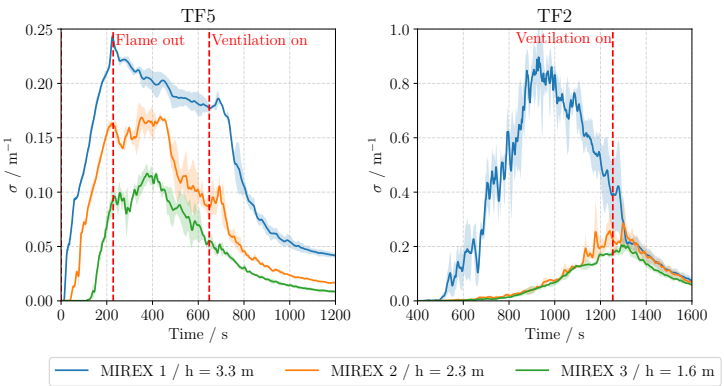

Figure 7: Mean value (solid lines) and ± 1 standard deviation (shaded areas) of the extinction coefficient of 3 TF5 and 3 TF2 tests, smoothed by a 10 s moving average. Measurements were taken by MIREX devices at heights 1.6 m, 2.3 m and 3.3 m above the floor.

For the TF5 tests, the mean extinction coefficient rapidly rises to $0.24\,\mathrm{m}^{-1}$, $0.16\,\mathrm{m}^{-1}$ and $0.10\,\mathrm{m}^{-1}$ for the top, middle and lower MIREX until around flame out at $\sim 220\,\mathrm{s}$. After that, the smoke layer can be observed to gradually settle down, which is evident from a decrease in the extinction coefficient at the top MIREX and an increase at the lower ones. From $\sim 400\,\mathrm{s}$ a steady drop occurs on all MIREX, followed by a spike when the ventilation is turned on at $\sim 620\,\mathrm{s}$ which results from the smoke being extracted close to the ceiling. For the TF2 the top MIREX rises to $0.85\,\mathrm{m}^{-1} \sim 900\,\mathrm{s}$ after the beginning of the heating phase before declining at a similar rate. The top MIREX decreases more rapidly after the fans are turned on $\sim 1{,}200\,\mathrm{s}$. The higher extinction coefficients, relative to the TF5 tests, may be the result of more or different particles and will be the subject of future analysis. The middle and lower MIREX indicate a much lower extinction coefficient, with a maximum peak of $0.28\,\mathrm{m}^{-1}$ and $0.20\,\mathrm{m}^{-1}$ respectively at $\sim 1{,}300\,\mathrm{s}$.

The standard deviation results indicate good reproducibility of the TF5 experiments. Due to thermal dynamics in the burning phase, smoke propagation here is essentially driven by forced convection. With the fire extinguished and the buoyancy subsiding, the environmental boundary conditions start having a stronger effect. The TF2 tests, in contrast, feature considerably higher standard deviations, and thus lower reproducibility. As pyrolysis of the wooden sticks entails negligible heat release, the resulting smoke is driven by low buoyancy. Furthermore, the process is affected by inhomogeneous material properties and certain residual moisture.

4.2 LEDSA and Radiance Method with a Flaming Fire

Alignment of the extinction coefficients derived from LEDSA and the Radiance Methods, compared to the MIREX results, indicates that both methods are generally capable of assessing smoke density in a temporal and spatial context. Fig. 8 shows the extinction coefficient results for a representative TF5 test at the three MIREX heights (3.3 m, 2.3 m, 1.6 m). The red camera channel is analysed for the LEDSA and Radiance Method results in this work, since red light is closest to infrared light of the MIREX. For better comparability, the MIREX extinction coefficient measurements were linearly scaled by the factor $K_{\mathrm{m,(R)}}/K_{\mathrm{m,(IR)}}$ according to Eq. 2 with respect to the peak wavelength of the red LEDs ($\lambda_{\mathrm{R}} = 632\,\mathrm{nm}$) and the MIREX ($\lambda_{\mathrm{IR}} = 880\,\mathrm{nm}$), respectively. However, this scaling factor provides only a coarse approximation since the LEDs do not emit monochromatic light and the emitted spectrum does not correspond to the response spectrum of the cameras.

In general, the LEDSA and Radiance Method extinction coefficients align with the MIREX results, while LEDSA seems to match the smoke dynamics captured by the MIREX more precisely. However, the LEDSA results display fluctuations at the peripheral regions, as expected based on the numerical approach discussed in section 3.3. Indeed, the Radiance Method results are much closer to MIREX and LEDSA results than was expected based on the systematic discrepancies seen in comparison to synthetic data. A major influence that could not be accounted for in the prediction is that the illumination of the contrast boards is reduced via a smoke-induced attenuation of the incident light. Quantifying this influence will be the subject of future work.

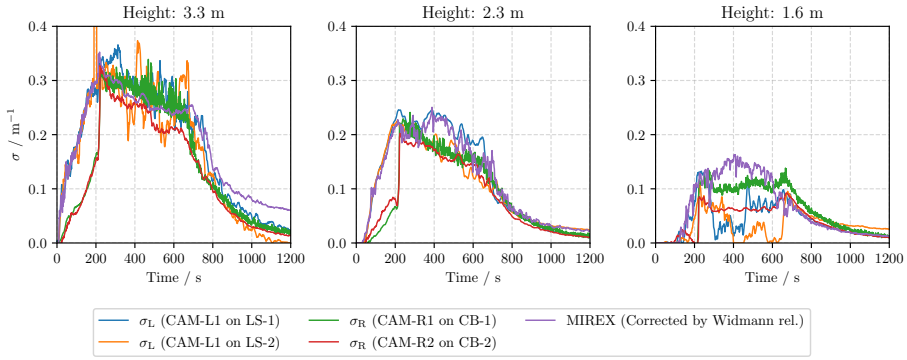

Figure 8: Extinction coefficients of the MIREX, LEDSA and Radiance Method at 3.3 m, 2.3 m and 1.6 m height for the TF5 test, smoothed by a 10 s moving average. The MIREX results are scaled by Eq. 2 according to the wavelength of the red LEDs.

During the burning period, the Radiance Method values fall below the MIREX and LEDSA results at all three heights. This difference was reduced by the applied flame correction, discussed in section 3.1. After flame out, the Radiance Method results are neither consistently above nor below LEDSA and MIREX results. After peaking at the same level around flame out, slightly lower values are measured by *Cam-L1* on *LS-2* and *Cam-R2* on *CB-2* than by *Cam-L1* on *LS-1* and *Cam-R1* on *CB-1* at each of the three heights, respectively. This may indicate an actual inhomogeneity of the smoke stratification. Similar deviations between measurements have already been observed in previous TF5 experiments with LEDSA [11]. Here, a centred LED strip was seen by two cameras to the left and right of the set-up at approximately the same distance.

Both methods show considerable deviations in the measured extinction coefficients compared to the MIREX at the height of 1.6 m after flame out. This can most likely be attributed to this area being in the smoke / ambient air transition zone.

Fig. 9 depicts a height profile of the extinction coefficients from the measurements of the MIREX, the *Cam-R1* and all the three LEDSA Cameras of the same representative TF5 experiment in the burning phase (100 s) and after flame out (300 s and 500 s).

At 100 s, all three measurements indicate minimal smoke below 1.8 m. LEDSA closely matches the MIREX results, with no significant effect of the height of the camera evident in the tomographic model. The results are underestimated by the Radiance Method and feature a differently shaped profile. At 300 s and 500 s LEDSA and the Radiance Method are in good agreement with the MIREX results, and each other, above 1.5 m. Below 1.5 m, there appears to be minimal smoke present in the post-flame, pre-ventilation period. Though, the LEDSA and Radiance Method results differ in this region, with values between ~ 0 and $0.1\,\mathrm{m}^{-1}$. It is likely that the LEDSA results at 300 s indicate a distinct smoke boundary at 1.5 m while the Radiance Method captures a more blurred transition here.

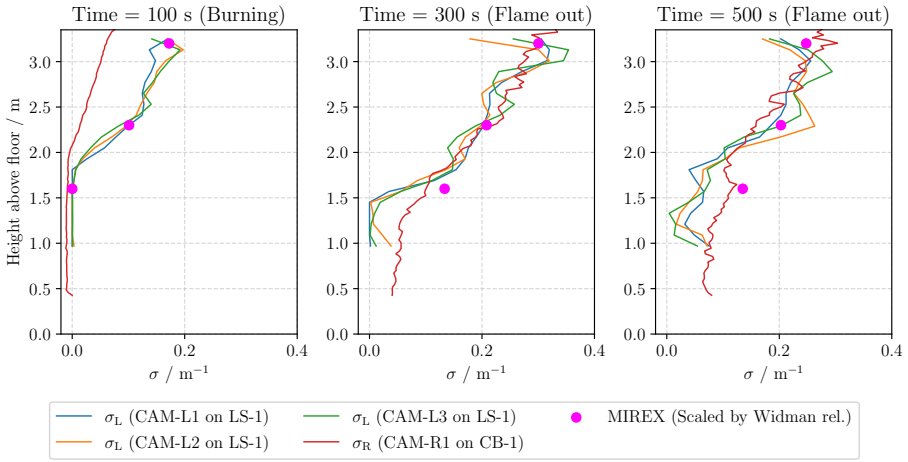

Figure 9: Extinction coefficients of the MIREX, LEDSA and Radiance Method for the TF5 test as a function of height at different times. The MIREX results are scaled by Eq. 2 according to the wavelength of the red LEDs.

4.3 LEDSA and Radiance Method with a Smouldering Fire

Despite being based on experiments involving flaming combustion, Eq. 2 appears to be at least a good approximation for scaling the TF2 MIREX results according to the wavelength of the red LED. Fig. 10 shows extinction coefficient results for a representative TF2 test at the three MIREX heights (3.3 m, 2.3 m, 1.6 m). Again, the red channel is used from the LEDSA and Radiance Method results to minimise MIREX data scaling error.

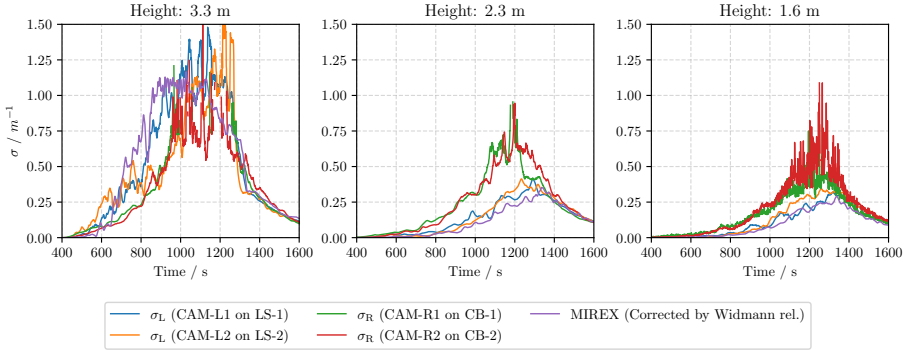

Figure 10: Extinction coefficients of the MIREX, LEDSA and Radiance Method at 3.3 m, 2.3 m and 1.6 m height for the TF2 test, smoothed by a 20 s moving average. The MIREX results are scaled by Eq. 2 according to the wavelength of the red LEDs.

Extinction coefficients measured by LEDSA at heights 2.3 m and 1.6 m closely match the MIREX results, while a significant overestimation by the Radiance Method

can be observed. The head-on exposure of the contrast boards by the LEDs is likely to cause a significant amount of the light to be back scattered from the smoke particles. This influence results in a substantial drop in the contrast on the black and white areas, thus, in an underestimation of the transmittance and overestimation of extinction coefficient. At 3.3 m, the Radiance Method results fall below the MIREX and LEDSA results. However, considerable noise impedes the comparison at the uppermost measurement point. The noise is likely to be related to both the lighting inside the laboratory and the smoke characteristics. As with the TF5 tests, the LEDSA results display more fluctuations in value at the high locations, which is in line with the predicted model uncertainties at the boundary layers, as described in section 3.3.

5 Conclusions and Outlook

In this paper, two photometric measurement methods for the analysis of smoke density were presented and compared under known laboratory conditions. The novel LEDSA and Radiance Methods, involve low-cost setups and, unlike the established MIREX apparatus, target spatially and temporally resolved measurements of light extinction coefficients. LEDSA involves measuring transmission from dedicated light sources such as LEDs by high resolution DSLR cameras. At present, the method is designed for laboratory-scale measurements, rather than for field applications, especially in high-temperature environments. The current (unoptimised) version of LEDSA, requires significant computational effort, practically requiring parallel computation on an HPC (High Performance Computing) system for computing the extinction coefficients. Data analysis using the Radiance Method can be performed on a desktop computer and may therefore allow for real-time measurements in the future. The method was designed to work with low-cost cameras, with resolution proportional to the spatial domain of interest. Examining smoke propagation typically only requires multiple adjacent contrasting light and dark areas within the image which are illuminated by ambient light. However, to determine extinction coefficients comparable with the LEDSA results, contrast boards illuminated by the above-mentioned LEDs were used for the contrast measurements in the conducted experiments.

It was demonstrated that both methods are capable of capturing the dynamics of black smoke such as emerges from the investigated TF5 n-heptane fire. On a temporal and spatial scale, they show good agreement with local measurements from the established MIREX system. In case of white smoke from the TF2 wood smouldering pyrolysis fire, the Radiance Method can provide an indication of the smoke density patterns but not accurate measured values under the given experimental conditions. This can likely be attributed to considerable backscattering of the incident light on the smoke particles, resulting in poor contrast between the light and dark areas on the images. LEDSA, on the other hand, can reproduce the MIREX measurements to a large extent. However, in the peripheral areas of the measurement range, the method partly exhibits increased uncertainty and noise due to the numerical model.

The Radiance Method showed much better accuracy than expected due to the model uncertainty revealed by a synthetic data set. Real experimental data anal-

ysis indicates that the model uncertainties may be competing with factors due to lighting conditions. A more in depth analysis and quantification of influences on the LEDSA and Radiance Methods will be the subject of future work. Analysis of additional TF2 and TF5 experiments will aid in better accuracy quantification. This includes analysis based on the remaining colour channels of the cameras, as well as investigation of different experimental setups.

Declaration of Competing Interest

The authors declare that they have no known competing financial interests or personal relationships that could have appeared to influence the work reported in this paper.

Data Availability

Data will be made available on request.

Acknowledgments

The authors gratefully acknowledge the financial support of the German Federal Ministry of Education and Research and the Natural Sciences and Engineering Research Council of Canada. The extensive LEDSA computations were performed largely on the high-performance computer system funded as part of the CoBra project with the grant number 13N15497.

References

[1] David A Purser and Jame L McAllister. "Assessment of Hazards to Occupants from Smoke, Toxic Gases, and Heat". In: *SFPE Handbook of Fire Protection Engineering*. Ed. by Morgan J. Hurley. New York: Springer, 2016. ISBN: 9781493925643. DOI: 10.1007/978-1-4939-2565-0.

[2] Kevin McGrattan, Simo Hostikka, Jason Floyd, Randall McDermott, and Marcos Vanella. "Fire Dynamics Simulator User's Guide – Version 6.7.9". In: (2022). DOI: 10.6028/NIST.SP.1019.

[3] Tadahisa Jin. "Visibility through Fire Smoke (I)". In: *Bulletin of Japan Association for Fire Science and Engineering* 19.2 (1970), pp. 1–8. ISSN: 0546-0794. DOI: 10.11196/kasai.19.2.1.

[4] M. Pierre Bouguer and William Edgar Knowles Middleton. *Optical Treatise on the Gradation of Light. Translated, with Introduction and Notes, by WE Knowles Middleton*. University of Toronto Press, 1961.

[5] George W. Mulholland and Carroll Croarkin. "Specific extinction coefficient of flame generated smoke". In: *Fire and Materials* 24.5 (2000), pp. 227–230. ISSN: 1099-1018. DOI: 10.1002/1099-1018(200009/10)24:5<227::aid-fam742>3.0.co;2-9.

[6] John F. Widmann. "Evaluation of the planck mean absorption coefficients for radiation transport through smoke". In: *Combustion Science and Technology* 175.12 (2003), pp. 2299–2308. ISSN: 0010-2202. DOI: 10.1080/714923279.

[7] Cerberus. *Ionization measuring chamber MIC Extinction measuring equipment MIREX*. Technical description. 1992.

[8] Kristian Börger, Alexander Belt, and Lukas Arnold. "LEDSA: A Python package for determining spatially and temporally resolved extinction coefficients of fire smoke". In: *Submitted to JOSS, The Journal of open source software* (2023).

[9] Jennifer Ellingham. "Measuring Smoke Evolution at FullScale with Video Recordings". MA thesis. University of Waterloo, 2021.

[10] International Organization for Standardization. *ISO 5659-2, Plastics -Smoke generation -Part 2: Determination of optical density by a single-chamber test.* 2006.

[11] Kristian Börger, Alexander Belt, Thorsten Schultze, and Lukas Arnold. "Remote Sensing of the Light-Obscuring Smoke Properties in Real-Scale Fires Using a Photometric Measurement Method". In: *Fire Technology* 60.1 (2024), pp. 19–45. ISSN: 0015-2684, 1572-8099. DOI: 10.1007/s10694-023-01470-z.

[12] The European Committee for Standardization. *EN 54— Fire detection and fire alarm systems, part 7: smoke detectors point detectors using scattered light, transmitted light or ionization.* 2000.

[13] *Gigahertz Optik BTS256-LED Tester*. Technical description. 2020.

[14] MD Abramoff, PJ Magelhaes, and SJ Ram. "Image processing with ImageJ". In: *Biophotonics Int* 11.7 (2004), pp. 36–42.

[15] Lukas Arnold, Alexander Belt, Thorsten Schultze, and Lea Sichma. "Spatiotemporal measurement of light extinction coefficients in compartment fires". In: *Fire and Materials* (2020). ISSN: 0308-0501. DOI: 10.1002/fam.2841.

[16] E. Fred Schubert. *Light-Emitting Diodes*. Vol. Second edition. New York: Cambridge University Press, 2006. DOI: 10.1017/BO9780511790546.

[17] E.M Patterson, R.M Duckworth, C.M Wyman, E.A Powell, and J.W Gooch. "Measurements of the optical properties of the smoke emissions from plastics, hydrocarbons, and other urban fuels for nuclear winter studies". In: *Atmospheric Environment. Part A. General Topics* 25.11 (1991), pp. 2539–2552. ISSN: 0960-1686. DOI: 10.1016/0960-1686(91)90171-3.

PUBLICATION III

A Waypoint Based Approach to Visibility in Performance Based Fire Safety Design

Note: This article was published as Kristian Börger, Alexander Belt and Lukas Arnold. *A Waypoint Based Approach to Visibility in Performance Based Fire Safety Design.* Fire Safety Journal, 2024. 104269, ISSN 0379-7112, https://doi.org/10.1016/j.firesaf.2024.104269.

Author Contributions

CONCEPTUALIZATION: Kristian Börger, Alexander Belt and Lukas Arnold
METHODOLOGY: Kristian Börger
SOFTWARE: Kristian Börger
VALIDATION: Kristian Börger
FORMAL ANALYSIS: Kristian Börger
INVESTIGATION: Kristian Börger
RESOURCES: Lukas Arnold
DATA CURATION: Kristian Börger
WRITING–ORIGINAL DRAFT: Kristian Börger
WRITING–REVIEW AND EDITING: Kristian Börger, Alexander Belt and Lukas Arnold
VISUALIZATION: Kristian Börger
SUPERVISION: Lukas Arnold
PROJECT ADMINISTRATION: Lukas Arnold
FUNDING ACQUISITION: Lukas Arnold

A Waypoint Based Approach to Visibility in Performance Based Fire Safety Design

Kristian Börger[1 2], Alexander Belt[2] and Lukas Arnold[1 2]

[1] Computational Civil Engineering, University of Wuppertal, Germany
[2] Institute for Advanced Simulation, Forschungszentrum Jülich, Germany

Abstract

In performance based fire safety design, ensuring safe egress, e.g. by visibility of safety signs, is a crucial safety goal. Compliance with the building requirements is often demonstrated by simulations of smoke spread. Numerical models like the Fire Dynamics Simulator generally compute visibility as a local quantity using the light extinction coefficient, without the consideration of the actual light path to a safety sign. Here, visibility maps are introduced, providing an approach for post-processing fire simulation data. They indicate safe areas along egress routes, with respect to visibility. At each location, the available visibility is calculated using Jin's empirical relation, as an integrated value of the extinction coefficient along the line of sight to the closest exit sign. The required visibility results from the distance between those points. Additional parameters like view angle or visual obstructions are considered. The presented method allows for temporal visibility assessment, e.g. in an ASET-RSET analysis.

Keywords: Visibility map; visibility; FDSVismap; computational fluid dynamics; smoke modelling; extinction coefficient; performance based design; ASET-RSET concept; Fire Dynamics Simulator

1 Introduction

Safety signs play a significant role in protecting building occupants by guiding them in the event of an emergency. Design principles of safety signs, incorporating dimensions and colorimetric and photometric characteristics, are internationally standardised in ISO 3864-1 [1]. Additionally, ISO 7010 [2] specifies certain safety signs, including exit signs. Exit signs are intended to ensure a safe egress by clearly indicating the location of the closest emergency exit. Hence, extensive research has been conducted in the past on various aspects that physically or physiologically affect the perception or interpretation of exit signs.

Chen et al. proposed an algorithm to optimise the arrangement of exit signs in public buildings in order to reduce the overall evacuation time [3]. They address the issue of most building codes not providing detailed guidelines or clear standards for placing exit signs. The algorithm is intended to maximise the coverage of the signs

and enhance the evacuation efficiency based on a cellular automaton evacuation model. In an experimental study, Shi et al. investigated the influence of different colours and types of exit signs on the attention and perceptual processing [4]. They conclude that the participants had a longer processing time for red than for green signs. Green signs on the other hand were causing stronger attention bias, which is an indicator for the difference in assigning attention to a certain stimulus when being faced with different stimuli.

The perception of exit signs in case of a smoke induced impairment of visibility was first comprehensively investigated by Jin in the 1970s [5]. From the visual obscuration threshold at which the sign can still be seen, he derived an empirical correlation of the smoke's light extinction coefficient σ and a visible distance (visibility) V. With constant boundary conditions of smoke density, smoke characteristics and ambient lightning, all factors affecting the contrast can be encapsulated by a single visibility factor C, simplifying this correlation to Eq. 1.

$$V = \frac{C}{\sigma} \tag{1}$$

For white smoke, as employed in his experiments, he found C to be $2 \sim 4$ for light reflecting signs and $5 \sim 10$ for light emitting signs. In subsequent studies, Jin examined the validity of this correlation for different types of smoke resulting from flaming combustion (black smoke) or smouldering (white smoke). He observed that at the same smoke density, black smoke allows for a greater visibility than white smoke [6]. Further research involving an actual exposure of participants with smoke revealed that visibility is significantly reduced by eye irritating effects when the smoke density exceeds a certain threshold. Impaired vision can result in psychological and physiological effects, like a decrease in walking speed [7].

In another study [8], Jin conducted measurements of the extinction coefficient at different wavelengths. At the beginning of the experiments, the extinction coefficient decreases with a higher wavelength in the visible range of light. With a dependence on the soot particle size distribution, the effect can change and even reverse with time due to the ageing effects of the aerosol. From these insights, he derived that the visibility for red and blue signs differs: the visibility for red signs within smoke with predominantly scattering properties (white smoke) is 20 - 40% higher, and within predominantly absorbing smoke, it is 20 - 30% higher. These conclusions have been drawn by directly correlating the extinction coefficient with visibility, rather than conducting separate investigations. The underlying assumption is that both signs have identical brightness and obscuration thresholds to be perceived. A different approach to assess visibility as a function of exit signs' colour was followed by Oh et al. [9]. They simulated a smoke-filled environment by having study participants wearing translucent eye patches featuring nine different levels of visual obstruction. Contrasting to Jin's conclusions, the visible distance at which exit signs were still detectable was significantly higher for blue signs than for red and green signs. Although the experiments did not take into account the wavelength-dependent characteristics of the fire smoke, a significant effect of colour on the perceived contrast and thus visibility can be drawn from their observations.

Jin's relation is still widely used to assess visibility in performance based fire safety design. It also serves as a standard model in numerical fire models such as the Fire

Dynamics Simulator (FDS). The model allows a temporally and spatially resolved output of the local visibility, as a function of the respective extinction coefficient. Awadallah et al. state that the interpretation of visibility on simulation data such as horizontal slices of the computational domain can be highly subjective when evaluated by different engineers [10]. They also note that Jin's analytical model was originally developed for the assessment of visibility in homogeneous smoke and should be used carefully on non-uniform smoke environments. Hence, they propose a numerical approach for averaging in the evaluation of visibility. The concept of an averaged extinction coefficient is also applied by Rinne et al. to evaluate the visibility of exit signs through an inhomogeneous smoke layer based on FDS simulation data [11]. Węgrzyński et al. propose a similar approach involving ray tracing for a more realistic assessment of visibility in the context of CFD (Computational Fluid Dynamics) simulations [12].

Husted et al. presented a model that allows considering an inhomogeneous smoke distribution when assessing visibility based on CFD simulations in the context of performance based design [13]. By applying a procedure for averaging the smoke density, their model allows to evaluate visibility with respect to the view point and viewing direction. Compared to a local or cell-based assessment of visibility, the approach allows indicating more realistically if an object would be recognisable in a real fire event. However, the model predominantly aims at the assessment of visibility in concise, single compartment geometries and thus may be unsuitable for evaluating escape scenarios in complex building structures.

In his PhD thesis [14], Zhang proposed an approach to create floor maps by assessing visibility via synthetically generated image data. The images were created from different view points on a regular grid, considering the smoke distribution and spanning the computational domain of a CFD fire model. In this context, a model was developed to measure visibility of objects as a function of contrast, brightness, and colour. The applied methodology to create photorealistic synthetic images from fire simulation data considering absorption and scattering phenomena on smoke particles was introduced by Rubini et al. [15].

In this study, an innovative method is presented to assess visibility in performance based design, utilising data from numerical fire models. The approach is designed for ease of application, providing a clear and realistic interpretation of visibility, even in complex building designs. It adopts Jin's relation for scenarios with inhomogeneous smoke distributions, as derived from CFD simulation results. A waypoint-based approach is introduced to evaluate visibility along the entire route of egress. These waypoints, representing exit signs, serve as key reference points for computing the maximum visual distance through fire smoke from the surrounding areas. A simple ray casting algorithm is applied to compute the averaged extinction coefficient along the line of sight. Finally, this process results in the creation of visibility maps. Visibility maps describe a two-dimensional matrix of binary values, providing a localised indication of whether the next exit sign is visible at every point along the route of egress.

Visibility maps enable a more realistic and distinct assessment of egress in case of fire, considering smoke induced reduction of visibility. No performance criteria need to be defined due to the automated consideration of the building's architectural

characteristics. Consequently, the personal bias in the interpretation of simulation results is significantly reduced, resulting in increased credibility in the approval process for building designs.

2 Visibility in Performance Based Design

Performance based design provides an alternative approach to applying prescriptive building regulations within the process of building approval. The SFPE Engineering Guide to Performance-Based Fire Protection [16] and the Interpretative Document Fire Safety of the European Commission [17] follow a similar definition of performance based design in fire safety as the engineering approach to satisfy fire safety goals and objectives. The primary safety goals of most national building codes, such as NFPA 101 [18], address the health of building occupants while ensuring safe egress in hazardous events. While fire safety goals usually represent fundamental requirements, they are specified by means of objectives to be met. This might include the structural integrity of the route of egress, limiting the occupants' exposure to toxic smoke products, or ensuring sufficient visibility in a smoke laden environment.

Prescriptive regulations typically require designated architectural, structural, technical, or operational measures to meet these objectives. Especially in modern buildings, characterised by a complex or open architectural designs, meeting these requirements can often be challenging or involve disproportionate efforts. Therefore, methods of performance based design are increasingly being utilised in fire safety engineering, to meet the specific needs of the building and its occupants. In this context, the objectives of the building regulations to be met are quantified as performance criteria that provide a threshold for compliance. Several national building codes, such as Switzerland [19], New Zealand [20], or the USA [18], natively implement performance based design and offer compliance with specific performance criteria as an alternative to satisfying prescriptive requirements.

In performance based fire safety design, evaluating a building design usually involves hazard calculations and fire dynamics calculations based on a predefined design fire scenario [21]. According to ISO 13943 [22] a fire scenario is defined as a "qualitative description of the course of a fire with respect to time, identifying key events that characterise the studied fire and differentiate it from other possible fires". From the chosen design fire scenario, the design fire can be derived, which is a "quantitative description of assumed fire characteristics". It typically reflects the temporal variation of key variables such as heat release rate (HRR), smoke production rate and the yields of toxic smoke products. Selecting relevant design scenarios from all potential scenarios may be conducted by either a deterministic or probabilistic approach. In contrast to consider "worst-case" scenarios, it should be aimed to select credible yet conservative scenarios, associated with the highest risk. This process may employ fully quantitative methods according to ISO 16732-1 [23] or qualitative or semi-quantitative approaches according to ISO 16733-1[24].

Significant uncertainties in the context of performance based design result from the input variables of fire models, in particular from the defined design fire scenario. Johanssen et al. have shown in a round-robin study among fire safety engineers that significant discrepancies can occur in modelling a fire in FDS, even when the scenario

is described in a high level of detail. Besides different assumptions, mistakes, insufficient knowledge about the software, they identified insufficient knowledge about fire dynamics as the biggest source of uncertainty [25].

Visibility in case of fire constitutes a central objective to ensure successful egress of buildings occupants. It depends on the irritant effect and the smoke density, having physiological and psychological effects on the evacuees. This inherently affects both their walking speed and the ability of way finding [26]. For buildings with high ceilings, like industrial facilities, the proof of safe egress can usually be provided by estimating the height of a low-smoke layer above the floor level. This simultaneously limits both excessive thermal stress and people's exposure to toxic smoke products. However, such evidence may be complicated to provide, especially in buildings with complex geometries, e.g. featuring a multi-storey spanning open design. In such cases, evaluating the actual impairment of visibility due to fire smoke may be advisable.

Proof of safe egress due to visibility based on numerical fire simulation models is usually conducted at a temporal level. In this context, the available time after the outbreak of the fire is determined until a route of egress is no longer passable and thus self-rescue is no longer possible. The evidence is provided if the Available Safe Egress Time (ASET) is greater than the Required Safe Egress Time (RSET) [27]. RSET can be specified as a global performance criterion or individually derived from an evacuation simulation, as outlined in [28].

Various tenability criteria for the minimum visibility required for a successful escape can be found in the literature. Those are subject to considerable scattering and depend largely on both the buildings and the occupants' characteristics. Short visible distances to emergency exits, for example, may require less stringent thresholds if the occupants are familiar with the building. Negative influences include poor lighting conditions, complex geometries, and expansive spaces [29]. Jin found visibility limits for occupants to be 4 m if they were familiar and 13 m if they are not familiar with the facilities [30]. Rasbash suggested a tenability criterion of 10 m for safe escape [31]. German building regulations refer to DIN 18009-2 [32] and vfdb guidelines [33], specifying a minimum visibility of 10 m to 20 m. Jin notes that wide variations in the proposed threshold values are probably due to differences in the geometry of the places and the composition of the group escaping from fire in the respective experimental investigations [26].

3 Visibility Maps

3.1 General Concept

The goal of visibility maps is to assess the accessibility of potential routes of egress and evacuation for building occupants in the presence of fire induced smoke. In the context of a performance based design, when numerical fire simulations are employed, visibility maps can become part of the building approval process. This makes it particularly important for the maps to be easily interpreted even by people without professional qualification.

Visibility maps represent building floor plans as Boolean matrices $M_{i,j}$ shaped in the same dimensions as the corresponding simulation mesh-grid. They label locations with physical Cartesian coordinates X_i, Y_j as safe (1 or True) or unsafe (0 or False) to walk through, with respect to sufficient visibility for safe egress. Here, i and j represent the two-dimensional indices of the cells, representing the walkable area. Only indices representing "agent cells" that are accessible to persons (agents in the sense of simulation) and are not populated by architectural elements are considered in the evaluation.

Visibility at a given location is calculated according to Jin's relation (Eq. 1), although it is not considered to be a local quantity. Here, an effective or averaged value of the extinction coefficient is computed in the line of sight between the viewpoint and an observed target to consider an inhomogeneous smoke distribution. Likewise, the required visibility automatically results from the distance between the viewpoint and the target. In accordance with Jin's relation, reflecting or light emitting safety signs are considered as such targets. The location and characteristics of the n exit signs along potential routes of egress are subsequently described as waypoints W_k with $k \in \{1, \ldots, n\}$.

Nomenclature note: The visibility map $M_{i,j}$ is subsequently used with different additional indices, indicating if it is waypoint and/or time related, see the summarising Table 2 in Appendix A further on. According to Eq. 2, the visibility map $M^t_{i,j,k}$, i.e. at a given time t for the waypoint W_k, is obtained by matching the available visibility ($V^t_{i,j,k}$) against the required visibility ($L_{i,j,k}$) for all agent cells i, j.

$$M^t_{i,j,k} = \begin{cases} 1, & \text{if } V^t_{i,j,k} \geq L_{i,j,k} \\ 0, & \text{otherwise} \end{cases} \tag{2}$$

$L_{i,j,k}$ denotes the Euclidean distance according to Eq. 3 between the observed exit sign at waypoint W_k with Cartesian coordinates X_k, Y_k and the agent cell i, j with Cartesian coordinates X_i, Y_j in the evaluation level.

$$L_{i,j,k} = \sqrt{(X_i - X_k)^2 + (Y_j - Y_k)^2} \tag{3}$$

An exemplary visualisation of the distance matrix $L_{i,j,k}$ is shown in Fig. 1a. The distance is only calculated in the observation plane and ignores any vertical height difference between the observer and the exit sign. In particular, for large distances, the resulting error is assumed to be negligible due to the small difference of lengths at narrow viewing angles.

$V^t_{i,j,k}$ (see Eq. 10) is the visibility based on the integrated extinction coefficient along the same visual axis.

The time dependent visibility map $M^t_{i,j}$ is derived from the superposition of all $M^t_{i,j,k}$ using a logical OR operation, as described in Eq. 4. The $M^t_{i,j,k}$ values are calculated independently for individual waypoints W_k. In this manner, all agent cells i, j within the route of egress are marked passable if at least one exit sign is visible from there.

$$M^t_{i,j} = \bigvee_{k=1}^{n} M^t_{i,j,k} \tag{4}$$

Thus, $M_{i,j}^t$ denotes a discrete temporal state of the visibility map, but can be further aggregated across a predefined set of time points T of the fire simulation, see Eq. 5. The time aggregated visibility map $M_{i,j}$ accordingly indicates whether the agent cells i, j satisfy the visibility criterion according to Eq. 2 corresponding to the respective waypoints W_k at each point in time $t \in T$.

$$M_{i,j} = \prod_{t \in T} M_{i,j}^t \tag{5}$$

The above approach provides several advantages over the traditional assessment of visibility solely based on the local smoke density. First, the visibility factor C in Jin's relation was empirically derived by experimentally evaluating people's perception of exit signs in a smoke laden environment. Accordingly, any such signs must also be taken as a reference when applying the model in performance based design approaches based on numerical fire simulations. Furthermore, the approach also allows taking into account further aspects, such as the viewing angle or visual obstructions between the exit sign and the observer. Last, it does not rely on predefined performance criteria, as these emerge intrinsically from geometric features of the compartment.

Generating visibility maps involves moderate computational effort and simply demands post-processing of simulation results from numerical field models. For this purpose, spatially and temporally resolved information of smoke density or the extinction coefficient can be used. The analysis is conducted by means of the Python package FDS*Vismap* [34], which was developed by the authors and is made freely available. Here, the required data is extracted from horizontal FDS slice files (in the global z-plane), providing a transfer file format for visualising simulations results on planar cuts through the domain in the FDS post-processor software Smokeview [35]. Employing the FDSReader, the data is transferred into two-dimensional NumPy arrays [36] according to the dimension of the underlying mesh-grid. The FDSReader is a Python package for extracting multiple kind of results data from binary output files of FDS simulations.

For simplicity, the occupant's eye level is considered to be at the same height above the floor as the exit signs. Thus, the integration of the extinction coefficient along the visual axis is reduced to a two-dimensional level. Accordingly, the required extinction coefficient or smoke density is extracted from a single slice data at a height of 2 m above the floor level. This simplifies the actual three-dimensional configuration, as in general the perceiving eye and the perceived sign are not at the same height. Additionally, this reduces the amount of data needed, as no volumetric data of the smoke density is needed. Yet, these are only technical limitations and can be addressed in future implementations using the proposed methodology and techniques.

Multiple visibility maps $M_{i,j}^t$ may also contribute to the creation of ASET maps, like suggested in [28]. Following the ASET-RSET concept, ASET maps locally indicate the time when a specific performance criterion is first met or exceeded. For this purpose, local scalar quantities such as temperature, gas concentrations or visibility can be employed. ASET maps can likewise be created by first generating visibility maps for every point in time $t \in T$ within the observation period. In a

"first order" ASET map, for a given set of points in time T, each agent cell i, j is assigned the time t at which the criterion according to Eq. 2 is not met for the first time (see Eq. 6). "First order" in this context refers to the respective times only indicating when the corresponding exit sign is no longer visible. Higher-order ASET maps could potentially take into account the entire route of egress. This would imply manually or automatically identifying route decisions and tracking for every potential origin agent cell. Especially in crowded areas involving a large number of agents or in case of dynamic fire events, a supplementary evacuation simulation may be required for this purpose. A detailed elaboration of this concept will be the subject of future work.

$$\mathrm{ASET}_{i,j} = \min\left\{t \mid M^t_{i,j} = 0, t \in T\right\} \tag{6}$$

The processing sequence to compute time aggregated visibility maps or ASET maps from the given input parameters is summarised in the program flowchart in Fig. 12 in Appendix B, while the following subsections provide further details about the procedure. Finally, it should be noted that processing data with high spatial (CFD grid) and temporal (number of evaluated points in time) resolution can take a considerable amount of time. Hence, it may be advisable to reduce the temporal increment outside critical periods of observation. This equally applies to the computation of time aggregated visibility maps and ASET maps.

3.2 Model Parameters and Variables

Waypoint parameters as well as the time points to be evaluated are defined detached from the imported fire simulation result data. A description of the required parameters and their respective data types and units is given in Table 1. The angles and physical coordinates refer to a global Cartesian coordinate system with the same origin and discretization as the underlying fire simulation model.

Table 1: Summarised description of the employed model parameters with their data types and units

Parameter	Type	Unit	Description
T	List	-	Set of points in time t to be evaluated
W_k	Integer	-	Identifier of a waypoint
X_k, Y_k	Float	m	Physical Cartesian coordinates of the waypoint W_k
C_k	Float	-	Visibility factor for the waypoint W_k, referring to the illumination type of the exit sign (usually $C = 3$ for reflecting signs and $C = 8$ for light emitting signs)
α_k	Float	°	Rotation angle of the exit signs' observation normal at waypoint W_k in the global coordinate system

All variables required to generate the visibility maps and ASET maps are described in Table 2 in Appendix A. This data is either loaded from the simulation

results or computed by means of simple mathematical or logical operations, taking into account the pre-defined waypoints. Most of these variables represent two-dimensional matrices of the same shape and extent as the fire simulation results data.

A detailed explanation of the employed mathematical and physical models is provided below. The variables labelled with subscript k are computed individually for each waypoint W_k. For reasons of computational efficiency, any computational operations will only be performed on agent cells i, j within a radius corresponding to the maximum visibility $V_{\max}$ (usually 30 m) around W_k.

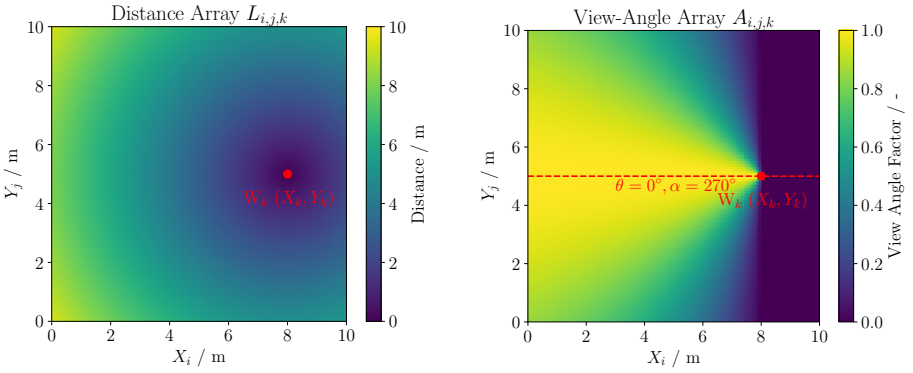

Figure 1: Exemplary visualisation of the distance matrix $L_{i,j,k}$ (b) and view-angle matrix $A_{i,j,k}$ (a) for the waypoint W_k as a function of the Cartesian coordinates X_i / Y_j of the agent cells i, j.

Viewing Angle

The observation of signs at a certain angle, different from the normal, reduces its effective area of projection. Accordingly, the physical distance at which they can be perceived is reduced. Reflective or light-emitting exit signs can be considered as Lambertian radiators, although this assumption is highly simplified depending on the sign's light source and surface. Hence, the visual distance is assumed to decrease by $\cos\theta$ with increasing view-angle θ to the sign [1]. This effect is represented by $A_{i,j,k}$ (see Eq. 7), considering that the sign can not be seen at view-angles $\theta \geq 90°$ ($\cos\theta \leq 0$). Calculating $\cos\theta$ involves the dot product of the sign's surface normal and the observer's visual axis, as well as the observation distance $L_{i,j,k}$. Fig. 2 provides an illustration of the involved orientation angles in the global coordinate system.

$$A_{i,j,k} = \max\left(0, \frac{\sin(\alpha_k) \cdot (X_i - X_k) + \cos(\alpha_k) \cdot (Y_j - Y_k)}{L_{i,j,k}}\right) \tag{7}$$

$A_{i,j,k}$ reduces the maximum intensity relative to the observation normal of the respective exit sign as seen from cell i, j. Given the linear relationship between light

transmission and the original intensity as stipulated by the Beer-Lambert law [37], this approach remains justified even when smoke is present in the observer's line of sight. An exemplary visualisation of the view-angle matrix $A_{i,j,k}$ is shown in Fig. 1b.

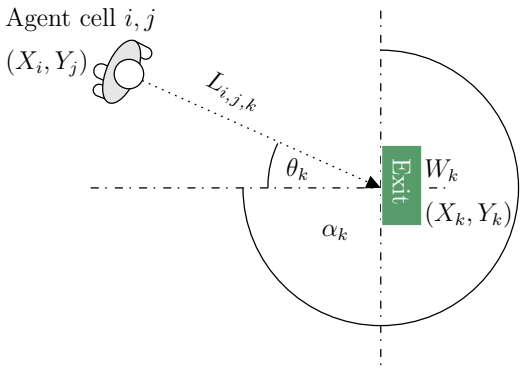

Figure 2: The projection surface of the exit sign being observed changes according to the viewing angle θ. θ can be described as a function of the orientation of the sign in the global z-plane, expressed by the rotation angle α_k, and the viewer's position at the agent cell i, j.

With the two-dimensional approach followed here, only the horizontal angle between the observer and the exit sign can be taken into account. However, since exit signs are usually located above the emergency exit doors and consequently, above the evaluation level, the approach entails a particular though minor degree of uncertainty. Incorporating the dependency of vertical viewing angles requires a spatial approach and will be the subject of future work.

Visual Obstruction

The visual obstruction of waypoints due to architectural elements is considered by the Boolean matrix $U_{i,j,k}$. For this purpose, an auxiliary Boolean type matrix $O_{i,j}$ is first created in the shape of the simulation mesh-grid. In this, all cells are marked that are populated by a building component at the height of the observation plane.

Detecting concealed cells, requires casting a ray from the waypoint to the individual cells to determine the collision coordinates with the obstruction cells. To obtain the number and location of the traversed cells until the collision point, the line of sight between the waypoint and the cells needs to be rasterised according to the respective mesh-grid. For this purpose, a simple drawing algorithm like the Bresenham's line algorithm [38] can be employed. In $U_{i,j,k}$ all cells $p \in P_{\text{cells}}$ along the line of sight are labelled as unconcealed (1, True) or concealed (0, False) when viewed from the waypoint W_k depending on their location before or behind the first collision with an obstruction cell. In order to reduce the number of cast rays and hence the required computational steps, only the edge cells of the mesh-grid are targeted in this process. An exemplary illustration of the ray casting procedure is given in Fig. 3.

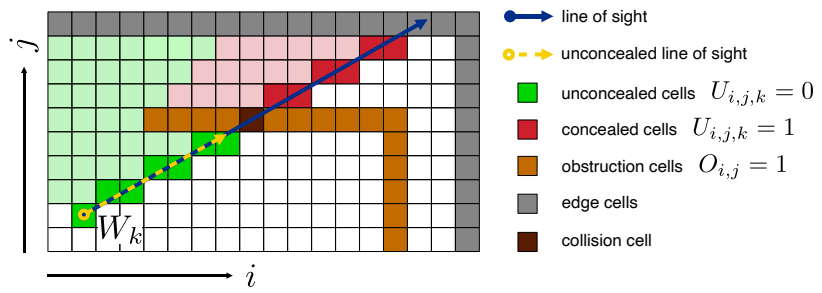

Figure 3: A ray casting algorithm is first employed to detect agent cells i, j that are concealed by obstruction cells. The line of sight between the waypoint W_k and the edge cells is rasterised by the Bresenham's line algorithm or an advanced algorithm involving anti-aliasing. In the next step, the algorithm is employed to identify all cells that are considered in computing the average extinction coefficient $\bar{\sigma}_{i,j,k}$ between the waypoint $\mathrm{W_k}$ and all unconcealed agent cells i, j. The domain is discretised in the same shape as the numerical grid of the fire simulation.

Collision detection can become unreliable if adjacent obstruction cells do not form an entirely closed barrier, since the line algorithm only draws a single cell staircase. Here an anti-aliasing technique, like introduced in [39] is employed to draw lines with a thickness of more than one cell. Such algorithm is computationally more complex than the Bresenham line algorithm, but is reasonable fast for the given application. The effect of applying an advanced line algorithm is illustrated by the visualisation of the matrix $U_{i,j,k}$ in Fig. 13 in Appendix C.

Available Visibility

Visibility according to Eq. 1 is primarily a function of the extinction coefficient σ of the (fire generated) smoke between the observer and a visual target. In general, σ can be expressed as a function of smoke mass density ρ_s and a mass specific extinction coefficient K_m. The latter indicates the contribution of the smoke to light extinction through absorption and scattering per unit mass. In compliance to the laws of classic electrodynamics K_m is a function of the wavelength λ of the incident light. A uniform value of $K_\mathrm{m} = 8{,}700\,\mathrm{m^2\,kg^{-1}}$ for red light at $\lambda = 633\,\mathrm{nm}$ is widely adopted for proof of visibility in performance based fire safety design, as it is the default value of many fire models. It was derived from experimental investigations involving 29 different fuels with well ventilated flaming combustion [40].

Assuming a uniform value for K_m, however, smoke density usually exhibits a temporal and spatial dependence. Given the general form of Beer Lambert's law, an effective or average extinction coefficient between the agent cell i, j and the waypoint W_k can be computed for penetrating an inhomogeneous medium at every time t by Eq. 8. Here $\rho^t_{\mathrm{s},k}(l)$ denotes the smoke density along the line of sight at the traversed distance l towards the waypoint W_k at time t. A similar approach to compute the

mean extinction coefficient along the visual path from a camera to an exit sign crossing an inhomogeneous smoke layer is followed by Rinne et al. [11].

$$\bar{\sigma}^t_{i,j,k} = \frac{K_\mathrm{m}(\lambda) \cdot \int_0^{L_{i,j,k}} \rho^t_{\mathrm{s},k}(l)dl}{L_{i,j,k}} \tag{8}$$

Eq. 8 can be simplified to Eq. 9, assuming that the covered distance in all traversed cells $p \in P_\mathrm{cells}$ is identical, so that calculating the path increments can be omitted. Thus, σ can be calculated directly as the arithmetic mean, depending on the number of traversed cells $|P_\mathrm{cells}|$. This approximation significantly reduces the algorithm's complexity and the associated computational effort, while any loss in accuracy remains tolerable, given a sufficiently fine discretisation of the floor. Further optimisation is achieved by applying the algorithm exclusively to unconcealed cells, i.e. where $U_{i,j,k} \equiv 1$.

$$\bar{\sigma}^t_{i,j,k} = \frac{K_\mathrm{m}(\lambda)}{|P_\mathrm{cells}|} \cdot \sum_{p \in P_\mathrm{cells}} \rho^t_{\mathrm{s},k,p} \tag{9}$$

The available visibility $V^t_{i,j,k}$ of agent cells i, j at time t with respect to the waypoint W_k can be calculated according to Eq. 10.

$$V^t_{i,j,k} = \min\left(U_{i,j,k} \cdot A_{i,j,k} \cdot \frac{C_k}{\bar{\sigma}^t_{i,j,k}}, V_\mathrm{max}\right) \tag{10}$$

In performance based design, visibility is often limited to an arbitrary upper boundary value of $V_\mathrm{max} = 30\,\mathrm{m}$, since Jin's relation is purely empirical and would imply an infinite visibility in the absence of smoke. Furthermore, the exit signs have a maximum visual distance even in a smoke-free environment.

4 Application Example

4.1 Design Fire Scenario

The concept of visibility maps outlined above is demonstrated by means of a basic application example featuring a small office facility with dimensions of approximately $20\,\mathrm{m} \times 10\,\mathrm{m}$, see Fig. 4. All rooms have a ceiling height of 3 m, and the foyer has a ceiling height of 4 m. As shown in Fig. 5, the buildings' geometry is mapped to a simple FDS model by discretising the computational domain with a uniform grid based on 8 meshes. In the context of a grid sensitivity analysis (see Appendix D), a total of 3 cases with cubic cells of 5 cm, 10 cm and 20 cm edge lengths are examined. It should be noted that this study does not provide an isolated examination of the discretisation of the CFD model and the ray casting procedure.

This example focuses on the assessment of unaided egress by the building's occupants. Accordingly, the design fire scenario is defined based on recommendations of the German VDI 6019 [41, 42] for an initial stage fire. The design fire assumes a linear increase of the heat release to $\dot{q}''_\mathrm{max} = 100\,\mathrm{kW}$ within 300 s followed by a constant progression on a constant burning area of $0.4\,\mathrm{m}^2$. The fuel is considered to

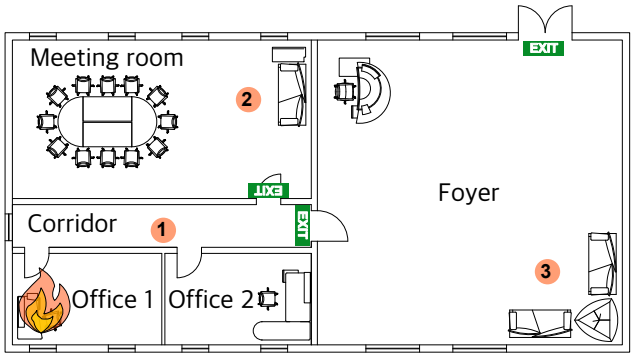

Figure 4: Floor plan of the office facility with dimensions of approximately 20 m × 10 m. All rooms have a ceiling height of 3 m, and the foyer has a ceiling height of 4 m. The design fire is located in Office 1. Exit signs are located in the meeting room, corridor, and foyer as marked with orientation facing inside the respective rooms. Locations 1 – 3 (red circles) denote exemplary sampling points that are considered for a study on grid sensitivity.

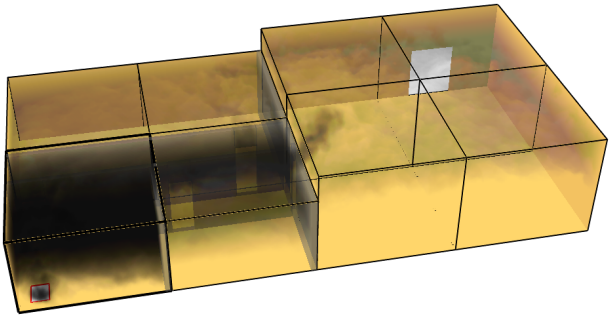

Figure 5: Smokeview visualisation of the FDS simulation model showing the spread of fire generated smoke at $t = 300\,\mathrm{s}$. The computational domain is discretised by a uniform grid based on 8 meshes. The mesh boundaries represent the compartment enclosure, while the inner walls and doors are modelled as obstructions and holes.

be heptane, with a heat of combustion of $\Delta h_\mathrm{c} = 44.6\,\mathrm{MJ\,kg^{-1}}$ and a soot yield of $y_\mathrm{s} = 0.037$, according to the SFPE Handbook of Fire Protection Engineering [43], assuming well ventilated combustion. The soot yield was adapted to $y_\mathrm{s} = 0.04$ as a recommended value following ISO 13571 [44] for a typical plastic fire, applicable for performance based design proof of visibility in case of fire. The soot mass flux, introducing the combustion products in the computational domain, is given by Eq. 11.

$$\dot{m}''_{\mathrm{f,s}} t = \frac{\dot{q}'' t}{\Delta h_\mathrm{c}} \cdot y_\mathrm{s} \tag{11}$$

In order to create the visibility maps, the spatio-temporal values of $\sigma_{i,j}^{t}$ are read from a single z-plane slice. $\sigma_{i,j}^{t}$ is as a function of the smoke density $\rho_{\mathrm{s},i,j}$ and the mass specific extinction coefficient K_{m}, which is set to $8{,}700\,\mathrm{m^2\,kg^{-1}}$.

The Python code for processing the fire simulation data by using the FDSVismap package is given in the GitHub repository [34].

4.2 Results and Discussion

Figure 6 illustrates the challenges in interpreting visibility results as a direct output of a fire simulation. It exemplarily shows the local visibility according to Eq. 1 for a visibility factor of $C = 3$, 400 s after the fire breakout.

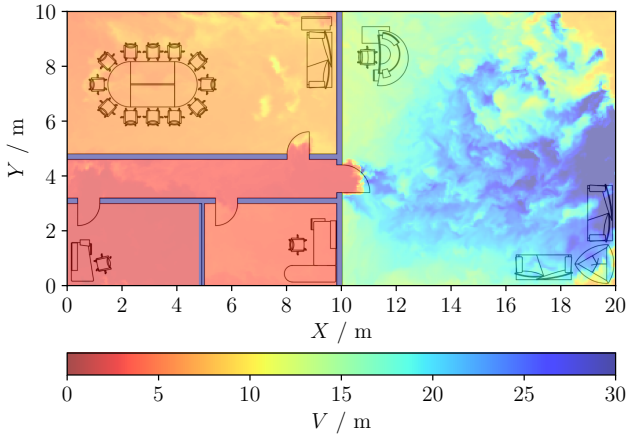

Figure 6: Visualisation of the FDS Slice with quantity `VISIBILITY` at $t = 400\,\mathrm{s}$, 2 m above the floor. The simulation has a uniform 5 cm mesh-grid. Visibility was calculated with $C = 3$ and truncated at a maximum boundary of 30 m.

Fig. 7 indicates that the chosen performance criterion, e.g. $V \geq 10\,\mathrm{m}$ is only extensively met in the foyer. However, analysing and visualising the same scenario ($C_k = 3$ for all W_k, $t = 400\,\mathrm{s}$) by means of visibility maps results in a different assessment of the escape routes.

In Fig. 8, the visibility matrices $V_{i,j,k}^{t}$ according to Eq. 10 at the same time ($t = 400\,\mathrm{s}$) are shown for waypoints W_1 - W_3. The visibility map can subsequently be obtained by matching the available and required visibility (see Eq. 2) and aggregating $M_{i,j,k}^{t}$ for all W_k according to Eq. 4. The visibility map (see Fig. 9) reveals that the corridor and foyer may be safely accessible by people escaping from the meeting room, while they might not see the exit sign inside the room. The primary distinction lies in the visibility map incorporating the actual boundary conditions and constraints throughout the designated escape route. The viewing angle significantly influences the perception of the exit sign, making it not visible in large parts of the meeting room. Conversely, for the considered escape scenario, a limited visibility is deemed acceptable in the corridor due to the shorter distance over which it is traversed.

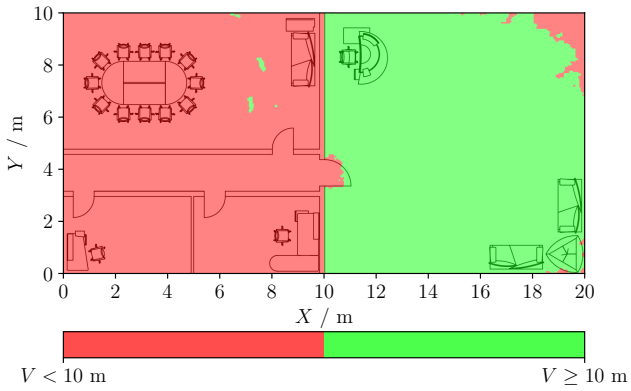

Figure 7: Map based on an FDS slice with quantity `EXTINCTION COEFFICIENT` at $t = 400\,\mathrm{s}$, $2\,\mathrm{m}$ above the floor. The simulation has a uniform $5\,\mathrm{cm}$ mesh-grid. Colours locally indicate if the visibility is above or below the chosen performance criterion of $V_{\mathrm{min}} = 10\,\mathrm{m}$. A global visibility factor of $C = 3$ was chosen for all cells.

Fig. 10 shows a visibility map based on the same data but with a visibility factor of $C = 8$ applied (recommended value for light emitting signs) for all exit signs. The map reveals that, to a large extent, conditions for safe egress in terms of visibility can be satisfied for occupants in the meeting room. However, it is important to note that this should not be considered as a comprehensive proof of safety. Due to potentially high local concentrations of smoke, individuals may be affected by other factors, such as eye irritation or reduced movement speed. Additional evidence may be required to ensure that tenable exposure to toxic smoke components is not exceeded.

Each of the visibility maps in Figs. 9 and 10 present $M^t_{i,j}$ at discrete points in time, but with different values of C. An aggregated analysis spanning multiple temporal intervals may be advisable when the design fire scenario encompasses dynamic events that potentially affect smoke propagation. Such events could include opening and closing of doors and windows, as well as the operation of systems for natural or mechanical smoke extraction. Furthermore, automatic or manual fire suppression will consequentially affect the course of the fire.

Significant differences in the interpretation of local and path wise integrated visibility also become apparent in the representation as ASET maps (see Fig. 11) according to Eq. 6. Both maps each are based on a visibility factor of $C = 3$ for all exit signs. For the local ASET map, a lower visibility limit of $10\,\mathrm{m}$ was defined. In case of the ASET map based on visibility maps, the required visibility is geometrically derived from the distances to the respective exit signs. Accordingly, both maps can only be compared on a qualitative level. The visibility map based ASET map indicates, certain areas of the floor plan do not have sufficient visibility even at time $t = 0$. This primarily results from these areas being geometrically concealed from the exit signs. Hence, a critical interpretation by the user is required in such cases. Summarising, it can be noted that neither of the approaches can be generally considered as conservative. However, both the time aggregated visibility

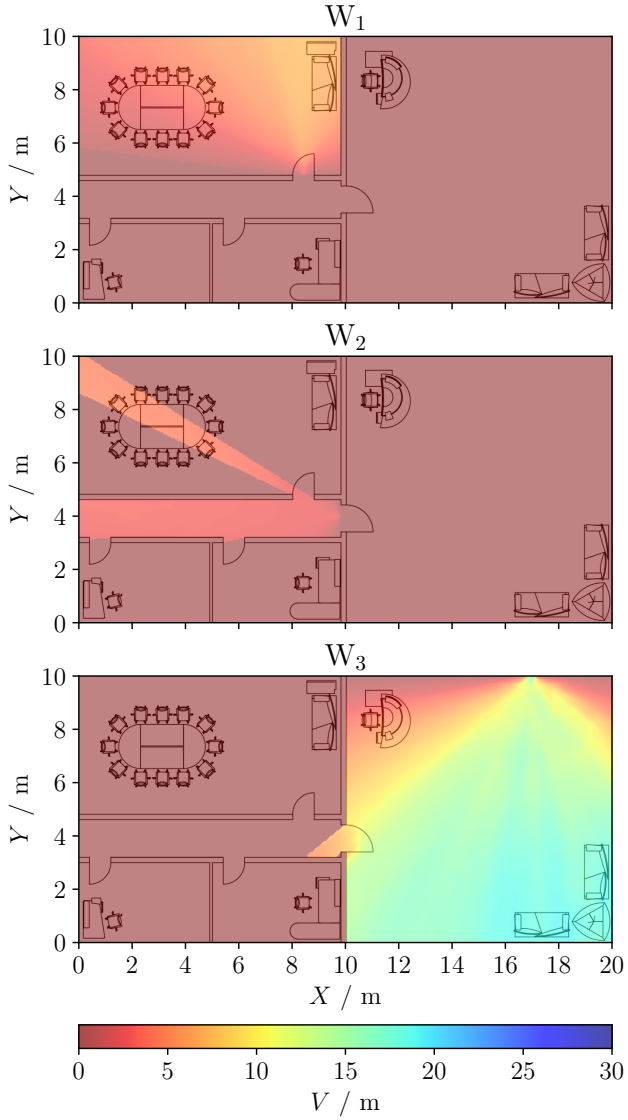

Figure 8: Visualisation of the visibility matrices $V^t_{i,j,k}$ for the waypoints $W_0 - W_2$ based on the FDS slice with quantity `EXTINCTION COEFFICIENT` at $t = 400\,\text{s}$, 2 m above the floor. The simulation has a uniform 5 cm mesh-grid.Visibility was calculated with $C = 3$ and truncated at a maximum boundary of 30 m.

maps and the corresponding ASET map can reveal potential hazards (blind spots) that may not be recognised in a local assessment of visibility. Likewise, examining the local visibility can provide conclusions about potentially dangerous areas where occupants are likely to be exposed to an enhanced smoke concentration.

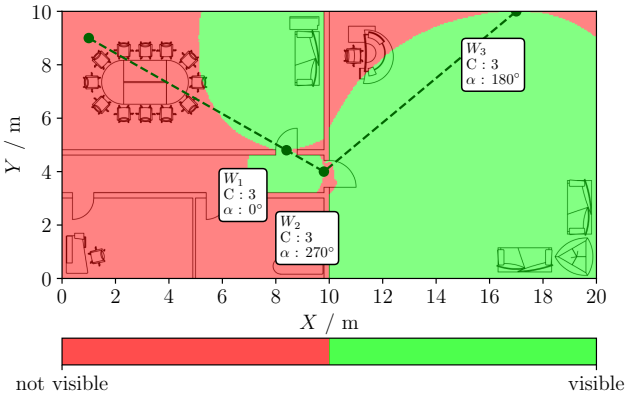

Figure 9: Visibility map based on an FDS slice with quantity `EXTINCTION COEFFICIENT` at $t = 400\,\mathrm{s}$, $2\,\mathrm{m}$ above the floor. The simulation has a uniform $5\,\mathrm{cm}$ mesh-grid. Colours indicate if the visibility criterion according to Eq. 2 is met (green) or not (red). All exit signs were assigned a visibility factor of $C = 3$.

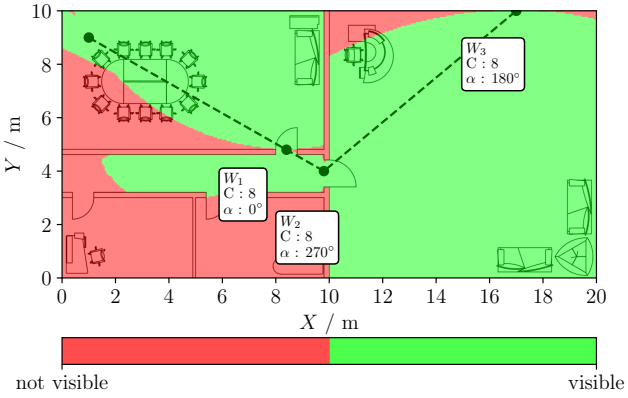

Figure 10: Visibility map based on an FDS slice with quantity `EXTINCTION COEFFICIENT` at $t = 400\,\mathrm{s}$, $2\,\mathrm{m}$ above the floor. The simulation has a uniform $5\,\mathrm{cm}$ mesh-grid. Colours indicate if the visibility criterion according to Eq. 2 is met (green) or not (red). All exit signs were assigned a visibility factor $C = 8$.

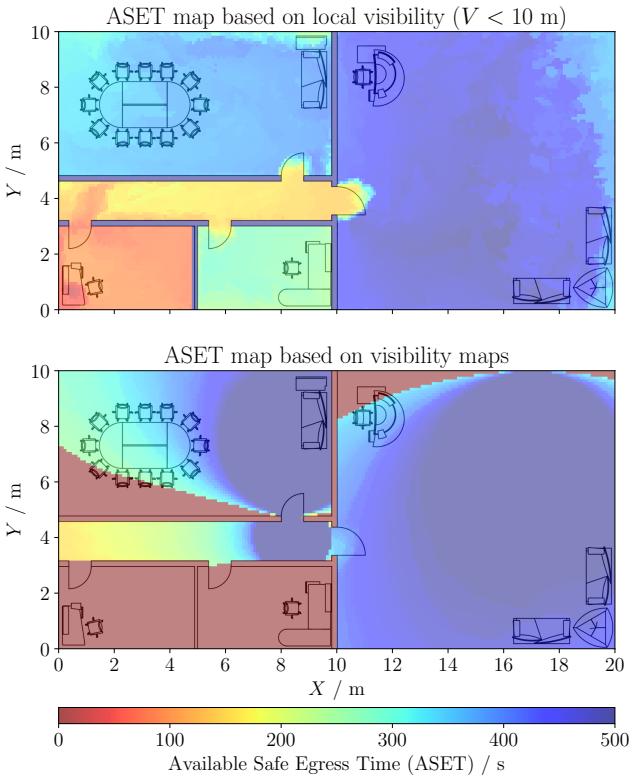

Figure 11: ASET maps based on local visibility and visibility maps. Both maps rely on the same FDS slice with quantity `EXTINCTION COEFFICIENT`, 2 m above the floor for time series $T = \{t \mid t = 0, 1, 2, ..., 400\,\text{s}\}$. The simulation has a uniform 5 cm mesh-grid. All exit signs were assigned a visibility factor of $C = 3$.

5 Summary

In this paper, an alternative approach is presented to assess visibility in case of a fire in the context of performance based design. It adapts the commonly applied empirical relation of Jin for use with inhomogeneous smoke distribution, as provided by CFD models. The method surpasses the traditional way of assessing local visibility, as commonly applied in fire safety engineering, by incorporating the location, orientation, and type of exit signs (reflecting or light emitting) in the analysis.

The proposed approach enables a comprehensive assessment of egress routes, providing visibility maps or, in a more advanced form, ASET maps through post-processing of simulation data. It obviates the need for predefined visibility performance criteria, as these emerge naturally from the compartment's geometry and the distance between exit signs and observers. Additionally, the model automatically accounts for factors affecting the perception of exit signs, such as viewing angles and potential visual obstructions within the occupants' line of sight.

It was demonstrated that the commonly employed visualisation of visibility data based on the local smoke density shows a substantially different pattern compared to the introduced waypoint-based approach. The derived visibility maps allow a simple and distinct assessment of the simulation results. This can particularly contribute in identifying potential blind spots within a building design. Moreover, visibility maps are easy to interpret also by people without professional qualification and may therefore become part of the approval process for building designs. However, the straightforward nature of the data's visual representation should not prevent users from critically reviewing the applied model parameters and the resulting simulation results.

The introduced model was implemented as a Python package, which is made freely available: the Python package FDSVismap operates as a dedicated post-processor for data from fire simulation models such as FDS, requiring only small additional effort from the user. The import of FDS data is handled with the open source Python module FDSReader. However, the data of any numerical fire model can generally be used to create visibility maps, if provided in a suitable transfer format. At the current state, the application generally requires moderate computational effort. However, especially for large simulations with dense mesh-grid discretisation involving multiple time steps to be evaluated, generating visibility maps can be highly time-consuming. An optimisation of the model is the subject of future work.

6 Outlook

A significant focus of future work will be directed towards optimising the algorithms of the Python implemented FDSVismap model. This especially involves vectorisation of computational operations, particularly concerning ray casting and data caching, to avoid redundant computations. Additionally, implementing advanced techniques like quad tree algorithms could significantly improve collision detection with obstruction cells.

Future iterations of the model aim to facilitate a spatial analysis, allowing exit signs to be considered that are located beyond the horizontal observation plane.

This would allow for an enhanced assessment of escape scenarios in more complex, multi-storey building environments. At this stage, ASET maps, generated on the basis of the visibility maps, still need to be interpreted in the context of a particular evacuation scenario. However, higher-order ASET maps may encompass the entire route of egress, requiring (automatic) identification of location based escape route decisions, potentially integrating data from pedestrian dynamics simulations.

Regardless of the presented approach, it is important to point out that the frequently used visibility model according to Jin needs to be fundamentally revised. Notably, the existing model does not adequately account for the absorbing and scattering behaviour of different kinds of smoke that might emerge from flaming or smouldering combustion. The model also provides limited scope in considering environmental effects, such as ambient light, which can significantly affect the contrast and thus the visibility of exit signs. To overcome these limitations, extensive experimental investigations and model developments will be required in the future.

Acknowledgements

This work was largely funded by the NextVIS project of the German Research Foundation (Deutsche Forschungsgemeinschaft – DFG) with the grant number 465392452. The authors gratefully acknowledge the financial support of the German Federal Ministry of Education and Research. The extensive computations of FDS simulations were performed largely on the high-performance computer system funded as part of the CoBra project with the grant number 13N15497.

Appendix

Appendix A – Description of the Employed Model Variables with their Data Types and Units

Table 2: Summarised description of the employed model variables with their data types and units

Variable	Type	Unit	Description
X_i, Y_j	Float	m	Physical Cartesian coordinates of the agent cell i, j
θ_k	Float	°	Viewing angle from the agent cell i, j towards the observation normal of the exit sign at waypoint W_k
$O_{i,j}$	Boolean	-	Indicating if cell i, j is populated by an obstruction element (1 or True) or not (0 or False)
$L_{i,j,k}$	Float	m	Euclidean distance between agent cell i, j and waypoint W_k
$A_{i,j,k}$	Float	–	Relative reduction of the emitted intensity as function of the view angle θ from agent cell i, j towards the surface normal of an exit sign at waypoint W_k
$U_{i,j,k}$	Boolean	-	Indicating whether the agent cell i, j is unconcealed (True or 1) or not (False or 0) from the waypoint W_k
$\rho^t_{\mathrm{s},k}(l)$	Float	$\mathrm{kg\,m^{-1}}$	Smoke density at distance l from the agent cell i, j towards the waypoint W_k at time t
$\bar{\sigma}^t_{i,j,k}$	Float	$\mathrm{m^{-1}}$	Integrated mean extinction coefficient along the line of sight between waypoint W_k and agent cell i, j at time t
$V^t_{i,j,k}$	Float	m	Visibility at agent cell i, j at time t with respect to the waypoint W_k
$M^t_{i,j,k}$	Boolean	-	Indicating if the exit sign at waypoint W_k is visible (1 or True) or not (0 or False) from agent cell i, j at time t
$M^t_{i,j}$	Boolean	-	Indicating if any exit sign is visible (1 or True) or not (0 or False) from agent cell i, j at time t
$M_{i,j}$	Boolean	-	Indicating if any exit sign is visible (1 or True) or not (0 or False) from agent cell i, j at all points in time $t \in T$
$\mathrm{ASET}_{i,j}$	Float	s	Indicating the first point in time $t \in T$, the visibility criterion according to Eq. 2 is not satisfied at agent cell i, j

Appendix B – Flowchart for the Creation of Visibility Maps and the Subsequent ASET Maps

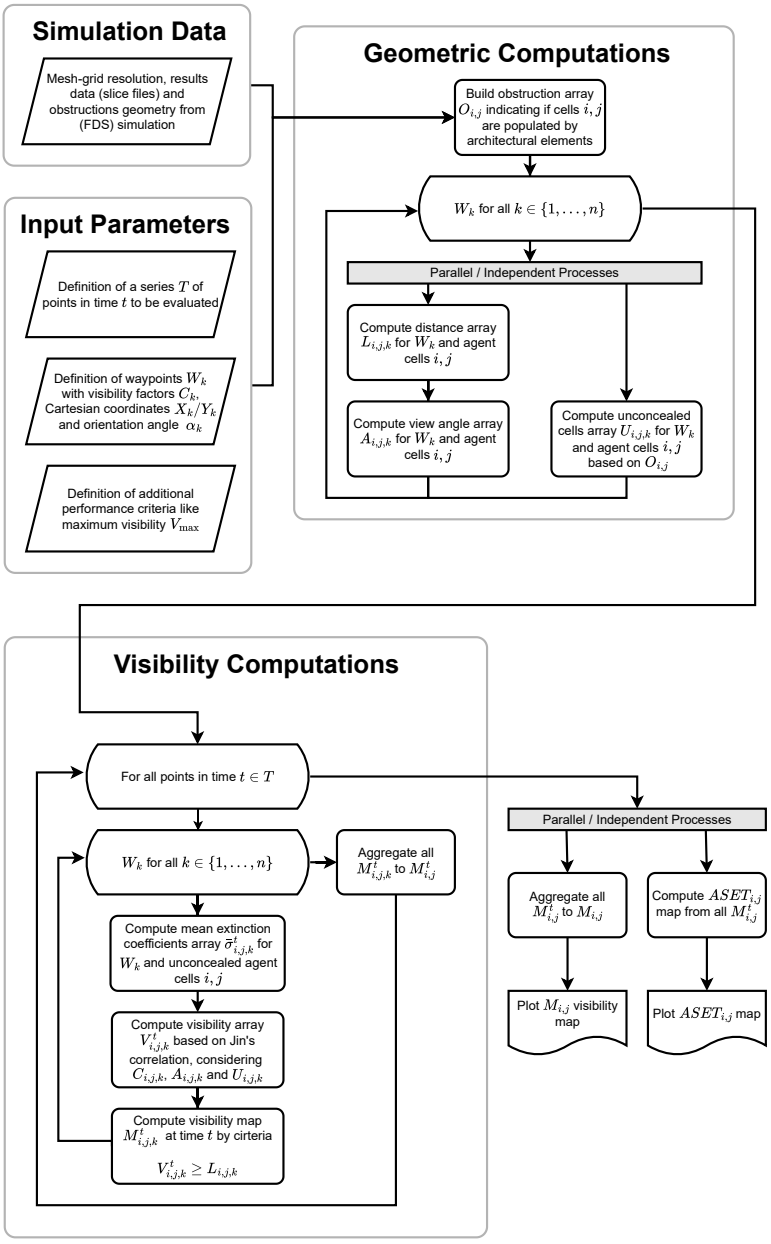

Figure 12: Flow chart for the computation of visibility maps $M_{i,j}$ and $\mathrm{ASET}_{i,j}$ maps based on fire simulation data. The algorithm can be subdivided into geometric computations and visibility computations. Both processes build on the simulation's boundary conditions and results, and on the defined waypoint parameters.

Appendix C – Visualisation of the Ray Casting Algorithm, using Different Techniques

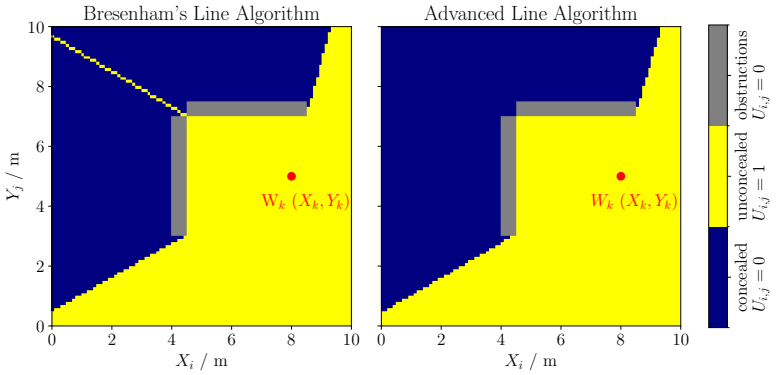

Figure 13: In $U_{i,j,k}$ all agent cells i, j are labelled as unconcealed (1, True) or concealed (0, False) when viewed from the waypoint W_k depending on their location before or behind the first collision cell. When adjacent obstruction cells do not form an entirely closed barrier, a collision point may not occur with the rasterised line of sight. A more advanced ray casting algorithm with a line thickness > 1 cell, e.g. using anti-aliasing, may then be applied to enforce an intersection.

Appendix D – Grid Sensitivity Analysis for Visibility Maps based on Different Mesh-grid Resolutions

Exemplary, the extinction coefficients at the locations Loc 1 - Loc 3 as (marked as red circles in Fig. 4) were evaluated for three simulations with identical geometry and boundary conditions but different grid sizes (see Fig. 14). The results of the three simulations generally show a consistent pattern, but exhibit quantitative discrepancies. At Loc 1, the 5 cm and 10 cm results are in good agreement, while the 20 cm results lie somewhat below them. At Loc 2, all three simulations show the same rank but notable deviations that increase over time. No clear pattern is evident, resulting from the different grid resolutions at Loc 3, while the ranking of the extinction coefficient values reverses. Notable differences are also evident in the visibility maps generated from each simulation (see Fig. 9 and Figs. 15 and 16). It is important to note that deviations resulting from different levels of discretisation may not solely be attributed to the simulation results, but also the conducted post-processing in generating the visibility maps. However, the influences from the simulation results appears to be dominant, as the ratio of the extinction coefficients according to Fig. 14 corresponds to the visibility range in the respective visibility maps.

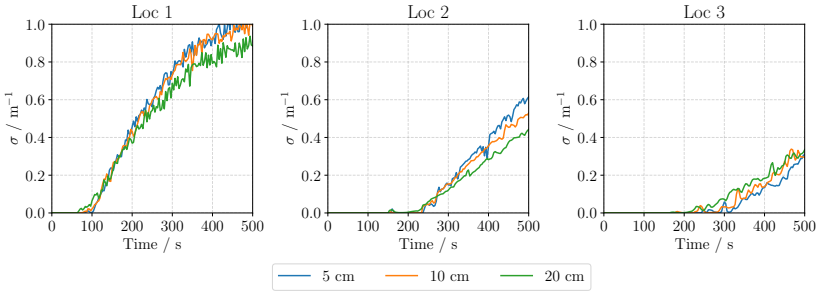

Figure 14: Extinction coefficients as a function of time for three different locations according Fig. 4. Values are given for three simulations with identical boundary conditions and geometry but different grid sizes with uniform cell sizes of 5 cm, 10 cm and 20 cm.

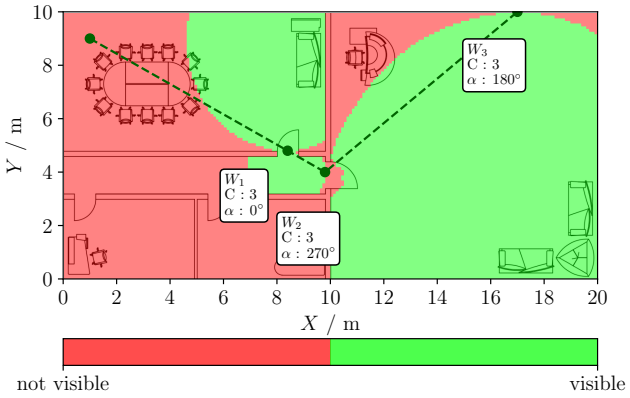

Figure 15: Visibility map based on an FDS slice file with quantity `EXTINCTION COEFFICIENT` at $t = 400\,\mathrm{s}$, 2 m above the floor. The simulation has a uniform 10 cm mesh-grid. Colours indicate if the visibility criterion according to Eq. 2 is met (green) or not (red). All exit signs were assigned a visibility factor of $C = 3$.

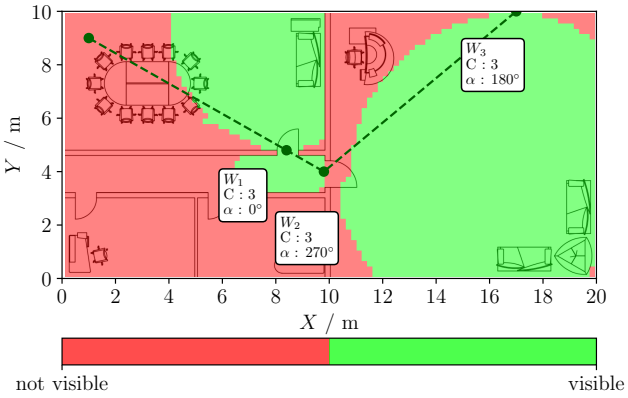

Figure 16: Visibility map based on an FDS slice file with quantity `EXTINCTION COEFFICIENT` at $t = 400\,\text{s}$, 2 m above the floor. The simulation has a uniform 20 cm mesh-grid. Colours indicate if the visibility criterion according to Eq. 2 is met (green) or not (red). All exit signs were assigned a visibility factor of $C = 3$.

References

[1] Deutsches Institut für Normung. *DIN ISO 3864-1: Graphische Symbole Sicherheitsfarben und Sicherheitszeichen Teil 1: Gestaltungsgrundlagen für Sicherheitszeichen und Sicherheitsmarkierungen (ISO 3864-1:2011)*. 2012.

[2] The International Organization for Standardization. *ISO 7010: Graphical symbols – Safety colours and safety signs – Registered safety signs*. 2020.

[3] Chunxiao Chen, Qiang Li, Shinji Kaneko, Jin Chen, and Xihong Cui. "Location optimization algorithm for emergency signs in public facilities and its application to a single-floor supermarket". In: *Fire Safety Journal* 44.1 (2009), pp. 113–120. ISSN: 03797112. DOI: 10.1016/j.firesaf.2008.05.006.

[4] Jiguang Shi, Ning Ding, and Fan Jiang. "The influence of color and direction on the perceptual processing of standard evacuation signs and the effect of attention bias". In: *Fire Safety Journal* 132 (2022), p. 103638. ISSN: 03797112. DOI: 10.1016/j.firesaf.2022.103638.

[5] Tadahisa Jin. "Visibility through Fire Smoke (I)". In: *Bulletin of Japan Association for Fire Science and Engineering* 19.2 (1970), pp. 1–8. DOI: 10.11196/kasai.19.2.1.

[6] Tadahisa Jin. "Visibility through Fire Smoke (II)". In: *Bulletin of Japan Association for Fire Science and Engineering* 21.1,1 (1971), pp. 17–23. ISSN: 18835600. DOI: 10.11196/kasai.21.17.

[7] Tadahisa Jin. "Visibility through Fire Smoke (III)". In: *Bulletin of Japan Association for Fire Science and Engineering* 22.1,2 (1972), pp. 11–15. DOI: 10.11196/kasai.22.11.

[8] Tadahisa Jin. "Visibility through Fire Smoke (IV)". In: *Bulletin of Japan Association for Fire Science and Engineering* 23.1,2 (1973), pp. 1–8. DOI: 10.11196/kasai.23.1_2_1.

[9] Ryun-Seok Oh, Young-Chan Kim, Young-Hoon Bae, and Jun-Ho Choi. "Evaluation of the Maximum Cognitive Distance Per Emergency Exit Sign Colour in a Smoke-Filled Environment Simulated Using a Translucent Eye Patch". In: *Fire Technology* (2023). ISSN: 0015-2684, 1572-8099. DOI: 10.1007/s10694-023-01474-9.

[10] Ahmed Ahmed Ali Awadallah and Konrad Wilkens Flecknoe-Brown. "(Mis)use of Visibility in Fire Safety Engineering". In: *Book of Abstracts Nordic Fire & Safety Days*. RISE Research Institutes of Sweden AB. 2022, pp. 32–33. ISBN: 978-91-89711-12-9. DOI: 10.23699/sgj7-kd69.

[11] Tuomo Rinne, Jukka Hietaniemi, and Simo Hostikka. *Experimental Validation of the FDS Simulations of Smoke and Toxic Gas Concentrations*. Tech. rep. VTT, 2007.

[12] Wojciech Węgrzyński and Gabriele Vigne. "Experimental and numerical evaluation of the influence of the soot yield on the visibility in smoke in CFD analysis". In: *Fire Safety Journal* 91 (2017), pp. 389–398. ISSN: 0379-7112. DOI: 10.1016/j.firesaf.2017.03.053.

[13] Bjarne Paulsen Husted, Jörgen Carlsson, and Ulf Göransson. "Visibility through inhomogeneous smoke using CFD". In: *Proceedings of the 10th International Fire Science and Engineering Conference. Interflam 2004*. Edinburgh, 2004. ISBN: 978-0954121631.

[14] Qihui Zhang. "Image based analysis of visibility in smoke laden environments". PhD thesis. Hull: University of Hull, 2010.

[15] P A Rubini and Q Zhang. "SIMULATION OF VISIBILITY IN SMOKE LADEN ENVIRONMENTS". In: *Proceedings of the 5th International Seminar on Fire and Explosion Hazards,* Edinburgh, 2007, p. 10.

[16] National Fire Protection Association and Society of Fire Protection Engineers, eds. *SFPE Engineering Guide to Performance-Based Fire Protection*. 2nd ed. National Fire Protection Association; Society of Fire Protection Engineers, 2007. ISBN: 978-0877657897.

[17] European Union. "Interpretative Document Essential Requirements No 2 'Safety in Case of Fire'". In: *Official Journal of the European Communities* (1994).

[18] National Fire Protection Association. *NFPA 101 Life Safety Code*. 2021.

[19] Vereinigung Kantonaler Feuerversicherungen (VKF). *Brandschutzrichtlinie: Nachweisverfahren im Brandschutz/ 27-15de*. Schweiz, 2017.

[20] Department of Building and Housing. *New Zealand Building Code Part C1-6: Protection from fire*. New Zealand, 2023.

[21] Morgan J Hurley and Eric R Rosenbaum. "Performance-Based Design". In: *SFPE Handbook of Fire Protection Engineering*. Ed. by Morgan J. Hurley. New York: Springer, 2016. ISBN: 9781493925643. DOI: 10.1007/978-1-4939-2565-0.

[22] The International Organization for Standardization. *ISO 13943:2017 - Fire safety - Vocabulary*. 2017.

[23] The International Organization for Standardization. *ISO 16732-1:2012 Fire safety engineering — Fire risk assessment — Part 1: General*. 2012.

[24] The International Organization for Standardization. *ISO 16733-1: Fire safety engineering — Selection of design fire scenarios and design fires — Part 1: Selection of design fire scenarios*. 2015.

[25] Nils Johansson and Madelene Ekholm. "Variation in Results Due to User Effects in a Simulation with FDS". In: *Fire Technology* 54.1 (2018), pp. 97–116. ISSN: 0015-2684, 1572-8099. DOI: 10.1007/s10694-017-0674-y.

[26] Tadahisa Jin. "Visibility and Human Behavior in Fire Smoke". In: *SFPE Handbook of Fire Protection Engineering*. Ed. by Philip J DiNenno. Third Edition. New York: National Fire Protection Association, 2002. ISBN: 087765-451-4.

[27] Leonard Y. Cooper. "A concept for estimating available safe egress time in fires". In: *Fire Safety Journal* 5.2 (1983), pp. 135–144. ISSN: 0379-7112. DOI: 10.1016/0379-7112(83)90006-1.

[28] Benjamin Schröder, Lukas Arnold, and Armin Seyfried. "A map representation of the ASET-RSET concept". In: *Fire Safety Journal* 115 (2020), p. 103154. ISSN: 0379-7112. DOI: 10.1016/j.firesaf.2020.103154.

[29] David A Purser. "Toxicity Assessment of Combustion Products". In: *SFPE Handbook of Fire Protection Engineering*. Ed. by Philip J DiNenno. Third Edition. New York: National Fire Protection Association, 2002. ISBN: 087765-451-4.

[30] Tadahisa Jin. "Studies on Human Behavior and Tenability in Fire Smoke". In: *FIRE SAFETY SCIENCE-PROCEEDINGS OF THE FIFTH INTERNATIONAL SYMPOSIUM*. Toranomon, Japan, 1997, pp. 3–21.

[31] David J. Rasbash. *International Seminar on Automatic Fire Detection, Aachen, Germany*. Aachen, Germany, 1975.

[32] Deutsches Institut für Normung. *DIN 18009-2:2016-09, Brandschutzingenieurwesen - Teil 2: Räumungssimulation und Personensicherheit*. 2022.

[33] Technisch-Wissenschaftlicher Beirat (TWB), Referat 4. *Guideline Fire Protection Engineering, 4th revised and supplemented edition*. Tech. rep. TB 04-01. Vereinigung zur Förderung des Deutschen Brandschutzes e.V. (vfdb), 2020.

[34] Kristian Börger. *FDSVismap - Github repository*. 2024. URL: https://github.com/FireDynamics/fdsvismap.git.

[35] Glenn P Forney. *Smokeview, A Tool for Visualizing Fire Dynamics Simulation Data Volume I: User's Guide*. Tech. rep. SP 1017-1. Gaithersburg, MD: National Institute of Standards and Technology, 2023.

[36] Charles R. Harris, K. Jarrod Millman, Stéfan J. van der Walt, Ralf Gommers, Pauli Virtanen, David Cournapeau, Eric Wieser, Julian Taylor, Sebastian Berg, Nathaniel J. Smith, Robert Kern, Matti Picus, Stephan Hoyer, Marten H. van Kerkwijk, Matthew Brett, Allan Haldane, Jaime Fernández del Río, Mark Wiebe, Pearu Peterson, Pierre Gérard-Marchant, Kevin Sheppard, Tyler Reddy, Warren Weckesser, Hameer Abbasi, Christoph Gohlke, and Travis E. Oliphant. "Array programming with NumPy". In: *Nature* 585.7825 (2020), pp. 357–362. DOI: 10.1038/s41586-020-2649-2.

[37] M. Pierre Bouguer and William Edgar Knowles Middleton. *Optical Treatise on the Gradation of Light. Translated, with Introduction and Notes, by WE Knowles Middleton*. University of Toronto Press, 1961.

[38] J. E. Bresenham. "Algorithm for computer control of a digital plotter". In: *IBM Systems Journal* 4.1 (1965), pp. 25–30. ISSN: 0018-8670. DOI: 10.1147/sj.41.0025.

[39] Wu Xiaolin. "An Efficient Antialiasing Technique". In: *Computer Graphics* (1991).

[40] George W. Mulholland and Carroll Croarkin. "Specific extinction coefficient of flame generated smoke". In: *Fire and Materials* 24.5 (2000), pp. 227–230. ISSN: 1099-1018. DOI: 10.1002/1099-1018(200009/10)24:5<227::aid-fam742>3.0.co;2-9.

[41] Verein Deutscher Ingenieure. *VDI 6019 – Part 1 – Engineering methods for the dimensioning of systems for the removal of smoke from buildings*. 2006.

[42] Verein Deutscher Ingenieure. *VDI 6019 – Part 2 – Engineering methods for the dimensioning of systems for the removal of smoke from buildings*. 2009.

[43] "Appendix 2: Thermophysical Property Data". In: *SFPE Handbook of Fire Protection Engineering*. Ed. by Morgan J. Hurley. New York: Springer, 2016. ISBN: 9781493925643. DOI: 10.1007/978-1-4939-2565-0.

[44] The International Organization for Standardization. *ISO 13571:2012 - Life-threatening components of fire - Guidelines for the estimation of time to compromised tenability in fires*. 2012.

Schriften des Forschungszentrums Jülich
IAS Series

Band / Volume 60
Elements for modeling pedestrian movement
from theory to application and back
M. Chraibi (2024), vi, 279 pp
ISBN: 978-3-95806-757-8

Band / Volume 61
Artificial Intelligence Framework for Video Analytics:
Detecting Pushing in Crowds
A. Alia (2024), xviii, 151 pp
ISBN: 978-3-95806-763-9

Band / Volume 62
The Relationship between Pedestrian Density, Walking Speed
and Psychological Stress:
Examining Physiological Arousal in Crowded Situations
M. Beermann (2024), xi, 117 pp
ISBN: 978-3-95806-764-6

Band / Volume 63
Eventify Meets Heterogeneity:
Enabling Fine-Grained Task-Parallelism on GPUs
L. Morgenstern (2024), xv, 110 pp
ISBN: 978-3-95806-765-3

Band / Volume 64
Dynamic Motivation in Crowds: Insights from Experiments
and Pedestrian Models for Goal-Directed Motion
E. Üsten (2024), ix, 121 pp
ISBN: 978-3-95806-773-8

Band / Volume 65
Propagation of Stimuli in Crowds:
Empirical insights into mutual influence in human crowds
H. Lügering (2024), xi, 123 pp
ISBN: 978-3-95806-775-2

Band / Volume 66
Classification of Pedestrian Streams: From Empirics to Modelling
J. Cordes (2024), vii, 176 pp
ISBN: 978-3-95806-780-6

Band / Volume 67
Optimizing Automated Shading Systems in Office Buildings by
Exploring Occupant Behaviour
G. Derbas (2024), 9, x, 168, ccxxiii
ISBN: 978-3-95806-787-5

Schriften des Forschungszentrums Jülich
IAS Series

Band / Volume 68
Speed-Density Analysis in Pedestrian Single-File Experiments
S. Paetzke (2025), XIII, 107 pp
ISBN: 978-3-95806-818-6

Band / Volume 69
Proceedings of the 35th Parallel Computational Fluid Dynamics International Conference 2024
A. Lintermann, S. S. Herff, J. H. Göbbert (2025), xv, 321 pp
ISBN: 978-3-95806-819-3

Band / Volume 70
Towards Improved Civil Safety: Experimental Insights into Impulse Propagation through Crowds
S. Feldmann (2025), xi, 99 pp
ISBN: 978-3-95806-828-5

Band / Volume 71
Development and Evaluation of Architecture Concepts for a System-on-Chip Based Neuromorphic Compute Node for Accelerated and Reproducible Simulations of Spiking Neural Networks in Neuroscience
G. Trensch (2025), 219, XXXV pp
ISBN: 978-3-95806-832-2

Band / Volume 72
The tube furnace as a new bench scale experiment for pyrolysis
K. De Lannoye (2025), ix, 70 pp
ISBN: 978-3-95806-839-1

Band / Volume 73
Single-file Movement: Literature Review, Empirical Analysis with Artificial Neural Networks, and Modeling
R. Subaih (2025), x, 115 pp
ISBN: 978-3-95806-843-8

Band / Volume 74
Improvement and Validation of Visibility Models in Fire Safety
K. Börger (2025), ix, 97 pp
ISBN: 978-3-95806-857-5

Weitere ***Schriften des Verlags im Forschungszentrum Jülich*** unter
http://wwwzb1.fz-juelich.de/verlagextern1/index.asp

IAS Series
Band / Volume 74
ISBN 978-3-95806-857-5

Mitglied der Helmholtz-Gemeinschaft